HELSINGIN YLIOPISTO
HELSINGFORS UNIVERSITET
UNIVERSITY OF HELSINKI

Master`s thesis
Department of Geoscience and Geography
Solid Earth Geophysics

VISUALIZATION AND INTERPRETATION OF THE SEISMIC REFLECTION DATA IN ARCHEAN BASEMENT IN SODANKYLÄ, LAPLAND

Noora Harjama
6/2020

Supervisors:

Suvi Heinonen (GTK)
Tuomo Karinen (GTK)
Ilmo Kukkonen (University of Helsinki)

UNIVERSITY OF HELSINKI
FACULTY OF SCIENCE
DEPARTMENT OF GEOSCIENCES AND GEOGRAPHY

PL 64 (Gustaf Hällströmin katu 2)
00014 Helsingin yliopisto

HELSINGIN YLIOPISTO
HELSINGFORS UNIVERSITET
UNIVERSITY OF HELSINKI

Tiedekunta / Faculty Faculty of Science	Koulutusohjelma / Degree program Master's Program in Geology and Geophysics	
Tekijä / Author Noora Heini Magdaleena Harjama		
Työn nimi / Title Visualization and Interpretation of the Seismic Reflection Data in Archean Basement in Sodankylä, Lapland		
Opintosuunta / Study track Solid Earth Geophysics		
Työn laji / Level Master's Thesis	Aika / Month and year 6 / 2020	Sivumäärä / Number of pages 62 + 2 attachments

Tiivistelmä / Abstract

The seismic reflection methods produce high-resolution images from the subsurface, which are useful in structural studies of geology. Northern Finland features a complex Precambrian geological history, including massive extension and compression stages, which has been extensively studied. The xSoDEx survey is the most recent seismic survey carried out in northern Finland by the Geological Survey of Finland (GTK). The XSoDEx concluded four survey lines, which are located in Central Lapland Greenstone Belt (CLGB) in Sodankylä, Lapland.

This thesis aims to find out whether the strong reflections shown in the xSoDEx Alaliesintie reflection profile, underneath the outcropping Archaean basement indicate a lithological contact or a fault zone. The Alaliesintie profile is characterized by Koitelainen intrusion, Archaean outcrops, and layers of younger Paleoproterozoic group rocks.

The work was carried out in stages, with the use of the SKUA - GOCAD 3D modeling software. The four stages are:

1. Create a 3D geological model based on the Alaliesintie reflection section and geological bedrock observations.
2. Use gravity and magnetic geophysical data from the study area to improve model reliability.
3. Use the geological 3D model and petrophysical data to build a synthetic seismic forward mode.
4. Analyze and evaluate the modeling result for understanding the possible origins of the reflections.

In the geological 3D model, I presented that the reflection would present lithological contacts and that the Archean bedrock would have folded and partly overthrust on top of the younger Proterozoic rocks. The seismic forward model is used as an experiment to test the geological 3D model's lithological contact respondence to the synthetic seismic signal and to discover the possible reflector underneath the Archaean basement. The results present that the seismic forward model can be used to perform the reflections and that the geological 3D model presented similar reflections in the seismic forward model comparing to the original Alaliesintie reflection data.

Avainsanat / Keywords
Geological 3D model, seismic forward model, reflection seismics, Archean basement, Central Lapland Greenstone Belt

Säilytyspaikka / Where deposited
HELDA- Digital repository of the University of Helsinki

Muita tietoja / Additional information
26 figures and 6 tables

HELSINGIN YLIOPISTO
HELSINGFORS UNIVERSITET
UNIVERSITY OF HELSINKI

Tiedekunta / Faculty Matemaattis-luonnontieteellinen tiedekunta	Koulutusohjelma / Degree program Geologian ja geofysiikan maisteriohjelma	
Tekijä / Author Noora Heini Magdaleena Harjama		
Työn nimi / Title Seismisen heijastusaineiston visualisointi ja tulkinta Arkeeisessa kallioperässä Sodankylässä, Lapissa		
Opintosuunta / Study track Kiinteän maan geofysiikka		
Työn laji / Level Pro gradu	Aika / Month and year 6 / 2020	Sivumäärä / Number of pages 62+ 2 liitettä

Tiivistelmä / Abstract

Seismiset heijastusluotausmenetelmät tuottavat maankamarasta korkearesoluutioista seismistä aineistoa, jota hyödynnetään rakennegeologisessa tutkimuksessa. Pohjois-Suomen kallioperä on monimutkaisen geologisen historian tulos, ja sisältää massiivisia tektonisia vaiheita, joissa kallioperä on repeytynyt ja poimuttunut, jota on tutkittu laajasti. XSoDEx-projekti on viimeisin Pohjois-Suomessa tehty seisminen heijastusluotaustutkimus, ja sen toteutti Geologian tutkimuskeskus (GTK). XSoDEx-projekti sisältää yhteensä neljä tutkimuslinjaa, jotka sijaitsevat Keski-Lapin vihreäkivivyöhykkeellä, Sodankylässä.

Tämän työn tarkoituksena on selvittää liittyvätkö xSoDEx, Alaliesintie-linjalla arkeeisen kallioperän alla olevat voimakkaat heijasteet litologiseen kontaktiin vai siirrokseen. Alaliesintien tutkimuslinjan kallioperä muodostuu Koitelaisen intruusiosta, arkeeisesta kallioperästä, sekä nuoremmista paleoproterotsooisista kivilajiryhmistä.

Työ toteutettiin käyttäen SKUA - GOCAD 3D-mallinnusohjelmistoa. Työ vaiheisiin kuuluivat:

1. Luoda geologinen 3D-malli, joka perustuu Alaliesintien heijastusluotaus aineistoon ja geologisiin kallioperähavaintoihin.
2. Käyttää tutkimusalueen muita geofysikaalisia aineistoja (painovoima- ja magneettista aineistoa) tukemaan geologista 3D-mallia.
3. Tehdä seisminen suoramallinnus geologisen 3D-mallin ja petrofysikaalisen aineiston pohjalta.
4. Analysoida seismisen suoramallinnuksen tuloksia Alaliesintien heijastusluotaus aineiston kanssa, jotta pystytään ymmärtämään paremmin heijastajien alkuperää.

Geologinen 3D-malli esittää, että heijasteet tulisivat litologisista kontakteista, jolloin alueen kallioperä olisi poimuttunut ja arkeeinen kallioperä olisi osittain ylityöntynyt nuorempien paleoproterotsooisten kivilajien päälle. Seismistä suoramallinnusta käytettiin tutkimaan geologisen 3D-mallin litologisten rajapintojen vaikutuksia seismiseen signaaliin, mikä mahdollistaisi löytämään heijastajien alkuperän. Tulokset osoittavat, että seimistä suoramallinnusta voidaan käyttää geologisen 3D-mallin tutkimukseen ja että seimisestä suoramallinnuksesta saaduissa heijasteissa on samankaltaisuuksia Alaliesintien aineiston kanssa.

Avainsanat / Keywords
Geologinen 3D-malli, seisminen suoramallinnus, seisminen heijastusluotaus, arkeeinen kallioperä, Keski-Lapin vihreäkivivyöhyke

Säilytyspaikka / Where deposited
HELDA- Helsingin yliopiston digitaalinen arkisto

Muita tietoja / Additional information
26 kuvaa ja 6 taulukkoa

TABLE OF CONTENTS

1. INTRODUCTION

Seismic wide-angle and reflection methods are a very effective means to study deep bedrock formations in the subsurface. Several seismic surveys have been completed in Finland, and the data has been used to create 3D models of the subsurface structures. Niiranen et al. (2014) report present the Central Lapland Greenstone Belt 3D modeling projects from 2007 – 2012, which includes investigations of orogenic Au deposit in Kittilä terrain, and Au-Cu ore deposit investigations with the use of HIRE seismic reflection survey data from Hanukainen-Rautuvaara region in the Kola area. In this thesis, I use the resent experiment of Sodankylä Deep Exploration (xSoDEx) reflection seismic dataset from Alaliesintie in the Sodankylä region (Figure 1), northern Finland.

Figure 1. Roadmap of northern Finland with the study area, where the Alaliesintie xSoDEx survey line is located.

The xSoDEx project acquired seismic data during the summer of 2017, in a co-operation between the Geological Survey of Finland (GTK), Freiberg University of Mining and Technology, and the University of Oulu (Heinonen et al. 2018). The purpose of the xSoDEx was to get a better understanding of the bedrock structures and mineral systems in the Sodankylä area. The xSoDEx reflection and refraction exploration included a total of four survey lines: Pomokairantie, Alaliesintie, Kuusivaarantie, and Sakatti profiles. In this thesis, I am focused on the Alaliesintie (15.5 km long) profile (Figure 1), in particular in the strong reflections underneath the Archean basement, which outcrops in the NW part of the profile and elsewhere in the study area.

The seismic data on the Alaliesintie profile revealed strong reflectivity underneath the Archean basement outcrops. Generally, the Archean basement is observed to be weakly reflective (Patison et al. 2006). This thesis focuses on studying the possible reasons for the strong reflections by analyzing their relationship with a lithological map and with other geophysical data. The thesis also utilizes petrophysical measurements and regional gravity and magnetic data in the study area. All the geophysical data set applied in this thesis have been acquired during the xSoDEx project or earlier by GTK.

To visualize the subsurface structures, I prepared a 3D-model of the study area by analyzing and combining the different data set with the use of the Subsurface Knowledge Unified Approach (SKUA) and Geologic Computer-Aided Design (GOCAD) 3D-modeling software. The software is designed for studying structurally complex areas, such as overthrust faults and multi-z surfaces (Emerson 2019). The SKUA – GOCAD has various tools for processing, combining, and creating structural and visual models from different datasets.

I took the following steps to reach and insight on the geological explanation for the reflection. First, I compiled a complied geological 3D model of the Alaliesintie profile, based on xSoDEx reflection data with surface observations from the (digital) geological bedrock map by GTK. Secondly, I used gravity and magnetic geophysical data, collected by GTK, to improve the 3D geological model. Finally, I created a synthetic seismic forward model using the geological 3D model surfaces and petrophysical parameters of rock samples in the study area. To find out whether the strong seismic reflections are due to lithological contacts as it is suggested in the geological

3D model or whether they are due to faulting, which has fractured the Archean basement. Thus, this study aids in understanding the structure and tectonic evolution of the study area as well as provide insight into the structures controlling the formation and locations of mineral deposits.

2. BACKGROUND

2.1. Geological setting of the area

2.1.1. Geology of the Central Lapland Greenstone Belt

The bedrock in northern Finland is characterized by the formations of the Archean craton, the Central Lapland Granitoid Complex (CLGC), the Central Lapland Greenstone Belt (CLGB), and the Lapland Granulite Belt (LGB) (Kukkonen et al. 2006) (Figure 2). The study area (16.9 km by 15.5 km) is located in the CLGB, around the Alaliesintie xSoDEx reflection seismic survey line. The Alaliesintie survey line runs on top of the Archean basement rocks, Paleoproterozoic supracrustal rocks, and the Koitelainen mafic-ultramafic layered intrusion.

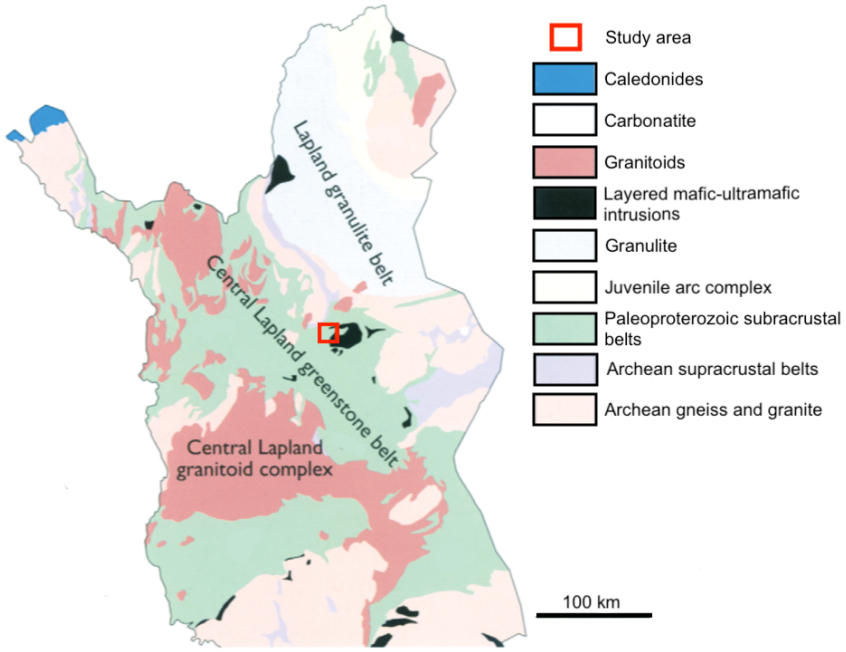

Figure 2. General geological units in northern Finland (modified after Korsman et al. 1997, Hanski and Huhma 2005), where the red box is presenting the study area.

The CLGB is the largest mafic volcanic-dominated province in Finland (Eilu et al. 2007). It is characterized by Paleoproterozoic supracrustal rocks, which are divided into lithostratigraphic groups from the youngest to the oldest: Kumpu group, Kittilä suite, Savukoski group, Sodankylä group, Kuusamo group, and Salla group (Figure 3) (Lehtonen et al. 1998, Hanski and Huhma 2005, Nironen 2017a). During its evolution, the CLGB has gone through continental accretion, continental extension, intense continent-continent collision, and orogenic collapse and stabilization, including five different deformation stages (Figure 4) (Table 1) (Köykkä et al. 2019). There is also evidence of Paleoproterozoic mantle plume-related eruptions of komatiitic and rhyolitic lavas, and emplacements of large layered sill-like mafic intrusions in 2.45 – 2.05 Ga (Hanski and Huhma 2005, Nironen 2017b).

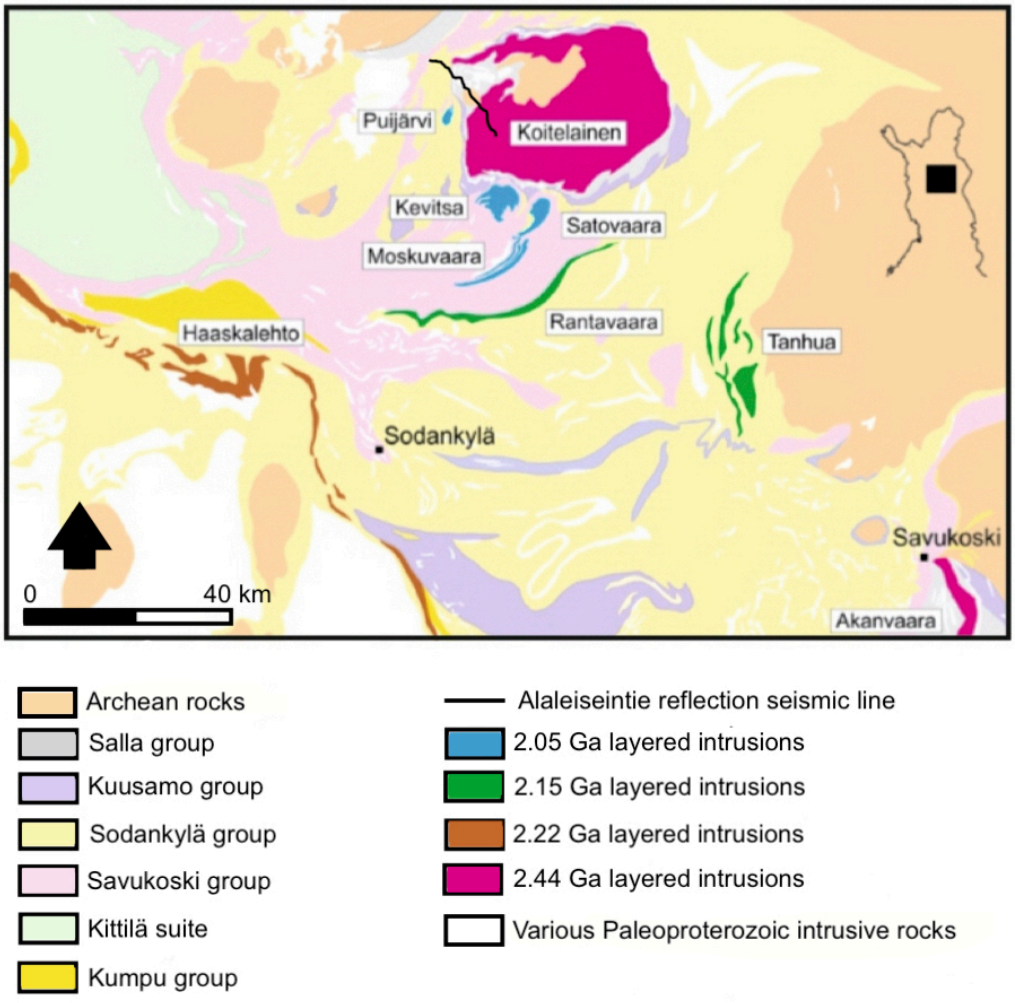

Figure 3. General geological map of Central Lapland Greenstone Belt (CLGB), with Paleoproterozoic lithostratigraphic groups (modified after Huhma et al. 2018). The location of the study area is around the Alaliesintie reflection seismic survey line.

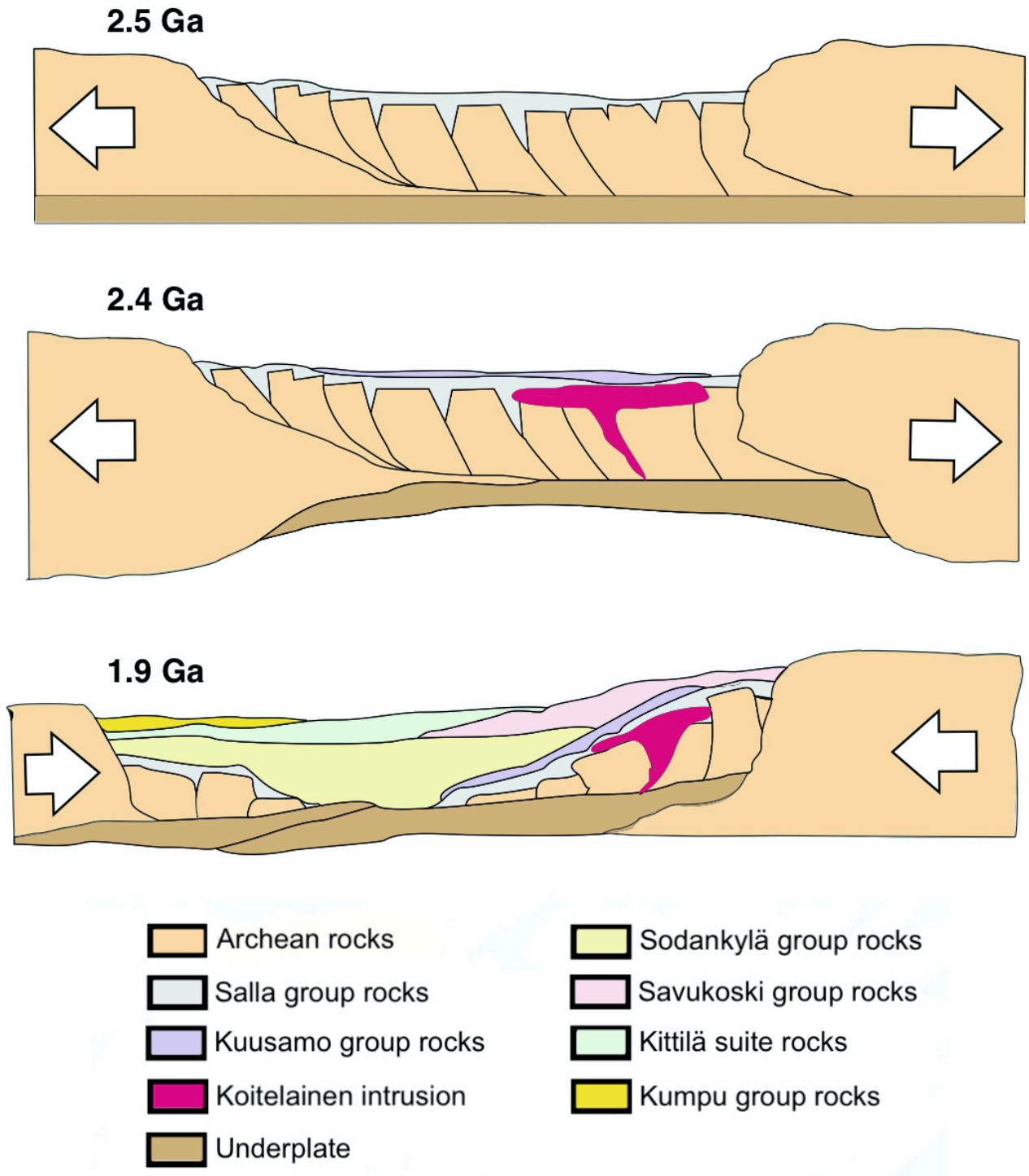

Figure 4. Sketch model is based on Köykkä et al. (2019) figures 8 and 9, which is summarizes the Central Lapland belt (CLB) lithologies and tectonic settings. The sketch is an illustration of the Central Lapland Greenstone Belt (CLGB) tectonic history between 3.20 – 1.9 Ga.

On the basis of previous studies (Hanski et al. 2005, Hanski and Huhma 2005, Nironen 2017a, b), the evolution of the CLGB is characterized by rifting of the Archean basin during 2.5 – 2.1 Ga, and deposition of the supracrustal rocks and the thrust belt development. The oldest lithostratigraphic unit in Paleoproterozoic CLGB is the Salla group. It consists of mainly intermediate to acid volcanic rocks, which were intruded by mafic-ultramafic intrusion (Koitelainen and Akanvaara) at 2.44 Ga (Hanski and Huhma 2005, Nironen 2017b, Huhma et al. 2018, Köykkä et al. 2019). The overlaying Kuusamo group is characterized by mafic volcanic rocks, which are present in the Koskimaa and Unikumpu formations (Köykkä et al. 2019).

Based on Köykkä et al. (2019), in the early stage of the CLGB evolution, the extension continued with volcanic activity, and the conditions turned into a mixed tidal and influenced shallow marine environment. The Sodankylä group includes metasedimentary successions with mafic volcanic rocks, formed during the beginning of the rifting and the rifting stage, and covered most of the CLGB. The first metasediments formed in the alluvial to the tidal stages, the shallow marine environment between 2.38 – 2.35 Ga (Hanski and Huhma 2005, Köykkä et al. 2019). The rest of the Sodankylä and Kivalo group of rocks formed during 2.35 – 2.15 Ga into a mix between tidally influenced shallow marine and clastic sedimentation (Köykkä et al. 2019). During this stage, the mafic-ultramafic intrusion in 2.22 Ga (Haaskalehto) intruded into the Sodankylä group (Köykkä et al. 2019).

The extension led to the oceanic opening of the basin into an ocean, where the Savukoski group, Rovaniemi super suite, Kittilä suite, and Martimo suite rocks formed in an environment of arc volcanism and a marine setting, between 2.15 – 1.92 Ga (Köykkä et al. 2019). The Savukoski group consists of mafic-ultramafic volcanic rocks, black schists, and greywackes (Köykkä et al. 2019). The Kittilä suite is par-allochthonous, meaning it is party overlays the Savukoski group of rocks, although the Kittilä suite rocks are the same as in the Savukoski group. The mafic-ultramafic intrusions intruded the Savukoski group in 2.15 Ga (Rautavaara gabbro) and 2.05 Ga (Puijärvi, Kevitsa, Satovaara, and Moskuvaara intrusions) (Hanski and Huhma 2005, Huhma et al. 2018, Köykkä et al. 2019). It is still uncertain if the magmatism was the reason of the continental breakup, but after the magmatism and related volcanism and intrusions, the continental breakup occurred between 2.50 – 2.10 Ga (Köykkä et al. 2019).

Table 1. Tectonic setting lithostratigraphic groups and formations and their relations to the tectonic evolution of the Central Lapland Greenstone Belt (CLGB). (LGB = Lapland Granulite Belt, CLB = Central Lapland Belt) (Compiled from Köykkä et al. 2019)

Age (Ga)	Group	Tectonic setting	Rock formation	Rock complex
3.50 – 2.75	Archean basement complex	PRE-RIFT	Granitoids and tantalite-trondhjemite-granodiorite	Archean Basement
2.61 – 2.38	Räväsjärvi and Haisujupukka suites	INITIAL RIFTING / EARLY SYN-RIFT Subaerial eruptions of ash and flood basalts in a subaqueous bimodal volcanism environment which has been the start of the continental extension	Quartzites and paragneisses	CLB
2.50 – 2.44	Salla	INITIAL RIFTING / EARLY SYN-RIFT Subaerial eruptions of ash and flood basalts in a subaqueous bimodal volcanism environment which has been the start of the continental extension	Felsic-intermediate volcanic and minor conglomerate-breccias	CLB
2.44	Intrusions	Koitelainen and Akanvaara		CLB
2.44 – 2.38	Kuusamo	INITIAL RIFTING / EARLY SYN-RIFT Subaerial eruptions of ash and flood basalts in a subaqueous bimodal volcanism environment which has been the start of the continental extension	Basaltic mafic volcanic and minor conglomerates	CLB
2.38 – 2.35	Virttiövaara and Vuojärvi suites	SYN-RIFT The rocks were formed to alluvial to tidally influenced shallow marine environment	Quartzites and mica schists	CLB
2.38 – 2.15	Sodankylä	SYN-RIFT/ EARLY POST-RIFT The rocks were formed to a mixed tidal and controlled shallow marine environment	Quartzites, siltstones carbonate rocks, mudstones, minor conglomerate-breccias and mafic volcanic with tuffites	CLB
2.22	Intrusion	Haaskalehto		CLB
2.15 – 2.05	Savukoski	PASSIVE MARGIN (POST-RIFT) The rocks formed into an arc volcanism and marine setting environment	Greywackes, BIFs, black schists, mafic to ultramafic volcanic, minor carbonate rocks, and tuffite	CLB
2.15 and 2.05	Intrusions	2.15 Ga Tanhua and Rantavaara and 2.05 Ga Puijärvi, Kevitsa, Satovaara, and Moskuvaara		CLB
2.15 – 1.88	Kittilä and Martimo suite	PASSIVE MARGIN (POST-RIFT) The rocks were formed to an arc volcanism and marine setting environment	Greywackes, BIFs, black schists, mafic to ultramafic volcanic, minor carbonate rocks, and tuffite	LGB, CLB
1.88 – 1.80	Kumpu	FORELAND SYSTEM The rocks were formed to marine and alluvia environment.	Conglomerates, arkose-quartzite, and felsic volcanic	LGB, CLB

After the open marine system, the initial compression collision started to occur in 1.94 Ga. Serval deformation phases characterized the compressional period in the Central Lapland Granitoid Complex (CLGC), Lapland Greenstone belt (LGB), and Central Lapland (CL)(Table 2), which have been interpreted by Lehtonen et al. 1998, Gaal et al. 1989, Ward et al. 1989, Evins and Laajoki 2002, Nironen and Mänttäri 2003, Patison et al. 2006, Hölttä et al. 2007, Niiranen et al. 2014a, Nironen 2017b, Lahtinen and Huhma 2019.

Table 2. Tectonic events and structures in CLGC and LGB between 1.92 – 1.76 Ga. (CLGC = Central Lapland Granitoid Complex, LGB = Lapland Granulite Bel, D1 = first deformation, D2 = second deformation, D3 = third deformation, D4 = fourth deformation, D5 = fifth deformation) (Lahtinen and Huhma 2019).

Age (Ga)	Main deformation direction	CLGC (Lahtinen et al. 2015, 2018)	Main deformation direction	LGB (Lahtinen and Huhma 2019)
1.92 – 1.91	↓	D1 E-W shortening, with E-vergent thrusting and folding	↙	D1 NW-SE shortening with, SW-vergent thrusting
1.89 – 1.88	←	D2 N-S shortening, with upright folding and N-vergent thrusting		Exhumation, appetites and granites.
1.88 – 1.87	↘	D3 SW-NE shortening, with NE-vergent thrusting and folding	↘	D2 SW -NE shortening with SW-vergent duplexing and NE-vergent folding
1.87 – 1.85	↙	D4 NNW-SSE shortening	↙	D3 NNW-SSE shortening with, radial conical folds, a strike-slip fault zone, and radial fractures
1.78 – 1.76	↓	D5 NNE-SSW shortening and folding and NNE-vergent thrusting	↓	NNE-SSW shortening, and extensional fractures

In this thesis, I follow the most recent interpretation of the tectonic evolution of CLGB and adjacent areas (Lahtinen and Huhma 2019). The main compression stage occurred in 1.92 – 1.88 Ga, which developed the foreland fold-trust belt (Köykkä et al. 2019). The Sodankylä area has south-divergent nappe structures, which are dislocated slabs of the basement. The nappes of Kelujärvi and Pyhätunturi are the development of a foreland fold and thrust belt and have then

been transported from the north during the D1 phase (Nironen 2017a). Lahtinen and Huhma (2019) present that large thrust nappes formed on the foreland fold and thrust belt. The D2 phase at 1.89 – 1.88 Ga, the shortening was north to south directed (Lahtinen and Huhma 2019). The D3 period occurred at 1.88 – 1.87 Ga with shortening in the southwest to northeast direction, the D4 phase took place at 1.87 – 1.81 Ga and the shortening was north-northeast to south-southeast directed (Lahtinen and Huhma 2019). During the D4 phase, the Kumpu group, Uusivirka suite, and Karunki formation formed into the marine environment, with clastic sedimentation and minor coeval felsic volcanism (Nironen 2017b, Köykkä et al. 2019). The latest deformation phase, the D5, occurred at 1.78 – 1.76 Ga and it had north-northeast to south-southwest directed shortening (Lahtinen et al. 2015, 2018, Lahtinen and Huhma 2019). Based on these deformation periods, very complicated structures were formed in the area with many deformation stages, which are important in investigating the structure of the area and understanding the reflective patterns in the seismic section.

2.1.2. Intrusions

The Archean shear zones were reactivated during the rifting at 2.5 – 1.9 Ga, and it led to the emplacement of layered intrusions (Nironen 2017a). The Koitelainen and Akanvaara mafic intrusions were emplaced and erupted during 2.45 – 2.44 Ga. The Koitelainen intrusion is the largest known layered intrusion in northern Finland. According to diamond drilling data, the intrusion is flat, with an area of 754 km^2 and a thickness of approximately 3 km (Mutanen and Huhma 2001). The Puijärvi intrusion is a considerably smaller mafic to ultramafic intrusion. It is located southwest from the Koitelainen intrusion. The Puijärvi was intruded into the Savukoski group of rocks at 2.05 Ga, the Kevitsa, and the Moskuvaara were as well intruded into the Savukoski group of rocks during this time (Huhma et al. 2018).

The Koitelainen intrusion is located between the Archean basement rocks and the Salla group of Proterozoic rocks, and during its history, it has been uplifted and eroded (Mutanen 1997, Hanski and Huhma 2005, Nironen 2017a). The intrusion is surrounded by the supracrustal rocks of the Salla and Kuusamo groups. The Koitelainen intrusion has been studied in detail, and the stratigraphy of the intrusion is well known. The top of the complex is on the NW side of the

intrusion. Mutanen (1989, 1997) divided the intrusion into four stratigraphic units: Lower Zone (LZ), Main Zone (MZ), Upper Zone (UZ), and granophyre, which is genetically related to the vulcanite rocks of the Salla group (Figure 5). Koitelainen intrusion is known for PGE-bearing chromite layers, upper (UC), and lower chromite (LC) and as well as layers of vanadium-bearing magnetite (Mutanen 1989, 1997, Hanski and Huhma 2005).

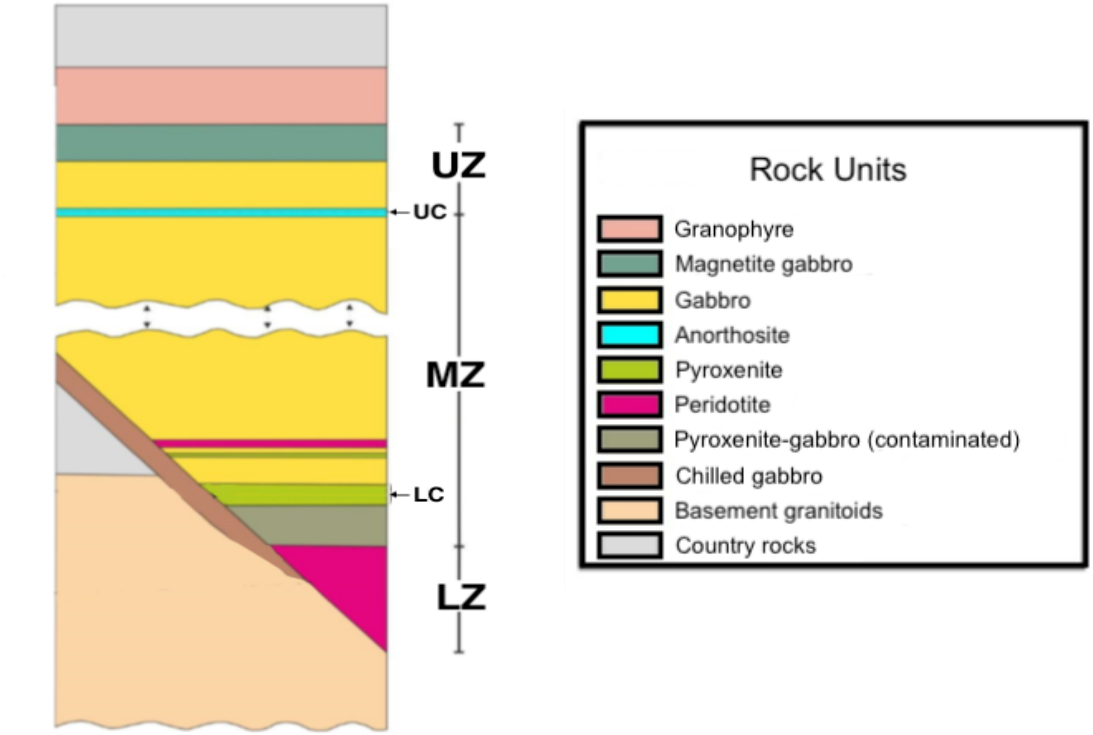

Figure 5. Stratigraphical units of the Koitelainen intrusion modified after Mutanen (1997). The rock units contain various rock types, and they are divided into the upper zone (UZ), main zone (MZ), and lower zones (LZ). The Koitelainen intrusion hosts PGE-bearing chromite layers (upper (UC) and lower chromite (LC)), which are located in the upper and main zones.

2.2. Theory of the reflection seismic method

2.2.1. Theoretical background

The seismic methods are based on the elasticity of rocks. The seismic wave's motion is a movement of the strain in the material, where the framework of rock-forming particles is expanding and compressing based on seismic motion and direction of propagation. The theory

behind the seismic waves is described in more detail by Shearer (2009), Stein and Wysession (2003), and Ylimaz (2001).

The seismic waves propagate in the subsurface in the bulk of the bedrock are called body waves. They are either compressional, i.e., P-waves or transverse waves, i.e., S-waves. The P-wave motion is parallel with the direction of wave propagation, whereas the S-wave is perpendicular to the direction of wave propagation. Waves move along the Earth's surface to obey a similar wave equation, but they are tied to the surface and attenuate and diminish rapidly with increasing depth from the surface. There are two basic types of surface waves, the Rayleigh waves, where the particle motion is elliptical in a vertical plane and parallel to the direction of propagation, and the Love waves, where the particle motion alternate transverse motion and perpendicular to the wave's propagation.

The P-wave (v_P) and the S-wave (v_s) velocities are defined by the elastic moduli, Lame's parameters μ and λ, and density ρ of the medium. The Lame's parameters μ and λ describe the linear stress-strain relation within an isotropic solid, which represents the material's response to shear stress, measuring the resistance to shearing. The body wave velocities can be defined as follows:

$$v_P = \sqrt{\frac{\lambda+2\mu}{\rho}} = \sqrt{\frac{\frac{4}{3}\mu+k}{\rho}} \tag{2.1}$$

$$v_S = \sqrt{\frac{\mu}{\rho}} \tag{2.2}$$

The ratio between the P-wave and the S-wave can be calculated with Poisson's ratio (Shearer 2009). Where the Poisson's solid ratio (φ), can be defined as:

$$\varphi = \frac{\lambda}{2(\lambda+\mu)} = \frac{\frac{1}{2}(V_P^2 - V_S^2)}{V_P^2 - V_S^2} \tag{2.3}$$

$$V_s = \frac{V_P}{\sqrt{3}} \tag{2.4}$$

where V_s and V_P are the S- and P-wave velocities respectively, and the $\sqrt{3}$ is the commonly used S-and P-wave Poisson solid ratio. The Poisson solid ratio is dimensionless, and most of the crustal rocks Poisson ration varies between 0.25 and 0.30 (Shearer 2009).

A seismic source (earthquake or vibroseis truck) creates a seismic wave to the subsurface, which is a spatial wavefront around the source point. The wave propagation is related to the Huygens principle, which presents that every point on a wavefront can be thought of as a new point source for waves generated in the direction the wave is traveling. When the wave motion hits the interface with different elastic properties, the wave reflects and refracts based on Snell's law. Snell's law describes the angle of the reflects and refracts waves, which can be defined as:

$$\frac{\sin i_1}{\sin i_2} = \frac{V_1}{V_2} \tag{2.5}$$

where i_1 is the angle between medium and incident wave, or medium and reflected wave, $i_2$is the angle between medium and refracted wave, and V_1 and V_2 are the velocities for the two materials.

The amplitude of the wave will change as in the Zoeppritz equations, which describe the partition of seismic wave energy at the interface (Sheriff 1995.). The Zoeppritz equations relate the amplitude of the incident P-wave and the amplitudes of the reflected and refracted P-and S-waves to the angle of incidence. The reflection coefficient (R) presents the reflected energy for incident wave, and the transmission coefficient (T) presents the refracted wave. For an incident wave meeting, the interface perpendicularly the coefficient are as follows:

$$R = \frac{A_r}{A_i} = \frac{\rho_2 V_2 - \rho_1 V_1}{\rho_2 V_2 + \rho_1 V_1} = \frac{Z_2 - Z_1}{Z_2 + Z_1} \tag{2.6}$$

$$T = \frac{A_t}{A_i} = \frac{2\rho_1 V_1}{\rho_2 V_2 + \rho_1 V_1} \tag{2.7}$$

where A_r is the amplitude of the reflected wave, A_t is the amplitude of the transmitted wave, and A_i is the amplitude of the incident wave. The acoustic impedances *Z* of the media are obtained as the products of the density ρ, and the velocity *V*. The reflection coefficient values range from +1 to -1., which indicates the polarity of the reflected wave.

2.2.2. Reflectivity and seismic resolution

There are two basic factors, which determine whether the potential reflector can be detected and imaged by seismic reflection techniques; the earlier presented acoustic impedance between the materials or horizon, and its surroundings, and its geometry (Salisbury and Snyder 2007). The strong reflectivity is related to the strength of the acoustic impedance contrast between two materials, meaning that the reflection coefficient defines the detection limit of the reflection from the interface. Basis of Salisbury et al. (1996), the reflection can be detected in practice in a reflection seismic survey when the reflection coefficient is bigger than 0.06, which is means that only 6% of the incident wave energy is reflected. The other factor is the geometry, especially the size, and the depth of the feature. The seismic resolution has vertical and horizontal theoretical limits that control what can be resolved in a survey (Kallweit and Woods 1982, Salisbury et al. 2007).

The vertical resolution expresses the minimum thickness of a layer, which can be resolved. The vertical resolution h_{min}, is defined as follows:

$$h_{min} = \frac{V}{4f_d} \tag{2.8}$$

where *V* is the average velocity, and f_d is the dominant acoustic frequency. Depending on the seismic source, the detected limits for vertical resolution are usually either 1/8 or 1/16 of the dominant wavelength, the smaller will be undetectable due to attenuation. The horizontal resolution separates the horizontal features by distinguishing them from the seismic section. The minimum separation d_F is defined as the width of the first Fresnel zone:

$$d_F = \sqrt{\frac{2zV}{f_d}} \tag{2.9}$$

where z is the depth, and V is the formation velocity. The first Fresnel zone is the area of a planar reflector from which the reflected energy in the 1/4 wavelength of the spherical wavefront that constructively interferes (Salisbury and Snyder 2007).

The resolution is related to the polarity of the wave phase. The seismic data is always acquired with offset separation between the source and receiver, meaning that part of the P-wave energy will be converted into a reflected and transmitted shear wave. Based on Simm and Bacon (2014), the amplitudes depend on the contrast in the Poisson's relation across the interface and the acoustic impedance change. If the polarity is positive, it means an increase of acoustic impedance between the contact materials, and vice versa, when the polarity is negative, the acoustic impedance is decreased between contact materials (Simma and Bacon 2014). When the thickness of the material gets too thin, it affects the amplitude polarity, which is a result of interference between the layers with opposite polarities, which partly cancel one another (Simma and Bacon 2014). Vice versa, when the layer gets thicker, the amplitude gets larger.

2.3. Seismic surveys in northern Finland

2.3.1. XSoDEx and other seismic surveys in northern Finland

Northern Finland has hosted numerous seismic refraction and reflection surveys, including the POLAR, the Finnish Reflection Experiment (FIRE), the Polar Earth Observing Network (POLENET/LAPNET), the High-Resolution Reflection Seismic for Ore (HIRE) seismic surveys, and the recent Sodankylä Deep Reflection Experiment (xSoDEx) (Figure 6) (Kukkonen et al. 2006, Patison et al. 2006, Kozlovskaya et al. 2016, Kukkonen et al. 2009, Heinonen et al. 2018). The POLAR project (1985) was a seismic refraction survey, which runs along a transect in the Archean and Early Proterozoic bedrock in a total length of 440 km (Luosto et al. 1989). Based on Luosto et al. (1989), the purpose of the study was to map the crustal structure and to understand the

development of the European lithosphere. The FIRE (2001 – 2005) project was a seismic reflection survey, the purpose of the study was to study the bedrock structure and evolution in the central and northern part of the Fennoscandian Shield (Kukkonen et al. 2006). The FIRE lines 4, 4A, and 4B were collected in the north of Finland and have a total length of 636 km (Kukkonen et al. 2006). The POLENET/LAPNET (2007 -2009) sub-project collected by Kozlovskaya et al. (2016) was a passive seismic array research experiment for the POLENET project, which studied the lithosphere-asthenosphere transition in the suture zone, between Arctic Proterozoic Svecofennian and Archean domains. The HIRE Exploration (2007 – 2010) reflection survey in Kittilä was a co-operation with Agnico-Eagle Ltd Finland (Kukkonen et al. 2009). The Kukkonen et al. (2009) study explored the geological structures of the Suurikuusikko gold mining area in the Central Lapland Greenstone Belt in Kittilä.

The xSoDEx project (2017) is the most recent reflection and refraction survey collected in northern Finland. The project was collected to improve the understanding of the tectonic evolution and structure. The FIRE project focused on the tectonic evolution of the area, by discovering that there is a north-dipping structure and boundary between the southern and central belts, even though the belt does not extend to the crust-mantle boundary or indicate Paleoproterozoic subduction zones (Patison et al. 2006). The Suurikuusikko HIRE survey implied that the reflections represent structures that form antiform folds and that the gold deposits are hosted by the Kiistala structure's quartz-carbonate veins (Kukkonen et al. 2009). Based on the Petäjäselkä HIRE project, the area hosts three Petäjäselkä thrust zones, which are connected to the Petäjäselkä and Kiistala thrust zones thought the Ruoppapalo shear zone (Niiranen 2015). The xSoDEx survey aim was to study the bedrock structures in the Sodankylä area to reveal the structural and lithological framework (Buske et al. 2019). The xSoDEx study connects the HIRE survey lines from Kittilä to Kevitsa, which helps to understand more about the mineral deposit structures in the area.

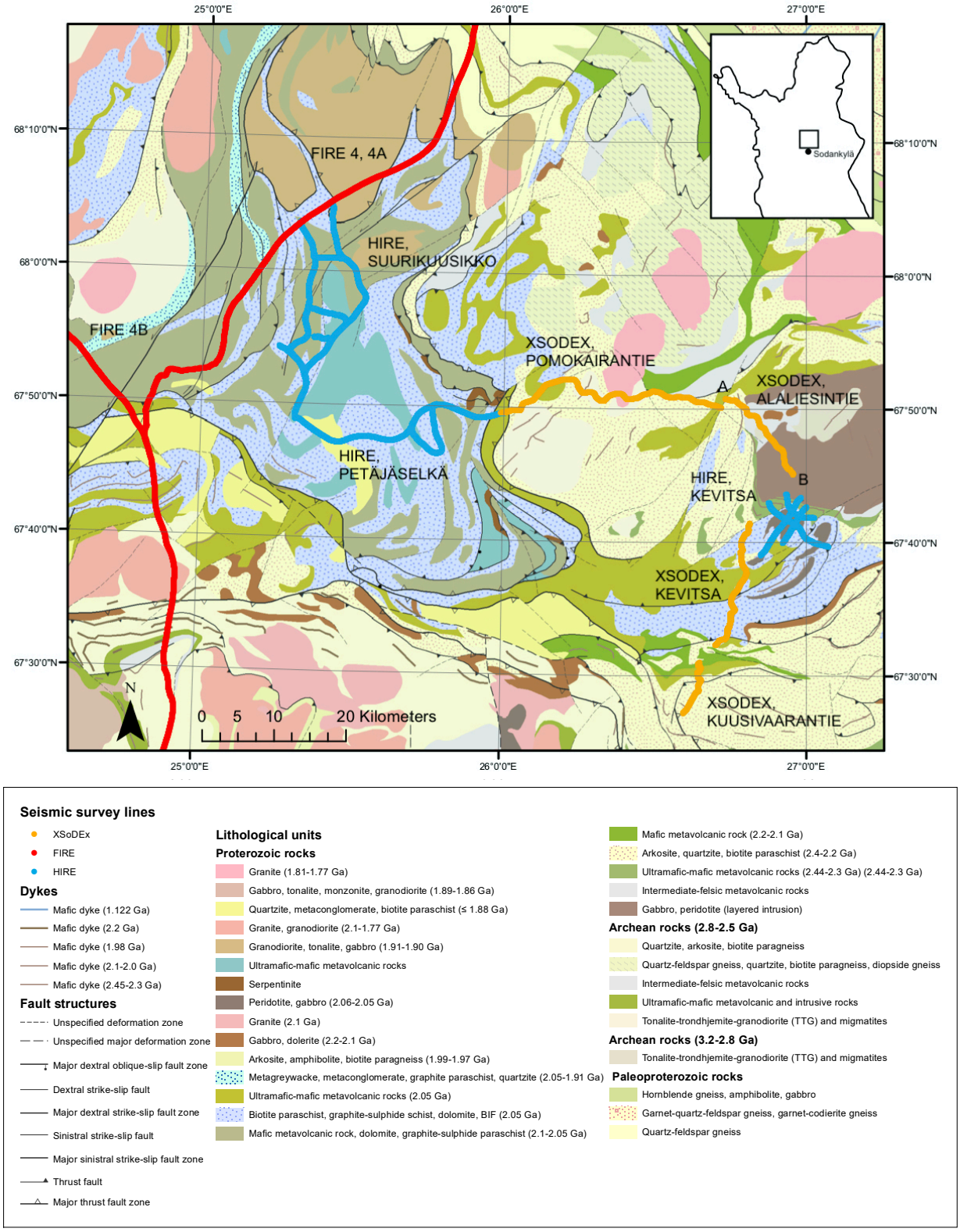

Figure 6. Presentations of the geology and the main seismic reflection surveys lines around the study area, in northern Finland. The recently collected xSoDEx reflection seismic survey lines are presented in orange.

The xSoDEx project provided seismic reflection data down to 8 km depth in the subsurface with a total length of 80 km of seismic reflection line. The survey consisted of four individual lines (Figure 6). The longest survey line is 35.5 km long and was gathered from Pomokairantie. The geology of the Pomokairantie area is characterized by contact between the Archean bedrock and the Paleoproterozoic rocks from Sodankylä and Savukoski groups. The Sakatti profile line is 22.5 km long and is located between the Kevitsa mine and the Sakatti exploration target. The geology of the area is characterized mostly by the Paleoproterozoic Savukoski group rocks as well as mafic intrusive rocks (Kevitsa intrusion) and other mafic sills. The Kuusivaarantie profile is located north from Sodankylä, and it is the shortest of the four profile lines, almost 9 km long. The geology of the area is characterized by the Paleoproterozoic Sodankylä and Savukoski group rocks. The last one of the four survey lines is the Alaliesintie survey (Figure 7), which is utilized in this study. The line is 15.5 km long, and it transects the Koitelainen intrusion, the Archean basement, and the Paleoproterozoic Kuusamo group and Salla group of rocks.

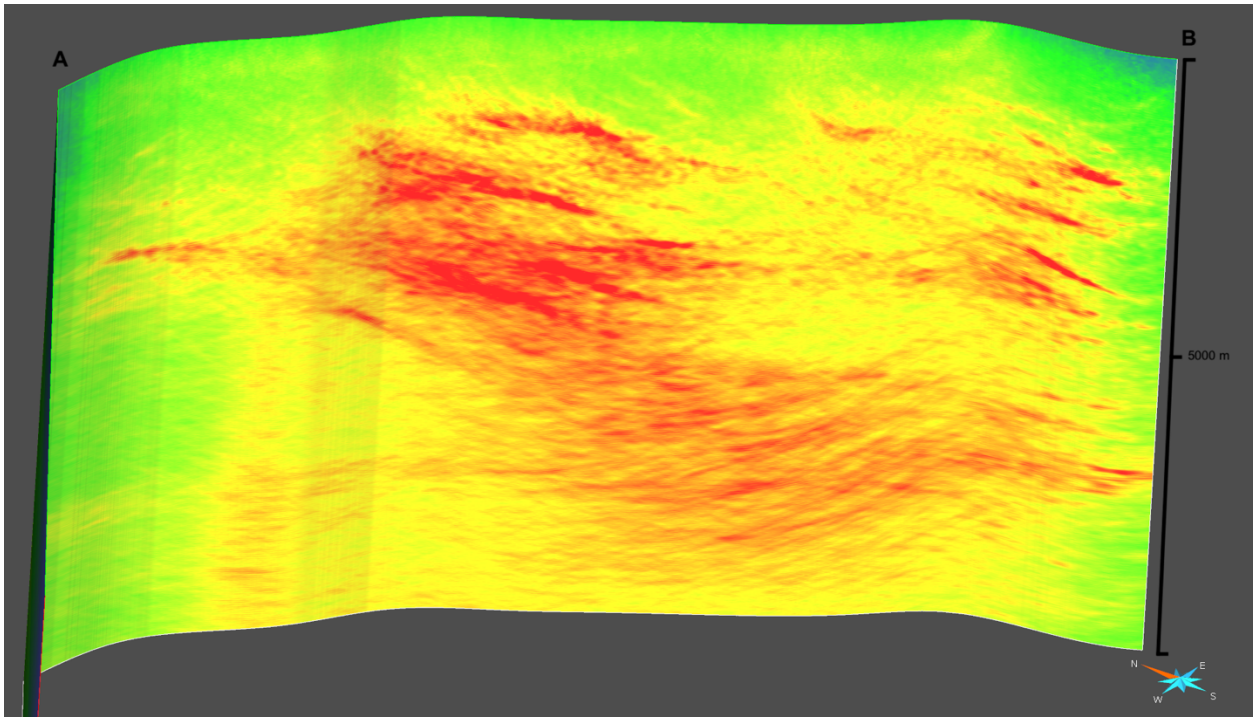

Figure 7. XSoDEx seismic reflection profile from Alaliesintie. The letters A and B are present the correct orientation of the seismic reflection section in the geological map in Figure 6.

2.3.2. Alaliesintie xSoDEx data acquisition

The xSoDEx data acquisition was carried out in co-operation with GTK, Oulu University, and Freiberg University of Mining and Technology. The description of the data acquisition and data processing is based on the xSoDEx report by Buske et al. (2019). Due to the landscape and the road accessibility, the xSoDEx survey was collected along gravel roads located closest to the geological area of interest. Figure 8 illustrates the xSoDEx seismic reflection survey set up. The total length of the receiver spread varied from 1800 m to 2400 m. The measurement used 8 or 14 Geometrics-Geode recording units. The Geometric-Geode recorder is a software interface to Geode as a network device, which can be viewed in a computer while recording (Geometrics Inc. visited 04.02.2020). One Geode has 24 channels connected to geophones deployed at 10 m intervals. The Geodes were connected by cables to vertical component 4.5 to 50 Hz geophones. The Thomas VIB3246, a 32 ton of vibroseis truck, created the active source. Shots were 40 m or 20 m apart, and the number of total receiver locations was 1559. The source sweep was 16 s duration, with the frequencies from 10 to 170 Hz. The listening time was 4 s, and the shots were stacked per shot location to improve the signal-noise ratio. The specifications of the Alaliesintie data acquisition are presented in Table 3.

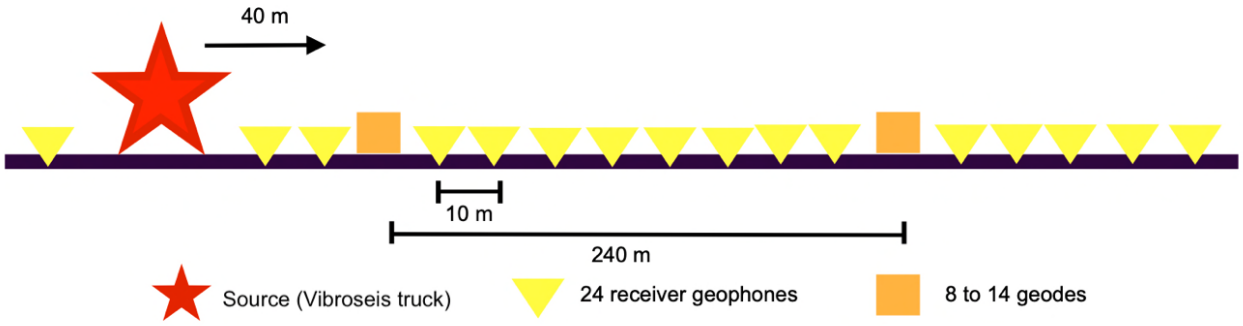

Figure 8. Presentation of the xSoDEx seismic reflection survey set up, where the source was produced in every 40 m. The reflections were collected with 24 geophones, which were connected to 8 or 14 geodes, depend on the survey line.

Table 3. The specifications of the data acquisition in Alaliesintie (Buske et al. 2019).

Total number of Geodes	8 – 14 (due to a thunderstorm, the number of Geodes was increased from 8 to 14 by the end of the survey)
Total number of Geophone	24
Geophone spacing	10 m
Total number of receiver locations	1559 (a distance of 15.59 km)
Source point intervals	40 m or 20 m
Number of sweeps per source point	3 – 4
Frequency	10 to 170 Hz
Total recording time	25 s (sweep 16 s)
Manual triggering	2 ms sampling interval

The main point in data processing is to strengthen the reflections from real geological structures and to eliminate interference signals. In crystalline bedrock, the optimal processing method is challenging to find due to the complex geology, weak signal to noise ratio, topographical variation, and steeply folded structures. The xSoDEx seismic data used in this study were processed at the Freiberg University of Mining and Technology, Germany. The pre-processing data methods are summarized in Figure 9, based on Buske et al. (2019).

First, in the pre-processing, the Jena cable recordings were reversed due to reverse geophone order, and then the data was converted into the Seismic Unix format. After this, the geometry was set up, including filling the trace headers with information from the field book, followed by the t0-time-shift, where the zero times were manually adjusted to absolute start time. This was done by picking the 0-offset trace within each shot. After this, the data format was converted into the file format of the Society of Exploration Geophysicists (SEG-Y) and correlated using a reference sweep with a total recording time of 4 s after correlation. This gives the P-wave velocity average of 5 to 6 skm^{-1} within subsurface and allows to image structures down to 10 to 12 km depth. In the next step, the data was processed with spike-muting by removing the spike-like signals by surgical muting. After this, the Vibroseis correlation takes place, which correlates the record with a reference sweep generated within the processing system. Followed the quality control, which is the visual inspection of correlated data and frequency spectra, vertical stacking occurs, where all the shot gathers are summed within the same Vibroseis source location.

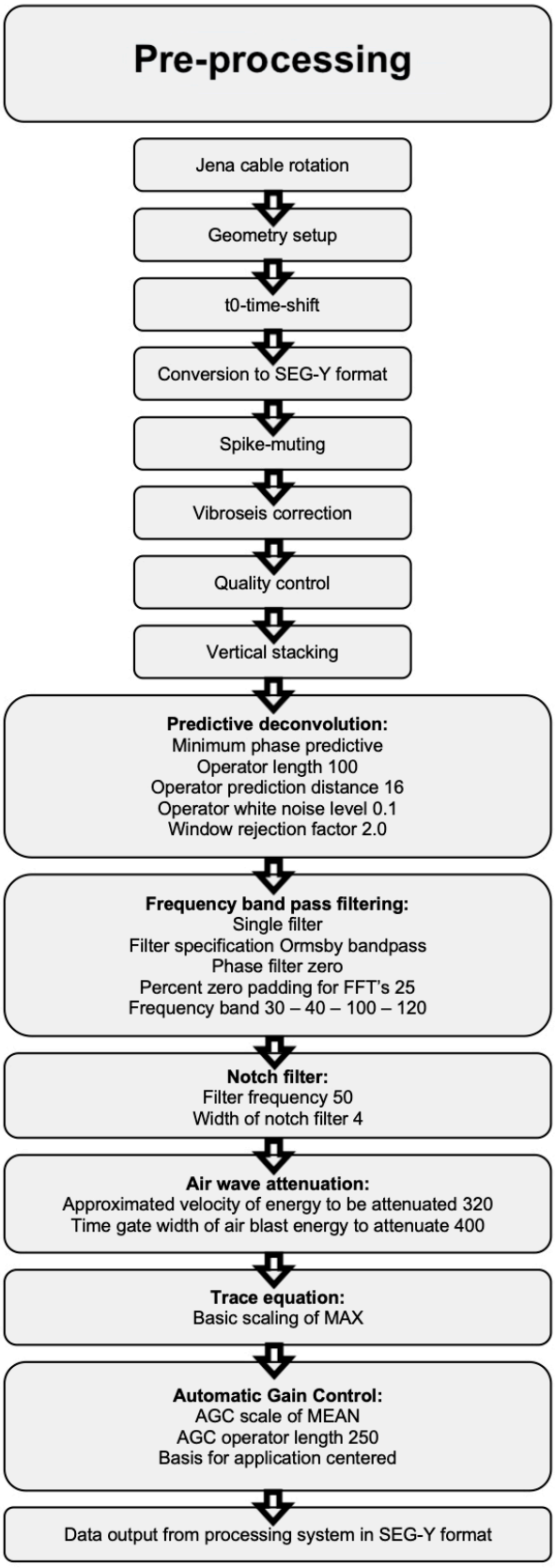

Figure 9. Alaliesintie reflection seismic data pre-processing flow based on Buske et al. (2019) report.

Then the predictive deconvolution is done. The deconvolution aims to improve the vertical resolution (Sheriff and Geldart 1982). In the xSoDEx Alaliesintie data processing, the predictive deconvolution type was minimum phase predictions, where the deconvolution operator length was 100 m, and the operator prediction distance was 16 m. The next step, the surface wave attenuation is filtered with a frequency bandpass of 30 – 40 – 100 – 120 Hz, this attenuates the effects of the surface waves. The airwave attenuation time gate width of air blast energy was fixed to be 400 ms^{-1}, with an approximate velocity of the energy of 320 ms^{-1}. The trace equalization was set up to be maximum, and the automatic gain control (AGC) type was centered and set to mean, with operator length of 250 m. Finally, the first arrival energy was eliminated by the top mute processing tool, and the data was output from the processing system in SEG-Y format. Finally, the Fresnel Volume Migration (FVM) of the pre-stack depth imaging approach was applied to the pre-processed shot gathers.

The FVM is a derivation of the emergent angle for the recorded wavefield (Hlousek and Buske 2016). The emergent angle is used as the initial condition of the ray-tracing-algorithm within FVM, which limits the migration operator to the physically relevant part of a reflector (Hlousek and Buske 2016). Based on Hlousek and Buske (2016), typically, the crystalline environment is characterized by a low signal-to-noise ratio and shows small-scale heterogeneities; therefore, the pre-stack depth migration is applied. The migration repositions the subsurface structures by replacing the reflectors by distributed sources with a magnitude proportional to the reflectivity (Sheriff and Geldart 1982). Based on Hlousek and Buske's (2016) report, the FVM results provide more detailed images of the structures.

2.4. Other geophysical measurements

2.4.1. Petrophysics

A total of 73 samples from 25 different rock types were collected by rock hammer on surface outcrops along the xSoDEx survey lines (Leväniemi et al. 2018). This study used a total of 26 samples, which were collected from Alaliesintie, and a small part of the Pomokairantie profile (Figure 10).

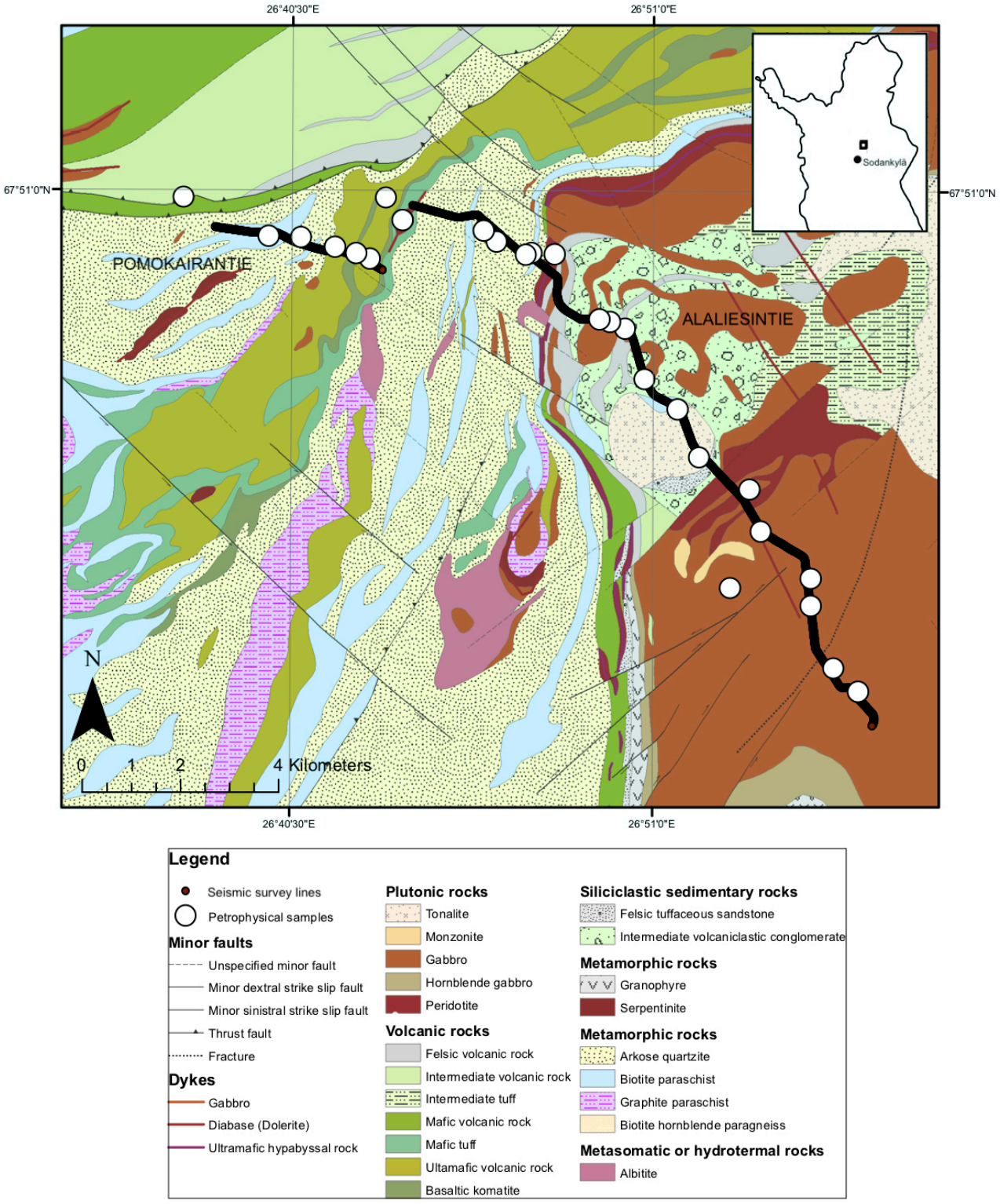

Figure 10. The petrophysical samples were taken around the Alaliesintie survey line and also around the east part of the Pomokairantie survey line.

Based on Leväniemi et al. (2018) study, all the sample measurements were carried out at the petrophysical laboratory of GTK. The measured properties included density, porosity, P-wave velocity, magnetic susceptibility, conductivity, resistivity, and intensity and direction of remanent magnetization. The used parameters for the samples in this study were densities and P-wave velocities. The rock density was measured with an Archimedean method, which measures the rock's weight difference in the air and water. P-wave velocity was determined from the wet rock samples, by use of the sonar element, where the transmitted time is measured with a pulse counter (Leväniemi et al. 2018).

2.4.2. Gravity measurements

The gravity method is based on measuring the variations of the gravity field (acceleration of gravity), which are caused by the density differences in the subsurface (Hinze et al. 2013). The gravity field is caused by the Earth's gravitational pull, which varies based on the elevation and density differences. The measurements are done with a gravimeter, which presents the gravity difference in 0.001 – 0.01 mgal accuracy (Peltoniemi 1988). Before the gravity data can be used in interpretation, it needs to be corrected. The corrections are described more in detail in Peltoniemi (1988). Based on Peltoniemi (1988), the gravity results cannot present the shape, mass, or size of the structure. The interpretation of gravity measurement is ambiguous, and therefore, the gravity survey is usually combined with another geophysical measurement.

The gravity data used in this study was acquired during the seismic xSoDEx survey. The measurements were collected with the CG-5 gravity meter, at a 100 m station interval along with the seismic profiles (Suvi Heinonen personal communication 2019), and the collected data was presented as inversion voxel model.

2.4.3. Magnetic measurements

In the magnetic measurement, the data indicate Earth's magnetic field variations due to the magnetic mineralization in the bedrock in different locations. All the materials are magnetic, but the amount of magnetism is measured based on how the magnetic properties within the content

behave when they are induced to the magnetic field (Schön 2011, Airo and Kiuru 2012). The main difference is that some materials the atoms are not related to the magnetic moments, and others are. The mineral's magnetic behavior can be either diamagnetic, paramagnetic, ferromagnetic, ferrimagnetic, or antiferromagnetic. Diamagnetic and paramagnetic materials do not have magnetic properties, nor they oriented based on the magnetic field, but ferromagnetic, ferrimagnetic, and antiferromagnetic materials are adapted based on the magnetic field at a specific temperature (Airo and Kiuru 2012). Based on Airo and Kiuru (2012), rocks magnetism is based on the magnetic properties in minerals, which is presented as the volume of susceptibility. The susceptibility is the ratio of the magnetization per unit volume to the external magnetic field strength (Schön 2011). The susceptibility is effect by the grain size and the purity of the materials composition (Airo and Kiuru 2012). Magnetism is usually found in rocks containing magnetite, pyrrhotite, and hematite (Schön 2011).

The measurements used in this study were collected earlier by GTK, in purpose to obtain the national database of magnetic fields in Finland (Niiranen et al. 2014a). The magnetic anomalies are caused by lateral contrast in the magnetic polarization or magnetization (Langel and Hinze 1998). The magnetic data in this study was presented as the Magnetic Vector Inversion (MVI) voxel models. The MVI voxel allows the susceptibility to be used directly in interpretation with a vector direction (MacLeod and Ellis 2013). The voxel inversion models can, therefore, accurately determine the direction of the magnetization, even when there are multiple directions existing in the same model area (MacLeod and Ellis 2013, 2015).

3. DATA AND METHODS

3.1. Available data

The following data sets were used in the modeling procedure:

- Different versions of the XSoDEx's seismic profiles were utilized as SEG-Y files. The SEG-Y files were imported into the SKUA – GOCAD 17 program as 2D surveys and also as 3D voxels.
- Two XYZ files of the seismic shot and receiver locations, which were brought into the SKUA – GOCAD 17 as column-based point sets (.txt).
- The geological bedrock maps were prepared in ArcMap 10.6.1, use of GTK's 1:50 000 lithological map and topographical map. The maps were imported to the SKUA – GOCAD 17 program as JPEG images.
- The outcrop observations XYZ files were collected from ArcMap 10.6.1, use of GTK's lithological map information properties, and brought into the SKUA – GOCAD 17 program as column-based point set (.vs), with information on layering, foliations, axial planes, joints, contacts, and faults of the area. The information included coordinates, dates of observations, the direction of dip, and strike (Attachment 1).
- The gravity data Koitelainen 3D and Gravity 3D (made by Ilkka Lahti, Geological Survey of Finland), were imported into the SKUA – GOCAD 17 program as an SGrid file and as a voxel.
- The two Magnetic Vector Inversion voxels (MVI4 and MVI5) (made by Hanna Leväniemi, GTK), were imported into the SKUA – GOCAD 17 program as SGrid files.
- The petrophysical measurement XYZ point data file was imported into the SKUA – GOCAD 17 program as a column-based point set (.vs). The petrophysical measurement data included sample density, magnetic susceptibility, conductivity, intensity, and direction of remanent magnetization, porosity, P-wave velocity, and resistivity values (Attachment 2).

3.2. Methods of building the geological 3D model

The geological 3D model was created in the SKUA – GOCAD 3D modeling software. The 3D geological model is based on the Alaliesintie xSoDEx reflection seismic reflections, geological bedrock map, and surface outcrop observations. The geological bedrock map of north Finland and the field observations data of the outcrops in the area have been collected earlier by GTK (collected

form the GTK digital databased on the 3rd of July 2019). Attachment 1. shows the collected field observation data such as faults, lineation, layering, etc.

The aim behind the geological 3D model was to build it based on the geological observations, the Alaliesintie seismic reflections, and the geological history of the CLGB. The geological lithostratigraphic groups in CLGB include the Archean bedrock, Koitelainen, and Puijärvi intrusions, and four Paleoproterozoic rock groups (Salla group, Kuusamo group, Sodankylä group, and Savukoski group rocks). The first part of the task was to create surfaces to represent these geological interfaces. The geological 3D model followed the typical structural model where the younger rock groups are displayed on top of the older rock groups. This applies unless the structure has not been intruded by an intrusion or has not been part of massive tectonic events. In the geological map, the Archean bedrock was detected as an outcrop, which means that the part of massive tectonic events, like it is detected in the geological history of the area (Köykkä et al. 2019).

The task started by outlining the Archean bedrock, which is detected to be weakly reflective. After this, the Puijärvi and Koitelainen intrusion surfaces were outlined. The Puijärvi intrusion surface was defined based on the geological map. The Koitelainen intrusion surfaces were defined in the model based on outcrop observations and drill hole studies by Mutanen (1997), which include lithologies of the intrusion based on diamond core drilling measurements. The dike was defined based on the geological map and similar reflections pattern in the FVM seismic profile. The fault was defined based on the field observation, which indicated it to slope towards the north-west. The Paleoproterozoic group's lithological contact surfaces were defined by reflections in the FVM seismic section and with the use of the geological maps lithological structure, and field observation data. The Sakatti and Pomokairantie seismic sections were also used to aid in shaping the surfaces at the edges of the study area.

Figure 11 presents the layering structure with the penny-shaped discs, which show that the younger formations are in the middle of the section, whereas the older formations are at the edges, which can be interpreted as a folded syncline structure. The folding repeats, and therefore several anticline formations are present in the structure. The axial plane observations indicate the same folding structure, where the Paleoproterozoic rocks are folded with the strongest shortening in the

northwest-southeast direction against the Archean basement (Figure 12). The layering dip directions indicate the syncline formation in Paleoproterozoic rocks (Figure 13). The structures feature the same tectonic events, as presented in Table 2.

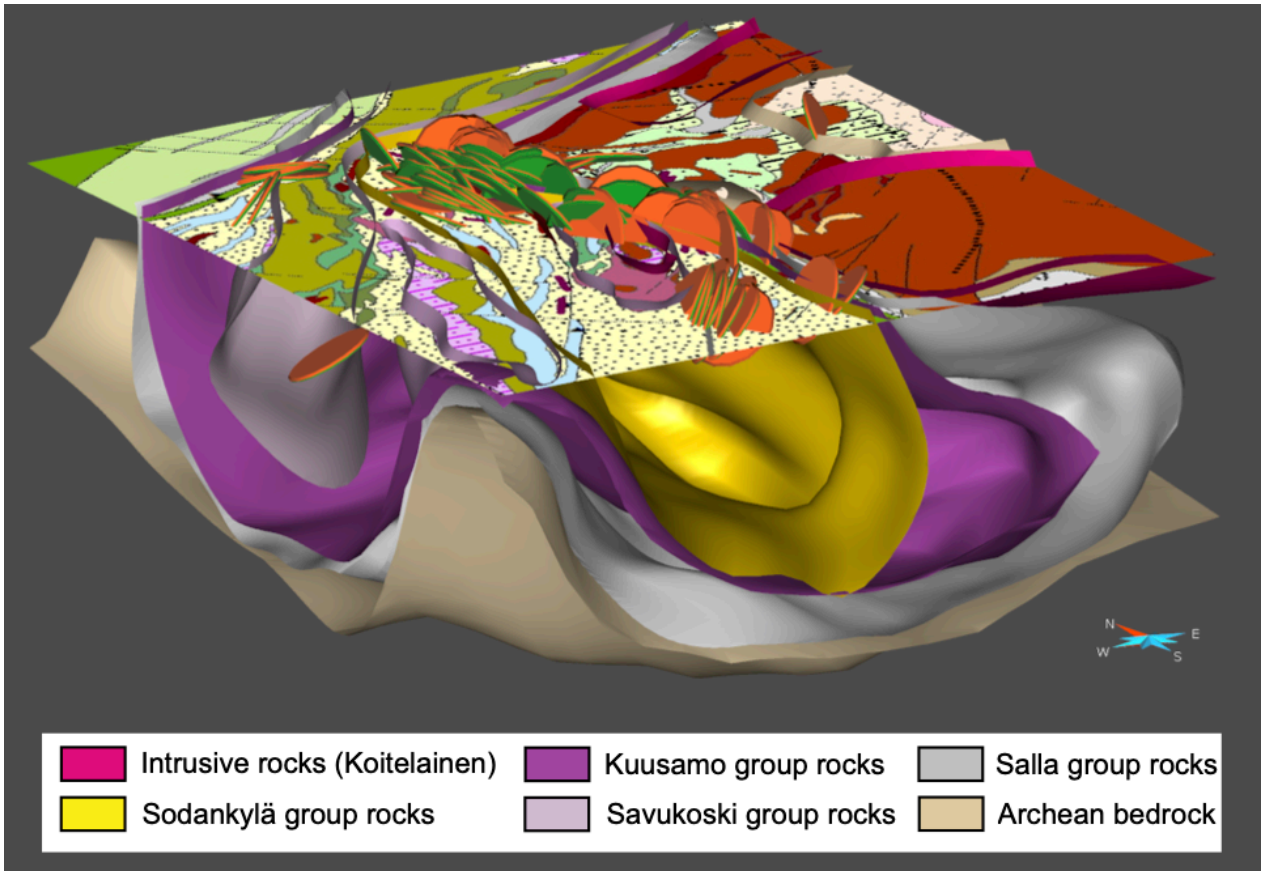

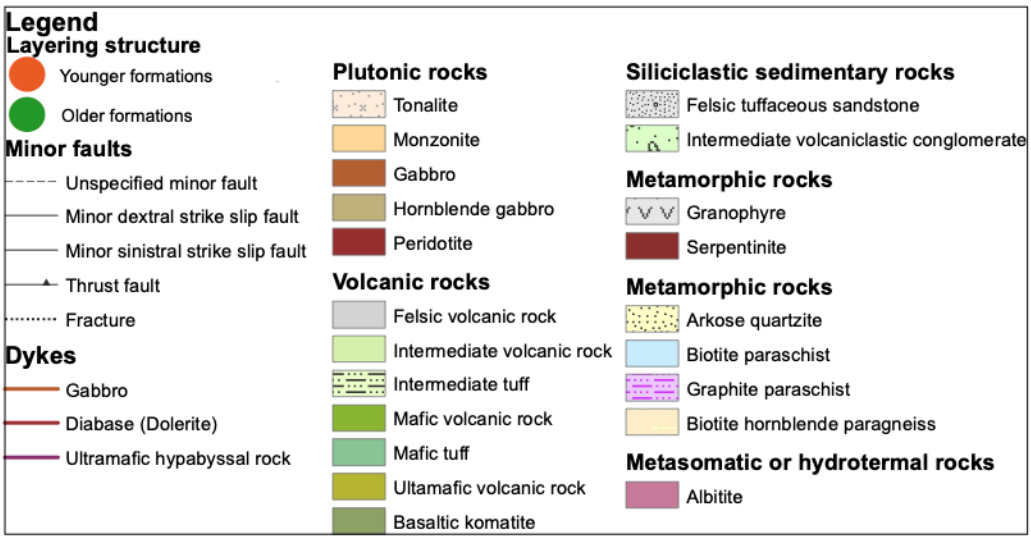

Figure 11. Presentation of how the geological map observations are combined with the geological 3D model. The symbols indicate the layering structure, where the red side of the penny-shaped disc presents the younger formations, and the green side of the disc represents the older formations, respectively.

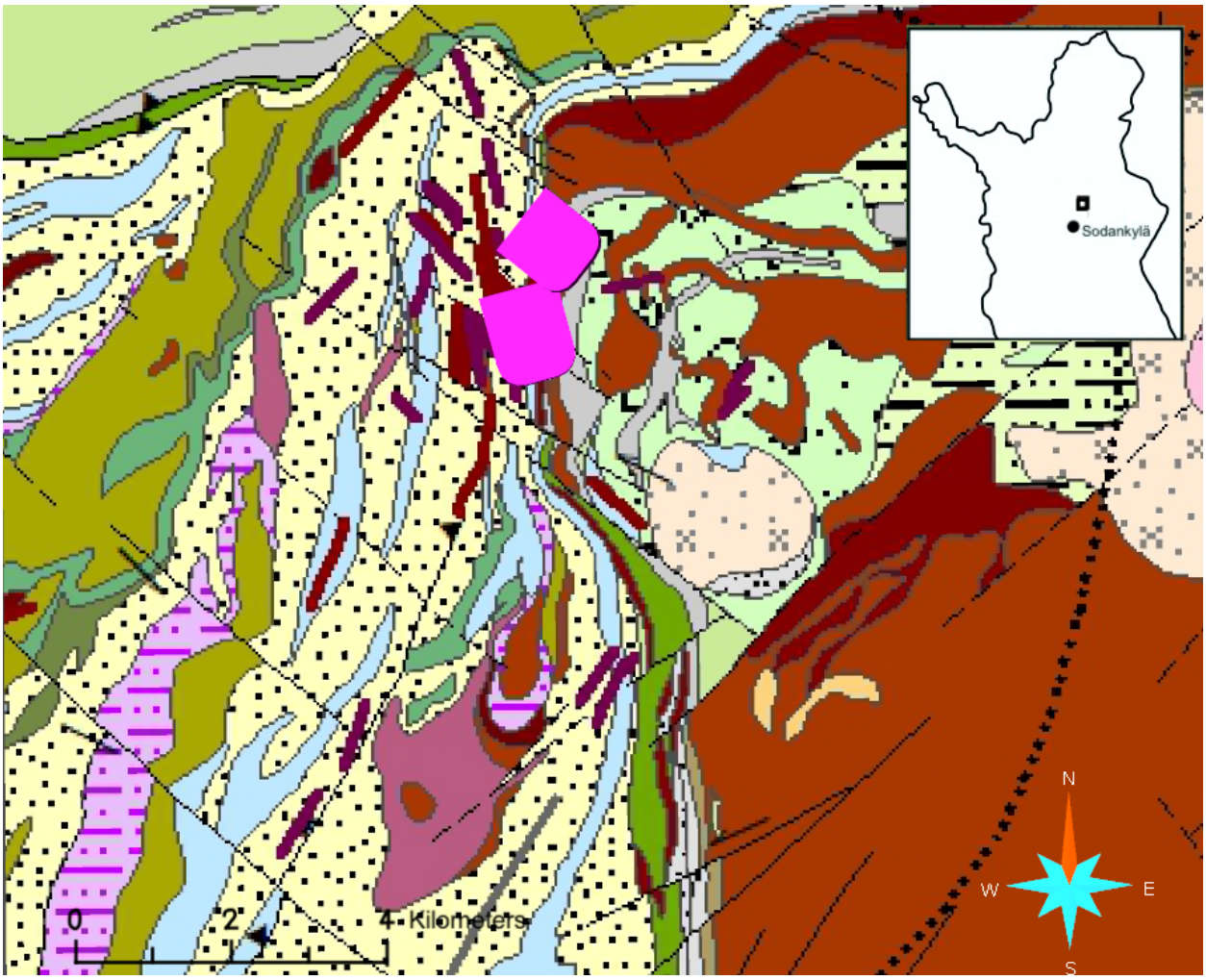

Legend

Axial plane

Minor faults
- Unspecified minor fault
- Minor dextral strike slip fault
- Minor sinistral strike slip fault
- Thrust fault
- Fracture

Dykes
- Gabbro
- Diabase (Dolerite)
- Ultramafic hypabyssal rock

Plutonic rocks
- Tonalite
- Monzonite
- Gabbro
- Hornblende gabbro
- Peridotite

Volcanic rocks
- Felsic volcanic rock
- Intermediate volcanic rock
- Intermediate tuff
- Mafic volcanic rock
- Mafic tuff
- Ultamafic volcanic rock
- Basaltic komatite

Siliciclastic sedimentary rocks
- Felsic tuffaceous sandstone
- Intermediate volcaniclastic conglomerate

Metamorphic rocks
- Granophyre
- Serpentinite

Metamorphic rocks
- Arkose quartzite
- Biotite paraschist
- Graphite paraschist
- Biotite hornblende paragneiss

Metasomatic or hydrotermal rocks
- Albitite

Figure 12. The symbols present the axial plane observation in the study area, based on GTK field observation in 1980 – 2018 (attachment 1). The axial plane observations indicate anticline structure in the Sodankylä group and Savukoski group rocks. The angle of the fold is almost horizontal, meaning that the structure is folded towards the east and the southeast.

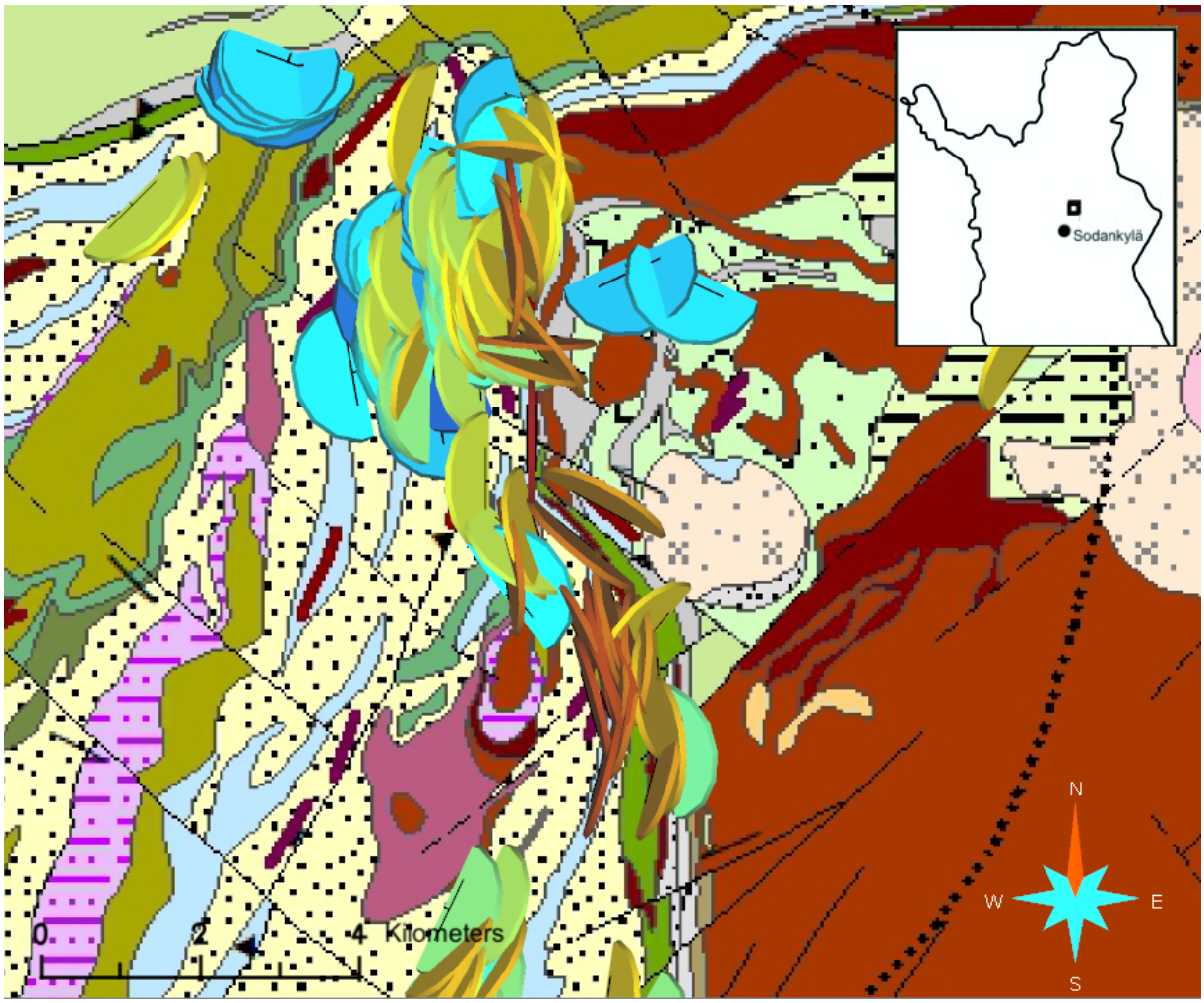

Legend

Angle of dip

0
1 - 15
16 - 30
31 - 45
46 - 60
61 - 75
76 - 89
90

Minor faults

- Unspecified minor fault
- Minor dextral strike slip fault
- Minor sinistral strike slip fault
- Thrust fault
- Fracture

Dykes

- Gabbro
- Diabase (Dolerite)
- Ultramafic hypabyssal rock

Plutonic rocks

- Tonalite
- Monzonite
- Gabbro
- Hornblende gabbro
- Peridotite

Volcanic rocks

- Felsic volcanic rock
- Intermediate volcanic rock
- Intermediate tuff
- Mafic volcanic rock
- Mafic tuff
- Ultamafic volcanic rock
- Basaltic komatite

Siliciclastic sedimentary rocks

- Felsic tuffaceous sandstone
- Intermediate volcaniclastic conglomerate

Metamorphic rocks

- Granophyre
- Serpentinite

Metamorphic rocks

- Arkose quartzite
- Biotite paraschist
- Graphite paraschist
- Biotite hornblende paragneiss

Metasomatic or hydrotermal rocks

- Albitite

Figure 13. The symbols present the layering angle of dip observation in the study area, based on GTK field observation in 1980 – 2018 (attachment 1). The layering structures show features that present syncline formation, where the Sodankylä group rocks top direction is next to the younger Savukoski group rocks. The colors indicate the dipping angle from 0° – 90°.

Some of the reflections were defined on the surface as lithological contrast, but several reflections could not be correlated with a lithological unit on the surface. Due to the data and applied processing (FVM), the seismic reflections are present in the section only at a depth deeper than 1 km This is caused by seismic data's weak signal due to the thickness and material of the overburden, as well as due to a lack of static corrections in the FVM seismic data processing. The bedrock observations were made prior to the xSoDEx project and for general mapping purposes. The difficulty of the bedrock survey in Finland is that only a small presentence of the Finnish bedrock is exposed. In the Alaliesintie, the bedrock is mostly underneath a lake and swamp or beneath a thick layer of soil, and therefore cannot be directly observed.

3.3. Use of other geophysical data

The second part of the project was to improve and analyze the compiled geological 3D model with the gravity and magnetic geophysical data. The gravity data reflects density differences in the subsurface, and the magnetic data reflects the variation of magnetic mineral content in the subsurface.

The gravity voxel present density distribution in 3D, allowing observations in multiple depths. The density variation shapes were produced based on the gravity voxel to demonstrate the voxel's 3D in the 2D image. The 3D gravity data was observed with the reflections, and also with the geological 3D model, to evaluate the continuity of the geological 3D model surfaces (Figure 14). The gravity data cannot directly be used to shape the lithological surfaces in the geological 3D model. The density distribution varies a lot in the middle of the Alaliesintie, which includes Archean basement rocks and Paleoproterozoic rock groups. The lithological surfaces were modified based on the lithological rock group's rock properties. The magnetic MVI voxels present magnetic mineralization in 3D, and the magnetization shapes were produced to present the MVI voxel's 3D in a 2D image. The mineralization was only able to be used to modify the shallowest surfaces because the MVI data was received between 190 m – 3 km (Figure 15).

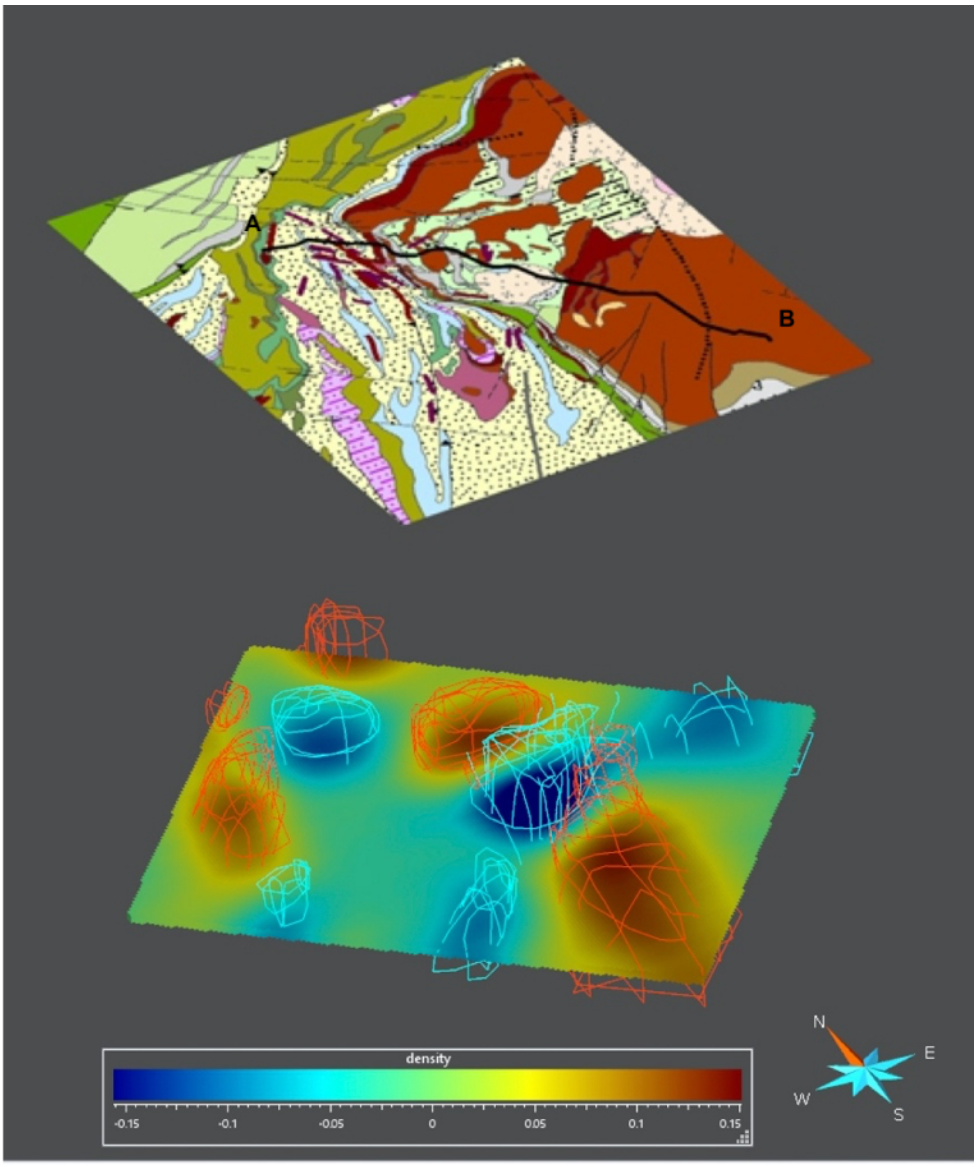

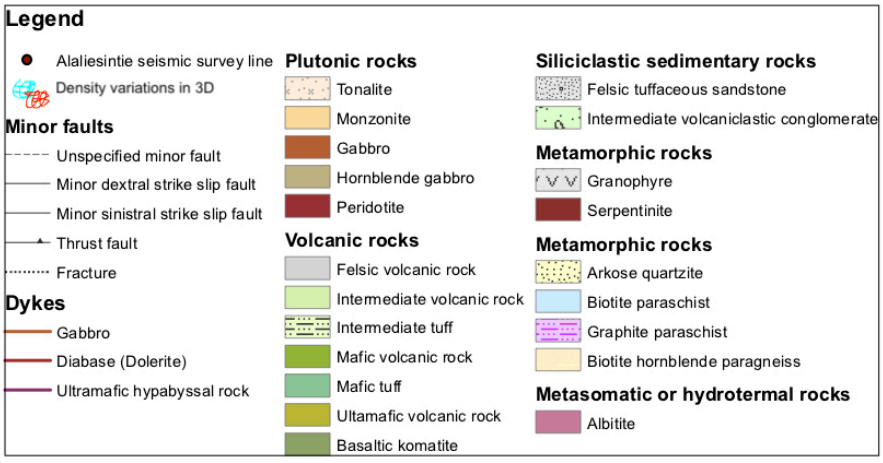

Figure 14. Density variations are presented in 3D with the gravity voxel over the study area. The black line illustrates the Alaliesintie survey line.

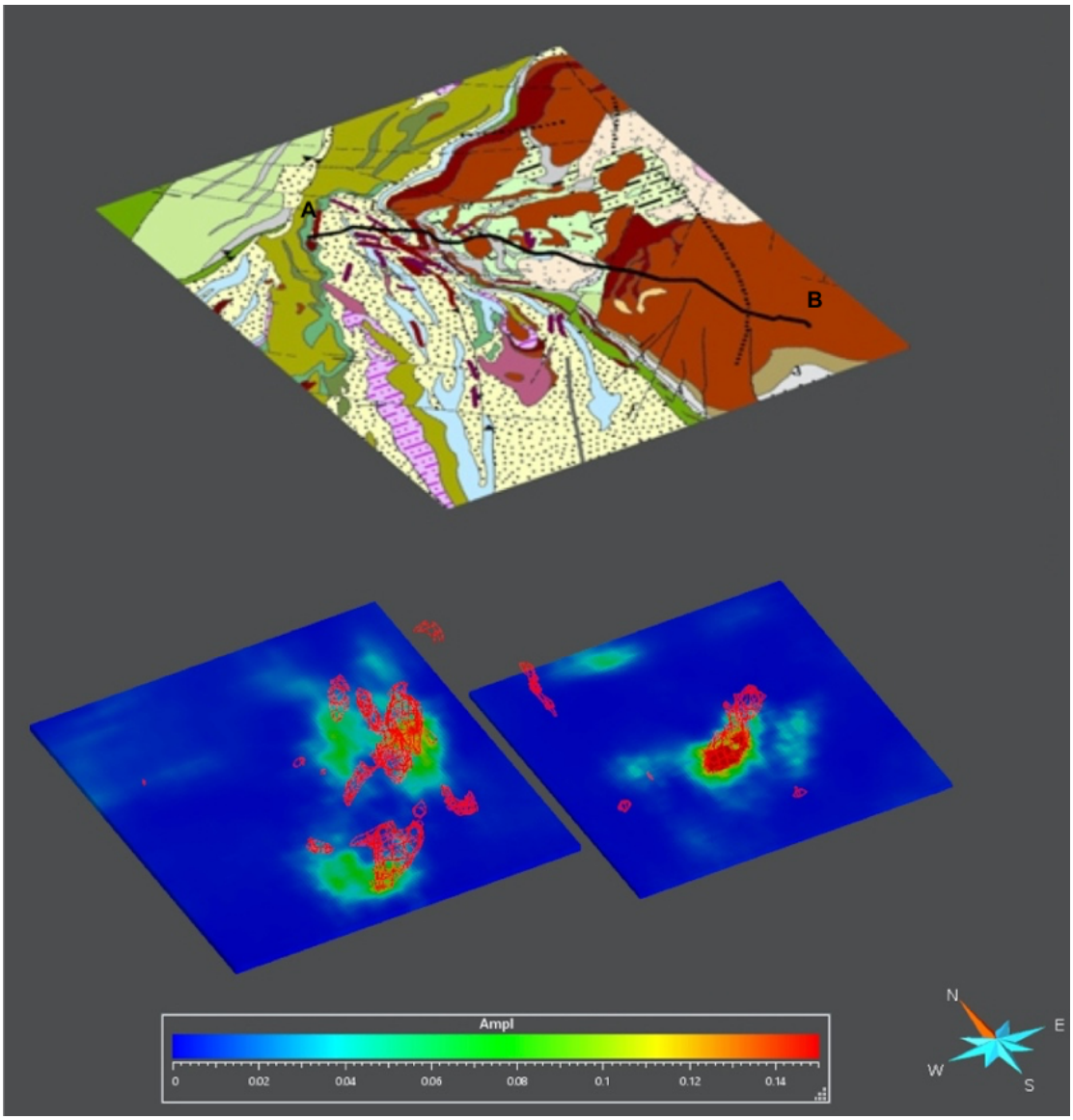

Legend

- Alaliesintie seismic survey line
- Magnetization in 3D

Minor faults

- Unspecified minor fault
- Minor dextral strike slip fault
- Minor sinistral strike slip fault
- Thrust fault
- Fracture

Dykes

- Gabbro
- Diabase (Dolerite)
- Ultramafic hypabyssal rock

Plutonic rocks

- Tonalite
- Monzonite
- Gabbro
- Hornblende gabbro
- Peridotite

Volcanic rocks

- Felsic volcanic rock
- Intermediate volcanic rock
- Intermediate tuff
- Mafic volcanic rock
- Mafic tuff
- Ultamafic volcanic rock
- Basaltic komatite

Siliciclastic sedimentary rocks

- Felsic tuffaceous sandstone
- Intermediate volcaniclastic conglomerate

Metamorphic rocks

- Granophyre
- Serpentinite

Metamorphic rocks

- Arkose quartzite
- Biotite paraschist
- Graphite paraschist
- Biotite hornblende paragneiss

Metasomatic or hydrothermal rocks

- Albitite

Figure 15. Magnetization in 3D with the MVI voxels over the study area. The black line illustrates the Alaliesintie survey line.

3.4. Methods in seismic forward modeling

The final part of the process was to produce a seismic forward model with the Mira feature in the SKUA-GOCAD program. The seismic forward model is a synthetic model, which presents synthetic seismic reflections off an object, in this case, the geological 3D model rock unit boundaries. The theory behind seismic forward modeling is a numerical solution of the wave equation, which is produced to reflect an object (Krebes 2004). The reflectivity at the interface between the lithological contact is described as the ratio between the reflected wave's amplitude and the incident wave's amplitude, where the geological model's depth is converted to the two-way transit time (Anderson and Cardimona 2002).

To be able to make the synthetic model, the geological 3D model's surfaces are supplemented with property parameters, namely the contrasts in density (DRO), and S- and P-wave velocities (DVS, DVP) based on the petrophysical data by Leväniemi et al. (2018). The seismic reflections depend on the reflection coefficients (eq. 2.6) at the lithological contacts of the 3D model. Like in real reflection seismic measurement, the synthetic seismic rays reflect from the geological models' surfaces based on the elastic properties. The synthetic seismic section allows a confident correlation with the observed reflections and the geological interfaces. It verifies that the seismic responses of interpreted conceptual to the geological 3D model's surfaces if they are consistent with the real seismic data. Afterward, the synthetic seismic section is compared with the FVM seismic section to present the similarities and possibilities for the reflection.

At first, the petrophysical data conducted by Leväniemi et al. (2018) was analyzed and cleared of the data entries unnecessary for the present study. The acoustic impedances were calculated based on the rock velocities and densities (eq. 2.6). Leväniemi et al. (2018) give only P-wave velocities for the rock types. Therefore, the S-wave velocities were calculated based on a Poisson's solid equation (eq. 2.4). The S-wave velocities confirm better results because the rock parameters affect the velocities between the rock types: the rock type and the orientation of the structures affect the wave motions. The results may differ in between bulk and shear modulus changes and therefore give different velocity values for the rock sample. Table 4 presents the measured densities, P-wave velocities, and calculated S-wave velocities for all the rock samples collected from the xSoDEx

survey sites. All the xSoDEx rock sample's average density and P-wave velocities are presented as an acoustic impedance graph in Figure 16. The ratio between the acoustic impedance points indicates the reflection coefficient, which presents the strength of the reflection.

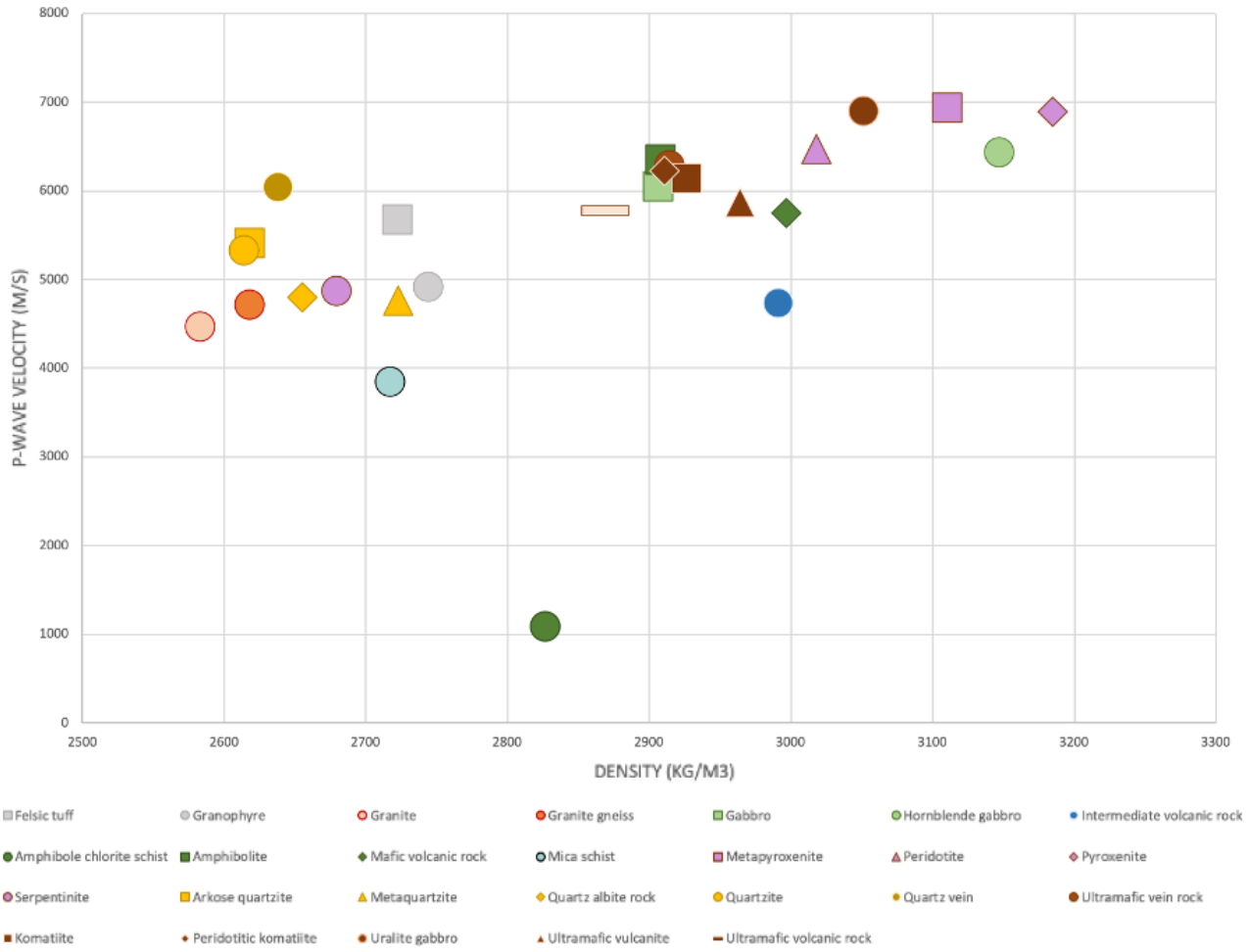

Figure 16. The density and P-wave velocity data of rock type averages in the XSoDEx project, based on Leväniemi et al. (2018) laboratory results.

Table 4. Density, P-wave, and S-wave velocities for all the rock units in the xSoDEx project. The densities and P-wave velocities are obtained from the laboratory results (Leväniemi et al. 2018) (Figure 9), and S-wave velocities are calculated based on Poisson's solid equation.

Rock types	P-wave velocity [m s^{-1}]			S-wave velocity [m s^{-1}]			Density [kg m^{-3}]	
	AVG.	MED.	Alaliesintie AVG.	AVG.	MED.	Alaliesintie AVG.	AVG.	Alaliesintie AVG.
Amphibole chlorite schist	1085	1085		767	626		2827	2843
Amphibolite	6355	6343	6355	3669	3662	3669	2908	2908
Arkose quartzite	5410	5432	5610	3123	3136	3239	2618	2653
Felsic tuff	5675	5675	5490	3276	3276	3882	2722	2681
Gabbro	6054	5975	6186	3495	3450	3571	2906	2926
Granite	4466	4435		2579	2561		2583	
Granite gneiss	4713	5133	5166	2721	2964	2983	2618	2650
Granophyre	4919	4591		2840	2651		2744	
Hornblende gabbro	6431	6411	6908	3713	3701	3988	3147	3294
Intermediate volcanic rock	4735	4735	4735	3348	3348	3348	2991	2991
Komatiite	6146	6437	5349	3548	3716	3782	2926	2813
Mafic volcanic rock	5747	5713	5713	3318	3392	3298	2997	2901
Metapyroxenite	6935	6935		4004	4004		3110	
Metaquartzite	4759	4759		2747	2747		2723	
Mica schist	3846	5338	3846	2461	3082	2220	2717	2717
Peridotite	6468	6468		4574	3734		3018	
Peridotitic komatiite	6224	6211		3593	3586		2911	
Pyroxenite	6894	6894	6894	4875	3980	4875	3185	3185
Quartz albite rock	4795	4795		3391	3391		2655	
Quartz vein	6040	6040		3487	3487		2638	
Quartzite	5332	5349		3079	3088		2614	
Serpentinite	4876	4876	4876	3448	2815	3448	2679	2679
Ultramafic vein rock	6285	6278		3629	3625		2914	
Ultramafic volcanic rock	5780	5780		3337	3337		2869	
Ultramafic vulcanite	5869	5765	5782	3388	3328	3338	2964	2939
Uralite gabbro	6900	6900	6900	3984	3984	3984	3051	3051

The next step in the seismic forward model is to identify the geological 3D model's surfaces with the correct rock types. The geological 3D model's surface presents a boundary between two rock types. The dike was detected to be uralite gabbro rock, based on its location in a geological map. The surface in the geological 3D model shows the contact between uralite gabbro and Archean granite gneiss. Other surfaces in the geological 3D model are presenting contacts between Archean basement granite gneiss and Salla group felsic tuffs, the Koitelainen intrusions gabbro and the Salla group felsic tuff, the Salla group felsic tuff and the Kuusamo group ultramafic rock, the Kuusamo group ultramafic rock and the Sodankylä group arkose quartzite, and the surface in between two Sodankylä group rocks. The Sodankylä group surface presents a contact between arkose quartz and mica schist, due to the appearance of strong reflections in the FVM seismic section and based on the acoustic impedance graph (Figure 16).

After defining the contact rock types, the contrasts in density and S-and P-wave velocities (DRO, DVS, DVP) were calculated for the surfaces. All the parameters needed for the seismic forward modeling are presented in Table 5. The DRO present the density difference between the two rock types at the boundary, and where the DVS and DVP present the velocity difference between the two rock types at the boundary. The DRO, DVS, DVP property values were calculated based on the equations:

$$DRO = 1 - \frac{\rho_1}{\rho_2} \tag{3.1}$$

$$DVS = 1 - \frac{v_{1,S}}{v_{2,S}} \tag{3.2}$$

$$DVP = 1 - \frac{v_{1,P}}{v_{2,P}} \tag{3.3}$$

where ρ_1 is the density for the upper lithology, ρ_2 is the density for the lower lithological unit, the $v_{1,SP}$ is the velocity for the upper lithology, and $v_{2,SP}$ is the velocity for the lower lithological unit (Tuomi 2016).

Table 5. Table of calculated DRO, DVP, and DVS values and the other parameters used in the seismic forward modeling. (DRO = density property value for the rock type interface, DVP = P-wave velocity property value for the rock type interface, DVS = S-wave velocity property value for the rock type interface).

Contact	Rock types	P-wave velocity [m s^{-1}]	DVP	S-wave velocity [m s^{-1}]	DVS	Density [kg m^{-3}]	DRO
Archean basement rock and dike	Granite gneiss	5166	0.251	2983	0.251	2650	0.131
	Uralite gabbro	6900		3984		3051	
Archean basement rock and Salla group	Granite gneiss	5166	0.059	2983	0.232	2650	0.012
	Felsic tuff	5490		3882		2681	
Koitelainen intrusion and Salla group	Gabbro	6186	-0.127	3571	0.080	2926	-0.091
	Felsic tuff	5490		3882		2681	
Salla group rock and Kuusamo group	Felsic tuff	5490		3882		2681	
	Ultramafic volcanic rock	5782	0.051	3338	-0.163	2939	0.088
Kuusamo group rock and Sodankylä group	Ultramafic volcanic rock	5782	-0.031	3338	-0.031	2939	-0.108
	Arkose quartzite	5610		3239		2653	
Sodankylä group rocks	Mica schist	2220	0.604	2717	0.161	3846	-0.450
	Arkose quartzite	5610		3239		2653	

P-wave background velocity [m s^{-1}]	6500
S-wave background velocity [m s^{-1}]	4600
Density [kg m^{-3}]	2700
Frequency [Hz]	10 – 170
Depth [m]	8000
A sampling interval of the receiver [m s^{-1}]	1

After this, the survey geometry was arranged, based on the coordinate system. The geometry was set to have the same source and receiver location as in the xSoDEx survey. The DRO, DVP, and DVS values were computed into the contact surfaces as property value, and finally, the synthetic seismic forward model was produced. The forward model was performed to individual contact surfaces, but as well to all the surfaces in the geological 3D model with frequencies of 10, 50, 90, 120, 150, and 170 Hz. This was done to evaluate the best suitable signal ratio in the subsurface for the geological 3D model contacts, as it is resaved in the real FVM seismic section.

4. OBSERVATIONS AND RESULTS

4.1. Geological 3D model

The geological 3D model (Figure 17) was made based on the geological ages of the lithological units and the observation results. The younger rock formations are displayed on top of the older structures. If this structural order is not defined, the geological display has gone through tectonic events, like in the study area case thought folding. In the geological history, the Archean basin has first gone through an extension which has created extensional folding to the basement, which was followed by Paleoproterozoic sedimentation and volcanism. The Palaeoproterozoic rocks confronted compression and subduction events, which are now distinguished from the surface observations. In the geological 3D model, the Archean basin and the Palaeoproterozoic metasediments and volcanic rocks show now folding and overthrusting features, creating anticline and syncline formations into the Paleoproterozoic rock groups. Figure 18 presents a cross-section of the geological 3D model's surfaces and their connections to the Alaliesintie FVM reflection seismic profile.

In Figure 18, the Savukoski group contact surfaces, the Puijärvi intrusion, or the fault line, are not detected by the seismic section, because they do not cross the seismic line. The Puijärvi intrusion is located inside the Savukoski group rocks right next to a fault zone, which is sloping towards the west. Therefore, the reflections in the seismic section are most likely not derived from the Savukoski group rocks. The Koitelainen intrusion contact with the Salla group of rocks is too shallow to be detected from the seismic section. The dike is shown in Figure 18 was detected from the surface by field observations, and a similar pattern was identified form reflections as well in the seismic section. The Archean bedrock was formed by outlining the seismic section and identified it as none or as weakly reflective areas, creating an anticline and syncline formation. The Paleoproterozoic rocks form a syncline against the Archean bedrock. This was detected based on the surface observations and the strength of strong reflections. The geological model indicates that the reflections are due to lithological contacts, which could be results of metamorphism.

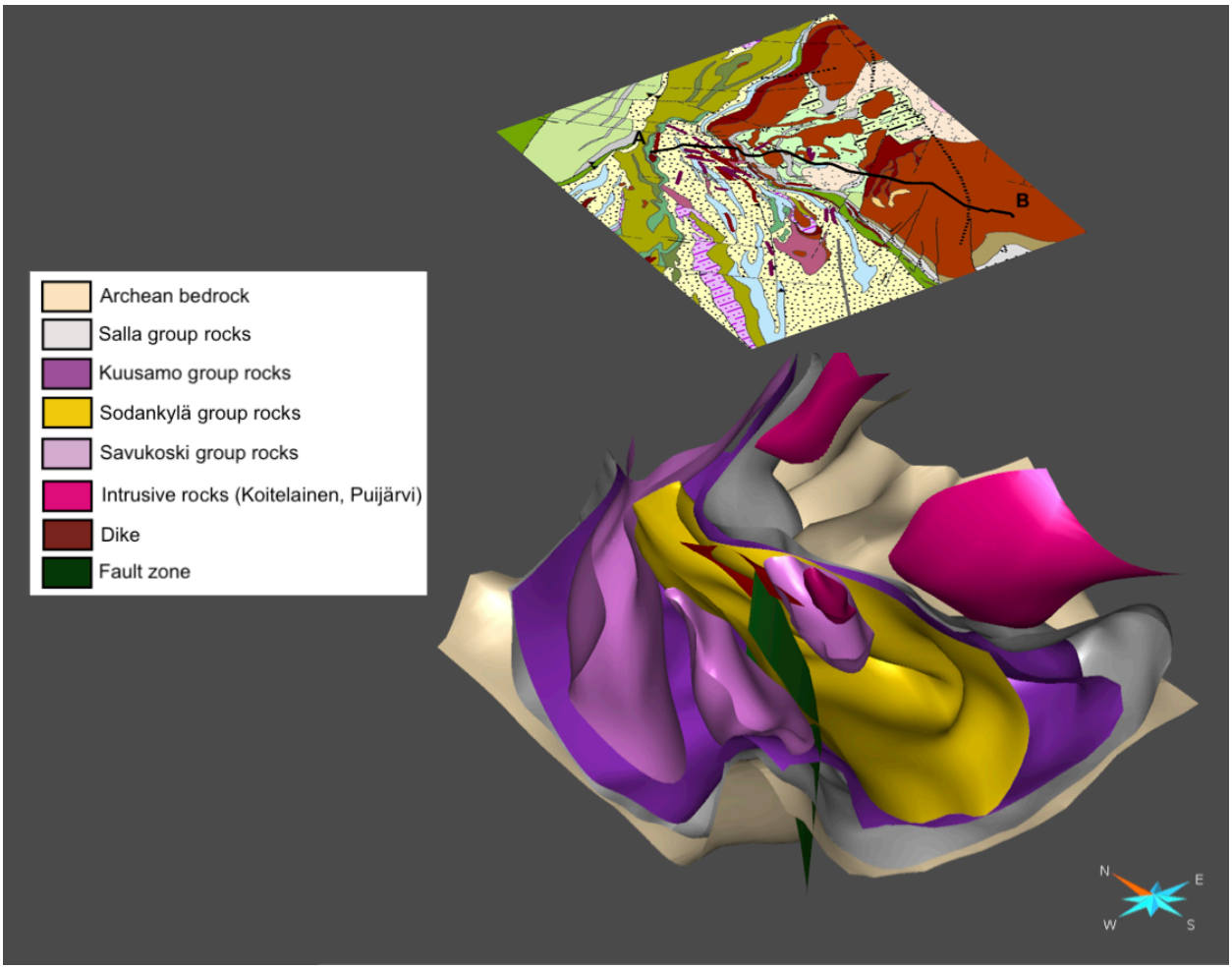

Legend

- XSoDEx seismic survey

Minor faults
- Unspecified minor fault
- Minor dextral strike slip fault
- Minor sinistral strike slip fault
- Thrust fault
- Fracture

Dykes
- Gabbro
- Diabase (Dolerite)
- Ultramafic hypabyssal rock

Plutonic rocks
- Tonalite
- Monzonite
- Gabbro
- Hornblende gabbro
- Peridotite

Volcanic rocks
- Felsic volcanic rock
- Intermediate volcanic rock
- Intermediate tuff
- Mafic volcanic rock
- Mafic tuff
- Ultamafic volcanic rock
- Basaltic komatite

Siliciclastic sedimentary rocks
- Felsic tuffaceous sandstone
- Intermediate volcaniclastic conglomerate

Metamorphic rocks
- Granophyre
- Serpentinite

Metamorphic rocks
- Arkose quartzite
- Biotite paraschist
- Graphite paraschist
- Biotite hornblende paragneiss

Metasomatic or hydrotermal rocks
- Albitite

Figure 17. The geological 3D model with the bedrock map of the study area. Some minor details were modified in the geological model after the seismic forward model was produced.

The seismic section presents that the Archean basement would still have some minor reflections, which are discovered as fractures—however, most of the reflections indicate Paleoproterozoic rock contacts. The strongest reflections are mainly between the Sodankylä group rock units, between the Kuusamo and Sodankylä group contacts, and also detected from the dike and contacts with its host rock.

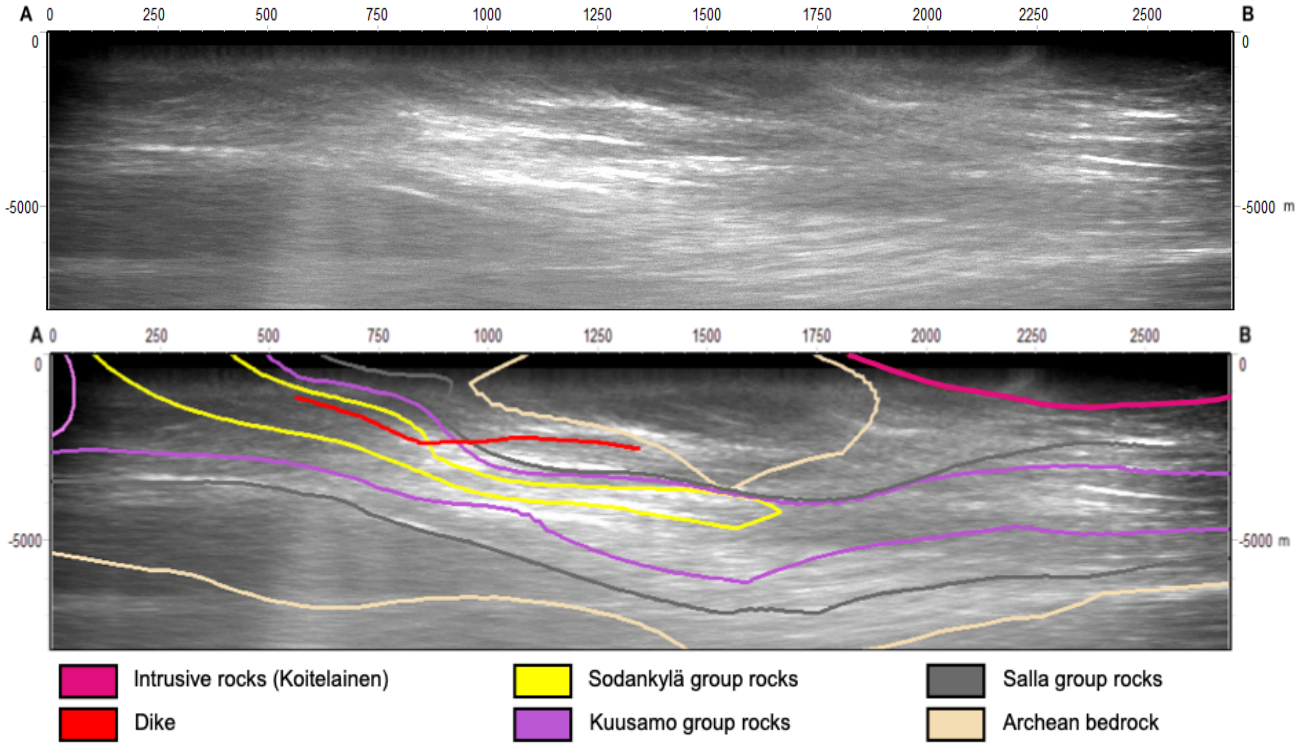

Figure 18. Cross-section of the geological 3D model's contact surfaces with the Alaliesintie reflection seismic section.

4.2. Correlation to gravity and magnetic geophysical data

The inversion models (made by Ilkka Lahti and Hanna Leväniemi in GTK) were used to improve and compare with the geological 3D model, as well as to identify structural components in the subsurface. As a result, the geological 3D model fits well with both of the inversion results, although, the reached depths were quite shallow.

4.2.1. Gravity data with the geological 3D model

The gravity inversion model reaches down to 5 km and therefore was not useful indeterminate the deep reflections at 7 km. The presented rock group descriptions fit well with the xSoDEx petrophysical measurements results. The mafic volcanic rocks have high density values and, therefore, create strong positive gravity anomalies. The granites and other felsic rocks create low gravity anomaly responses. In the gravity data, the Archean basement and the Sodankylä group rocks are detected to have low gravity anomaly responses. The Savukoski group rocks and the uralite gabbro dike, as well as the southern Salla and Kuusamo group rocks, show high anomaly values, which can be seen in Figure 19.

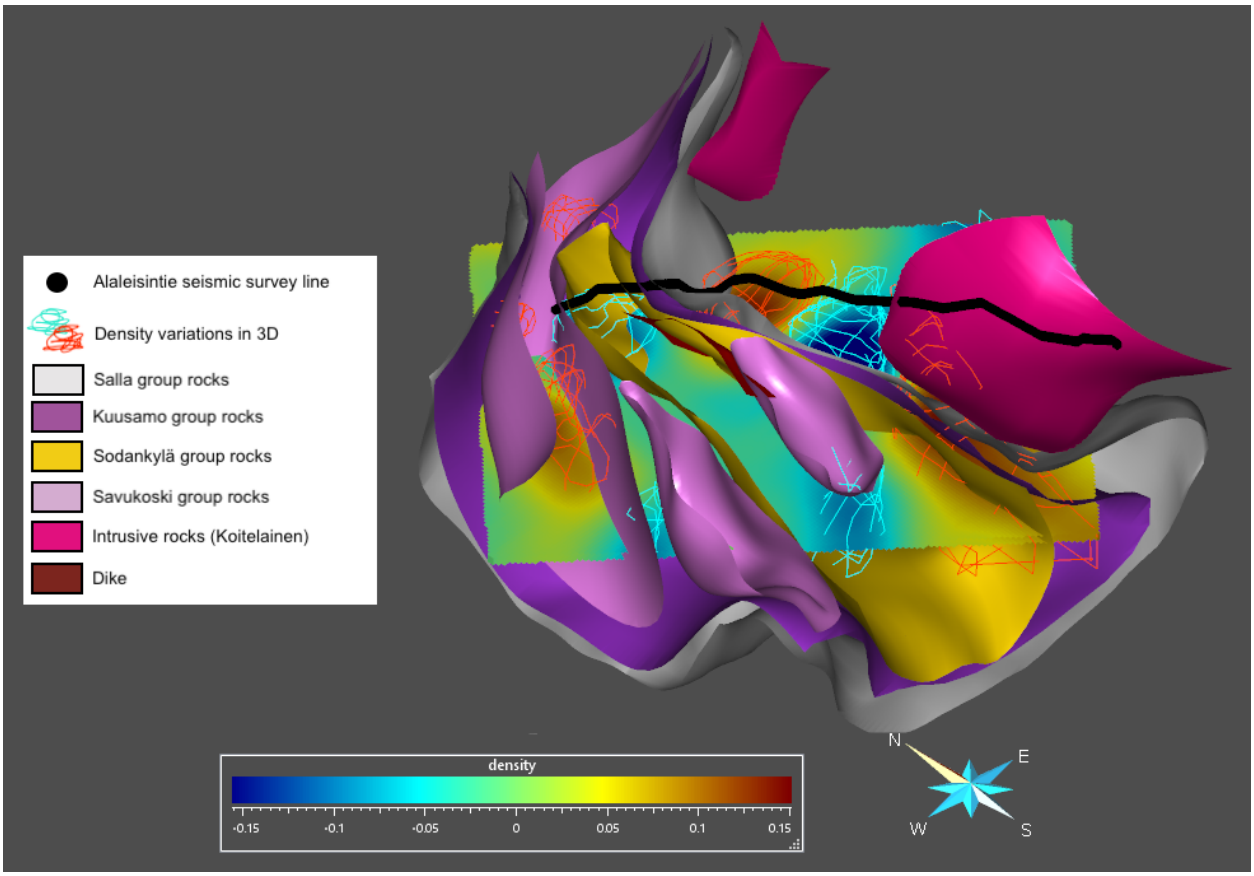

Figure 19. Gravity data and density variations shapes in 3D with the geological 3D model, where the black line illustrates the Alaliesintie seismic survey line.

The low anomaly results around the Archean basement reaches deeper than the modeled Achaean basement surface is presented in the geological 3D model, by continuing underneath the Archean

basement outcrop (Figure 20). The Archean basement was not modified to suit perfectly to the gravity data. The low anomaly results could be caused by Sodankylä group rocks, which are detected to cause low anomaly results in the gravity data in other parts of the model.

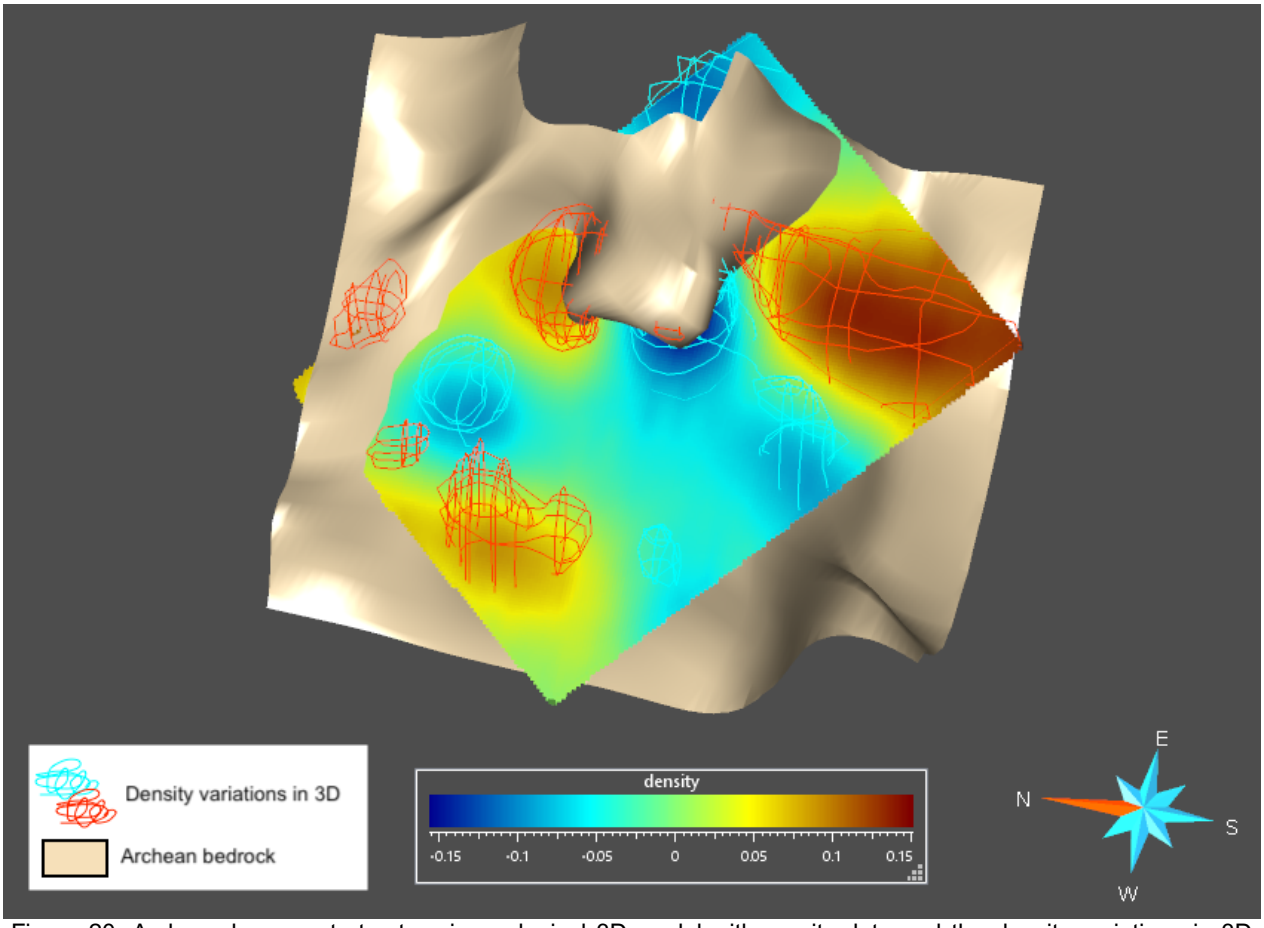

Figure 20. Archean basement structure in geological 3D model with gravity data and the density variations in 3D. Featuring that the low-density continues underneath the Archean bedrock even though the Archean bedrock surface is not continuing with it.

The comparison between the FVM seismic section and the gravity data show that there is a strong density alteration in parts of where there is no reflection in the seismic section (Figure 21). This could be related to the orientation of the lithological structures, which will not allow the reflection to be exposed in the seismic section. The fault or lithological structures that are near perpendicular towards the measurement profile are not revealed as reflections in the seismic section because the incident waves angle affects the reflection coefficient strength. Fault or lithological contact at this angle would be exposed in gravity data. Figure 21 shows the possible almost vertical structure in

between the high- and low-density variations in the right side on the FVM seismic section. The structure does not show any reflections on the Alaliesintie seismic profile.

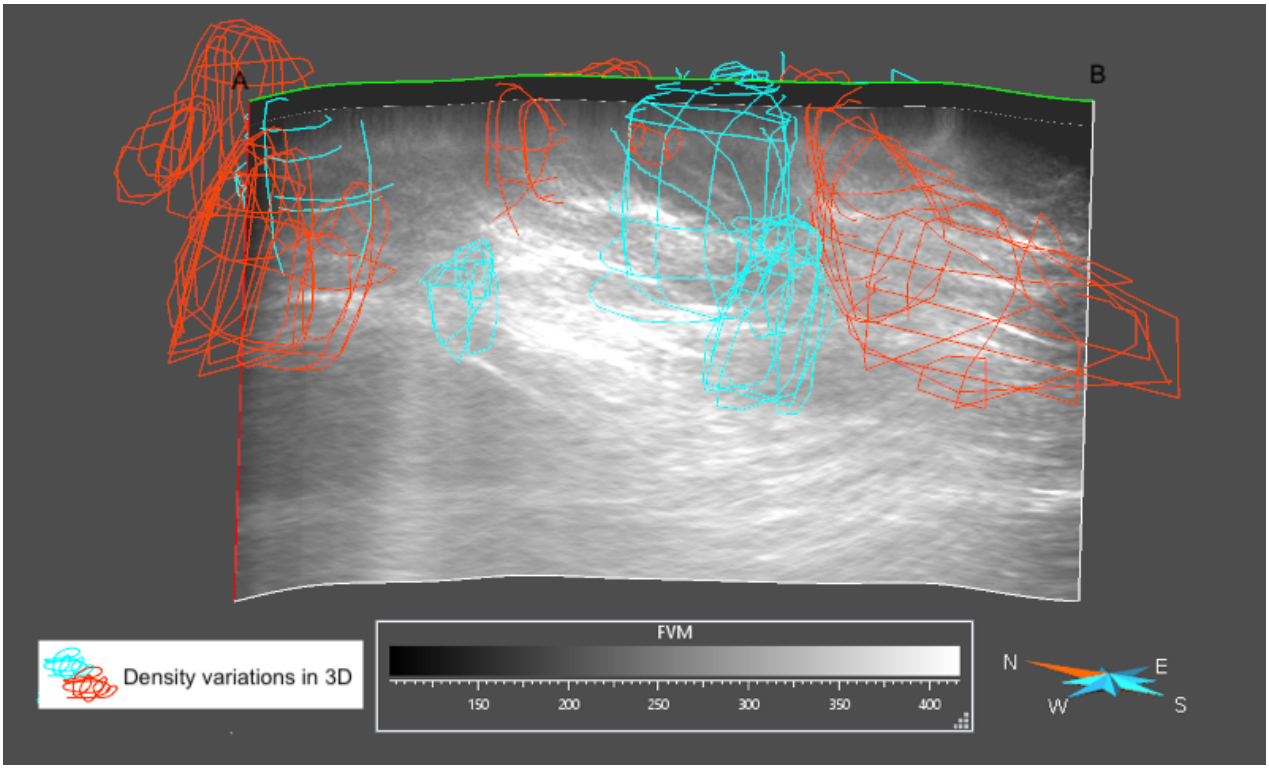

Figure 21. Alaliesintie seismic reflection profile with the 3D density variations.

4.2.2. Magnetic data with the geological 3D model

The magnetic inversion data is presented in two areas as MVI4 and MVI5. The MVI models reach down to 3 km and therefore are only used for shallow subsurface modeling. The data showed that the mafic volcanic rocks create high magnetic anomalies, but alternative felsic volcanic rocks can as well cause high magnetic responses. Low susceptibility values are usually distinguished from felsic volcanic rocks. The anomaly maximum was obtained from Savukoski group rocks (Figure 22). The Savukoski group metasediments are formed in arc volcanism and marine setting. The rock group consists of greywackes BIFs, black schist, mafic and ultramafic volcanic, graphite, and sulfide bearings. Magnetic maximums are as well recognized in contact between Koitelainen intrusion and the Salla group rocks and in contact between the Salla group and Archean basement rocks and as well from contact between the Puijärvi intrusion and the Savukoski group rocks (Figure 22).

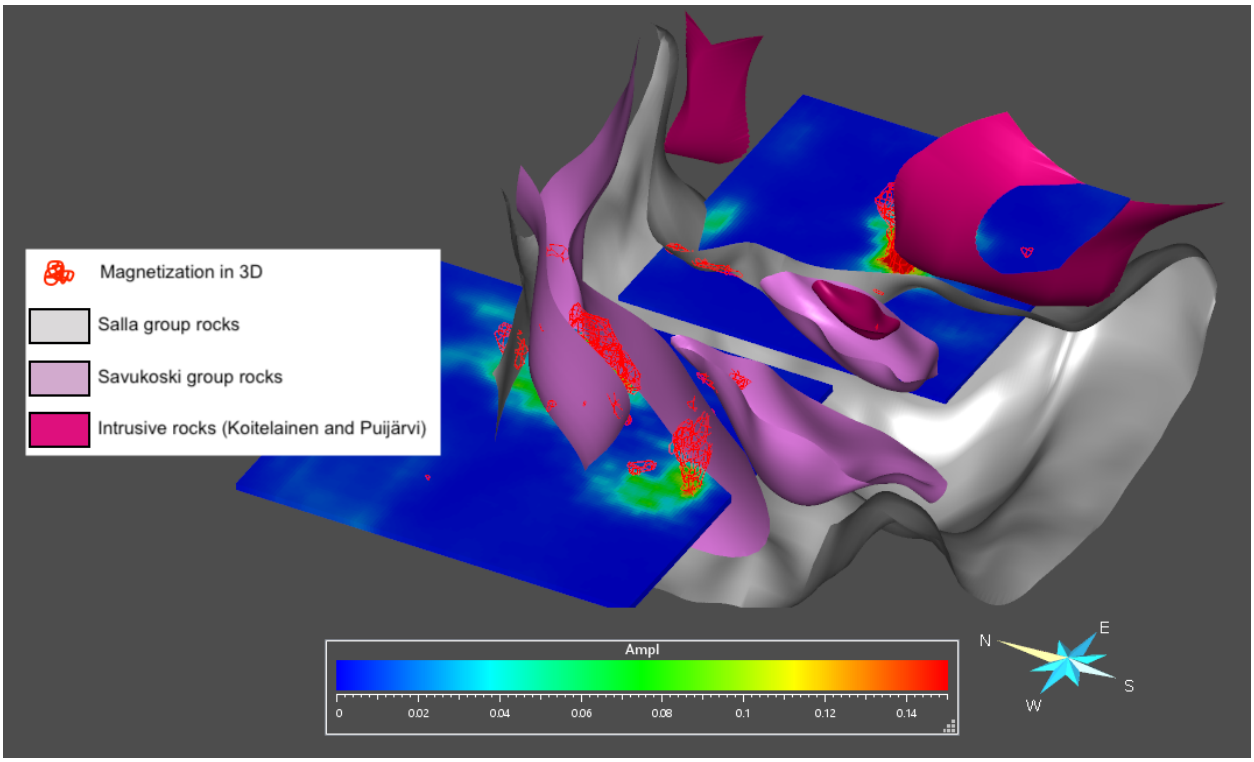

Figure 22. Two magnetic inversion models with the geological 3D model.

4.3. Seismic forward model

The 2D seismic forward model is a synthetic seismic section, which is based on the produced synthetic signal's correspondence with the geological 3D model. The acoustic impedance graph shows the reflection coefficients (Figure 23), indicate the reflection strength between the rock types presented in the geological 3D model. The acoustic impedance and reflection coefficient values are displayed in Table 6. Based on Table 6, the strongest reflections would appear between Sodankylä group rock contacts, which is the contact between arkose quartzite and mica schist, and also between Archean basement and dike, which is the contact between granite gneiss and uralite gabbro. The weakest reflections would appear between the Archean basement and Salla group rock contact, which is the contact between felsic tuff and granite gneiss. The contact between the Kuusamo group's ultramafic volcanic rock and Sodankylä groups' arkose quartzite contacts, reflection coefficient value is 0.066. Meaning that only 6% of the incident intensity is reflected and, therefore, may not be distinguished from the real seismic section. This also applies to the

surfaces between the Salla groups' felsic tuff and Kuusamo groups' ultramafic volcanic rocks contact.

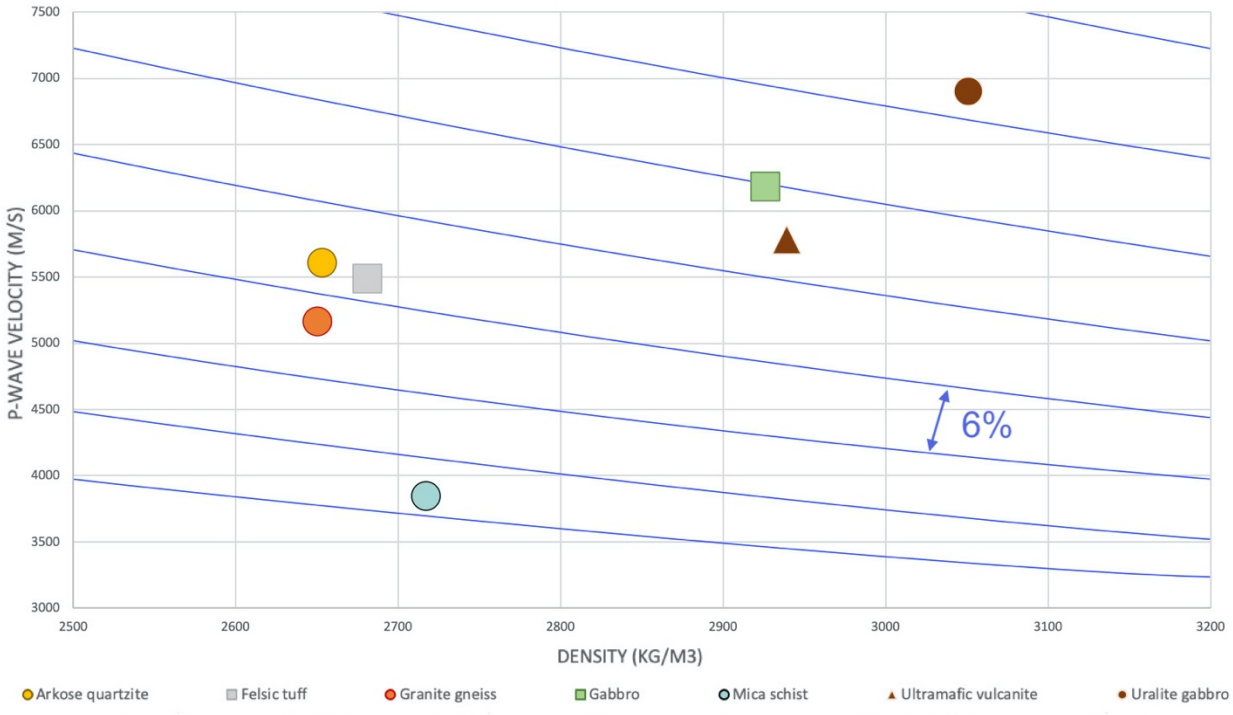

Figure 23. Average P-wave velocity versus density measurement of rocks in Alaliesintie, based on Leväniemi et al. (2018) laboratory results. The lines in the figure demonstrate the impedance units of 10^6 kg s m^{-2} with intervals of a normal incidence reflection coefficient of 0.06.

The synthetic reflections section presents the reflections without any disturbances, which cannot be fully ejected from the original FVM seismic section. The reflection can be coming from any direction in the subsurface space. In the FVM seismic section, the data is possessed to gain the best outcome by strengthening the reflectors in their exact locations. In the synthetic model, the reflection does not always present the contact or discontinuity directly underneath the source and receiver point. Figure 24 shows the problems with the synthetic model, where the marked locations present reflection, which is not resaved from the surface cutting thought the seismic section. The reflection is projected to the seismic section from other parts of the surface. This phenomenon can be fixed by phase shift migration, where the reflections are relocated to the correct position. The produced 2D seismic forward model has not been migrated, or processed like the FVM seismic section, and cannot be directly compared with the real seismic section.

Table 6. Presentation of the geological 3D model's rock contact surfaces acoustic impedances and the reflection coefficient ratio from Alaliesintie.

Contact	Rock types	Acoustic impedance [MPa s m^{-1}]	Reflection coefficient
Dike and Archean	Uralite gabbro	13.7	0.212
basement	Granite gneiss	21.1	
Archean and	Granite gneiss	13.7	0.036
Salla group	Felsic tuff	14.7	
Koitelainen intrusion and	Gabbro	18.1	-0.103
Salla group	Felsic tuff	14.7	
Salla group and Kuusamo	Felsic tuff	14.7	0.072
group	Ultramafic volcanic rock	17.0	
Kuusamo group and	Ultramafic volcanic rock	17.0	-0.066
Sodankylä group	Arkose quartzite	14.9	
Sodankylä group rocks	Mica schist	8.5	0.271
	Arkose quartzite	14.9	

The seismic forward model was produced with multiple frequencies between 10 – 170 Hz (Figure 25), to compare the seismic resolution. Seismic resolution distinguishes the features from one other. Low frequencies give low resolution to the data, and vice versa, the high frequencies provide a high resolution to the seismic data. In Figure 25, the reflections appear more transparent at the lower frequencies due to that it contains fewer details, and reflections with higher frequencies appear more detailed. The most comparable resolution to the Alaliesintie FVM seismic section was detected with a frequency of 50 Hz.

The 2D seismic forward model with frequency 50 Hz shows similarities with the Alaliesintie FVM seismic section (Figure 26). The 2D seismic forward model and FVM seismic section cannot be directly comparable since the synthetic seismic section is not processed with FVM. The results represent only possibilities and ideas for the reflections. The big difference comparison between the seismic sections is that the xSoDEx seismic section the data has disturbances. Also, the first kilometer in the data set has very little to no reflection due to the lack of static corrections and overburnt material, which caused disturbance to the data. In the forward model, these disturbances

are not detected. Like mention earlier, most of the reflections in the seismic forward model are a reflection of the surfaces from other locations that are not directly underneath the seismic profile.

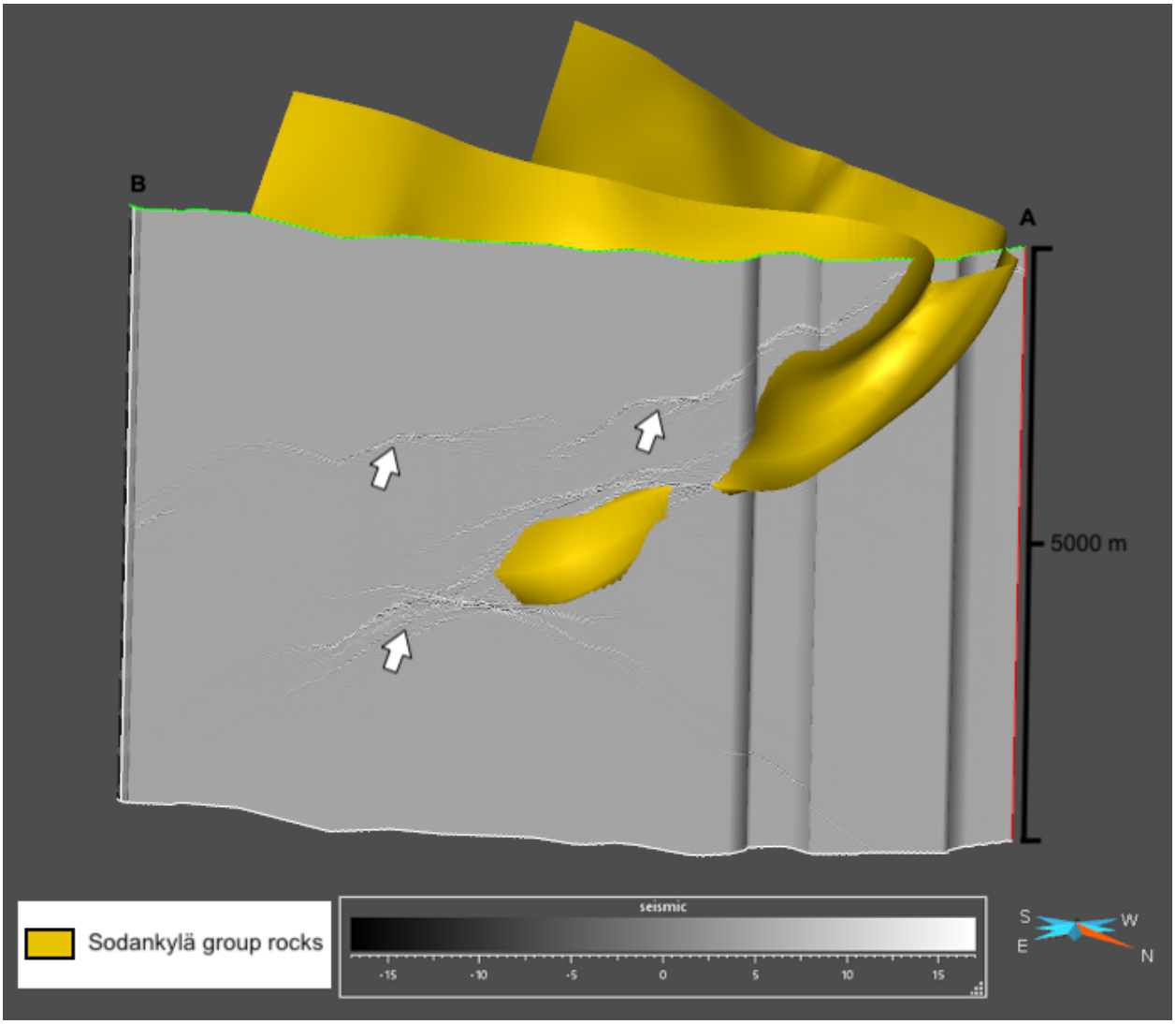

Figure 24. Synthetic seismic forward model of the Sodankylä group rock contact. The white arrows present reflections, which reflects from the side of the surface.

By comparing the visibility of the reflections to the calculated reflection coefficient values in Table 6., the strongest reflections are received from locations a, c, d, and e, which are presented in Figure 26. The reflection in locations a and b are detected to be coming from surfaces between the Salla groups' felsic tuff and Kuusamo groups' ultramafic volcanic rocks contact. The reflections in locations c and d are detected to be coming from the contact between Sodankylä group rocks arkose

quartzite and mica schist. The reflections in location e are detected to be coming from the surface, which is the contact between Archean basement granite gneiss and uralite gabbro dike.

The reflections in location f are unknown in an Alaliesintie FVM seismic section. In the forward model, the reflections in location f present reflections of contact between Sodankylä group rocks arkose quartzite and mica schist, but the reflections do not show similar features. In the FVM seismic section, the reflections curve upwards, and the reflections are not as strongly reflective as they are in the forward model. In the forward model, the reflections are from contact between Sodankylä group rocks. Some of the reflections reflect from the side, as it was shown in Figure 24. In the FVM seismic section, the reflections below the location f could indicate fractured structures that are not seen in the forward model.

The reflections in location g in Figure 26 are a result of a curving surface of the Koitelainen intrusion. The curving surface creates reflections shaped like a bow; these types of reflection patterns are also present in other areas in the forward model. The Koitelainen intrusion is detected from the seismic forward model with a strong reflection coefficient value. The structures are not clearly detected from the FVM seismic section because it is located in the shallow subsurface. The structure is disturbed by the overburnt material and the lack of static corrections during the data processing.

The FVM seismic section is detected to have stronger reflections in a certain part of the profile. This is due to the position of the surface. The surface angle towards the measurement line affects the reflection coefficient strength. Also, the rock type's physical properties and the mineral composition differs though out the lithological unit. The surfaces in the synthetic model have the same reflection coefficient thought out the surface, which does not really present the true bedrock environment, especially in old metamorphic areas where the rocks may have either fractured, partly melted, or reformed.

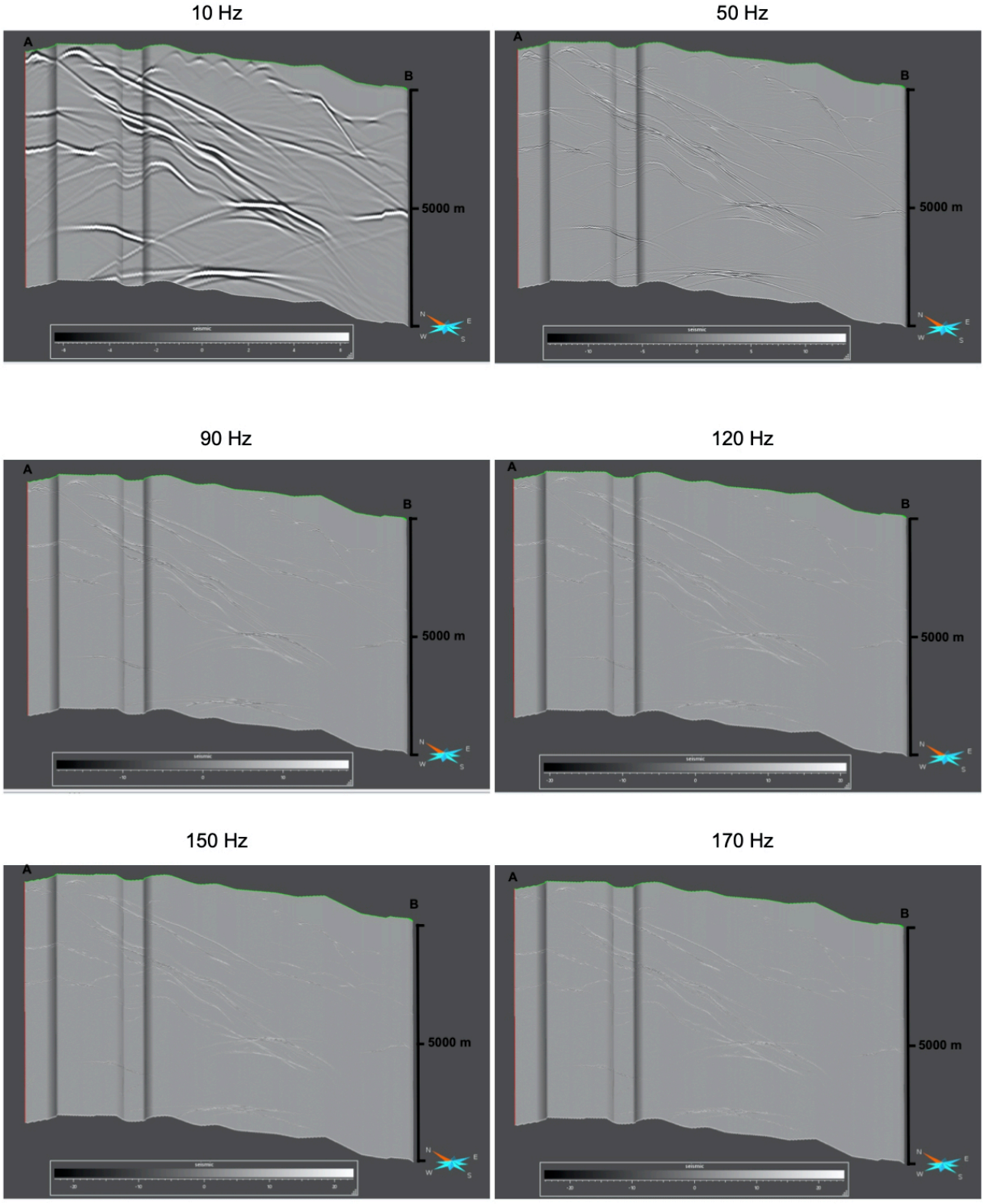

Figure 25. The seismic forward model was produced with different frequencies of 10 Hz, 50 Hz, 90 Hz, 120 Hz, 150 Hz, and 170 Hz.

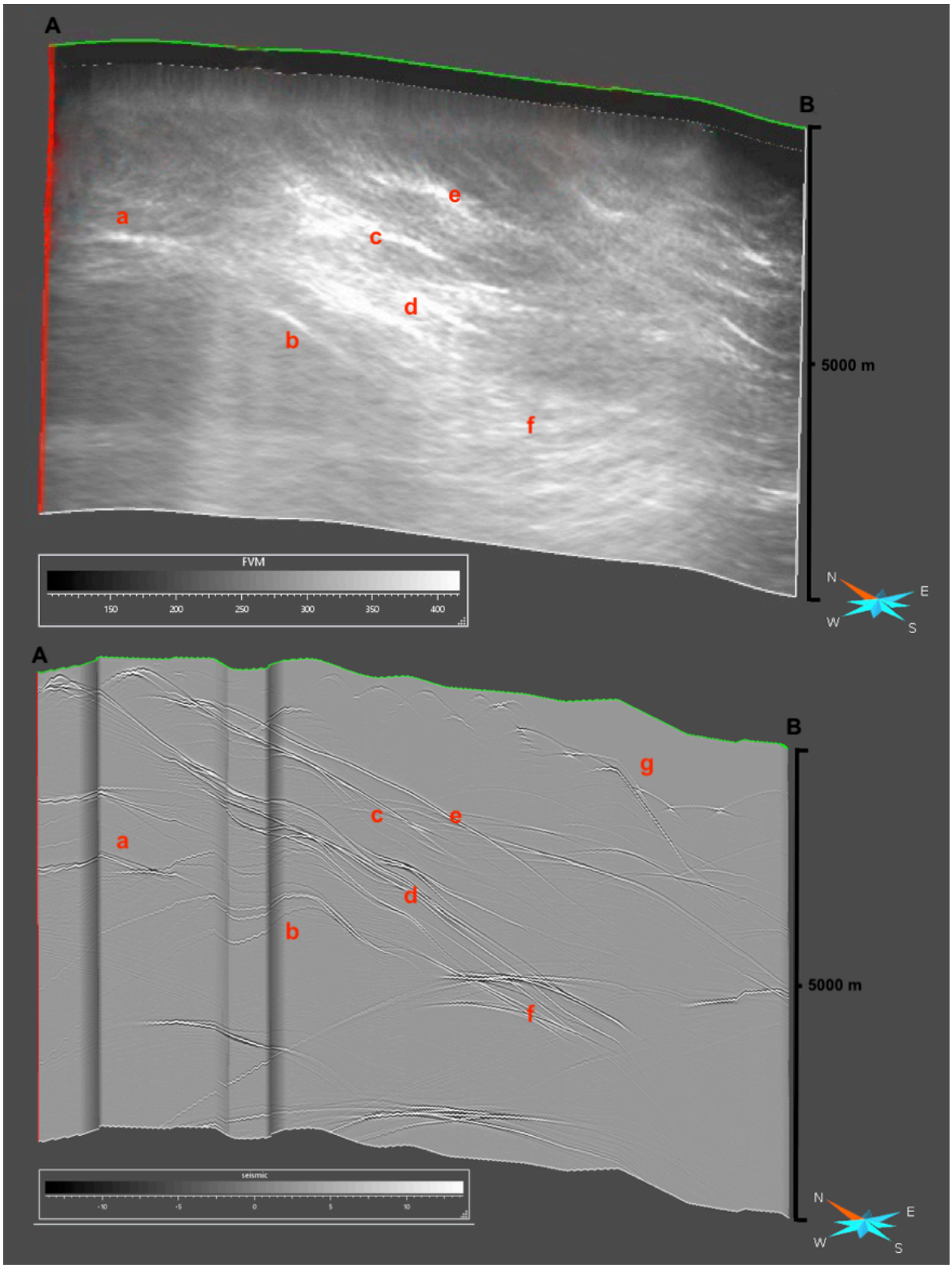

Figure 26. The original Alaliesintie FVM seismic section is in the above, and the syntactic seismic forward model was created with a frequency of 50 Hz is in the bottom. The marked alphabets present the similarities and differences between the seismic sections.

5. DISCUSSION

The geological feature in the produces seismic forward model shows similar features to the Alaliesintie FVM seismic section. The issues with the seismic forward model have are that it presents the same acoustic impedance values throughout the surface, which is not the same in the real subsurface structures. In Alaliesintie, the reflections are caused by mineral composition and tectonic impacts on the rocks. The seismic forward model presents that the Paleoproterozoic lithological contacts would create strong enough reflection to be detected from the seismic section. The seismic forward model's reflection in the Paleoproterozoic lithological contacts is although creating dipping reflection, which is not detected form the Alaliesintie FVM seismic section. The direction of the dip in the seismic profile is unknown in a 2D profile, the apparent amount of dip is always less than the true dip unless the interception angle is 90^{o} (Patison et al. 2006). The seismic forward model and Alaliesintie FVM seismic section show similarities, but they are not comparable due to the different processing methods. The migration of the seismic forward model's reflection would laterally shift the reflection to the correct possession.

The geological 3D model is built based on the available data and my interpretation of the area based on the earlier studies. Evidence-based on earlier studies indicate that the area has gone thought over thrust folding like it is presented in the geological 3D model. Buske et al. (2019) present in the xSoDEx report, that the reflections are dipping to the southeast direction in Alaliesintie, which are an indication that the structures continue underneath the Archean outcrop. Also, the evidence found out about the Koitelainen intrusion structure indicates that the top part of the intrusion is placed in the northern part of the Alaliesintie survey line, which agrees with the assumption that the area presents an anticline and a syncline formation. The HIRE Suurikuusikko reflection profile also shows the antiform fold structure in the seismic reflection profile (Kukkonen et al. 2009). The study by Kukkonen et al. (2009), presents that the reflections indicate a contact zone between mafic graphitic tuff rocks and mafic lavas. The study also presents similar features that show structures that are partly thrusting and folding. The Suurikuusikko area still presents different rock units comparing to the Alaliesintie, but the features indicate that the area has gone through similar tectonic processes.

In the geological 3D model, the Archean basement was interpreted as non-reflective, due to its homogeneity. The weak reflections underneath the Archean outcrop could be caused by deformation, metamorphism, or melting, which is mainly distinguished from transparent zone areas. In FIRE 4 profile, the Archean bedrock was determined to be brittle, and it shows reflectors in the seismic section (Patison et al. 2006). The poor reflectivity underneath the Archean basement could indicate shearing and breaking like Kukkonen et al. (2012) detected in Outokumpu FIRE 3 section. Only fractured Archean basement would not present as strong reflections. In the geological 3D model, the stronger reflections underneath the Archean basement were identified to be coming from Palaeoproterozoic rocks due to the rock's acoustic impedance values. In the FIRE profile, the strong reflections in the Archean basement were identified to be caused by mafic dikes, which were displayed there due to the breakup of the Archean basement (Kukkonen et al. 2006). This could be occurring as well in the study area because it has been tectonically active, and the area's history holds many intrusions. The Sodankylä geology has similar features to the FIRE under the Kainuu Belt, where the Archean craton is fractured and is associated with high reflectivity mafic magmatism (Kukkonen et al. 2006).

Kukkonen et al. (2012) report present that Outokumpu fault is shown as a non-reflective zone in the seismic profile; this shows similar features which were detected from Alaliesintie FVM seismic section in Figure 21. In the Outokumpu HIRE profile, the reflections were discovered to have a fault zone, in the north-west of the Outokumpu fault was discovered to represent the same lithologies based on Kukkonen et al. (2012) report. Many ore deposits are concentrated along the fluid pathways in fault zones, and therefore the fault zones should be detected based on the thickness of the fault zone if it is sufficiently large to produce reflections (Salisbury and Snyder 2007). Based on the Outokumpu studies (HIRE and FIRE), there is still a possibility that the structure could be a result of a normal fault that has moved the older Archean basement structure to the surface and over the younger Paleoproterozoic rocks. The fault zone could be under the later displayed lithological layers. As a now, no evidence on the surface indicates a fault zone; this would need more research.

In order to improve the modeling future, a new seismic reflection profile crossing the Alaliesintie profile would be a good addition to find out about the structures which could be hiding due to the

angle of the dip. Now the geological 3D model is created based on a 2D profile. Having another crossing profile would release the reflection surface angles and give subsurface interedition possibility in three dimensions. The result in the geological 3D model and seismic forward model should be replicated multiple times to enrich the overall aspect of the area, and the angle between the surface and the reflection could be perceived with the model. Borehole studies would be needed to find out the geological reasons for the reflections.

6. CONCLUSION

This study aims to reveal whether the strong seismic reflections underneath the Archean bedrock outcrop, in the Alaliesintie, are due to lithological contacts or a fault zone. The geological 3D model of the seismic reflections was produced based on the assumption that reflection image the lithological contacts. The geological 3D model was build based on surface observations, combined with the Alaliesintie FVM seismic section. The field observations indicate the geological history of the region, which has gone through massive extension stages, including sedimentation, volcanic rock deposition, and also compression stages, which reformed and deformed the structures. The compression shaped and relocated the subsurface structures, which are not displayed in the complex geological map. The tectonic events, including magmatism, of significant layer intrusion into the metasedimentary rocks. These Paleoproterozoic metasedimentary rocks are detected to be great deposition for ore mineralization, which is the reason for the active exploration and mines in the area.

The geological 3D model gives understanding to the tectonic evolution as well as to provide insight into the mineral system structures in the area. Based on this study, the geological 3D model presented that the Archean bedrock and Koitelainen intrusion outcrop presents an anticline and syncline formation, indicating that the Archean bedrock would have folded and overthrust to on top of the younger Paleoproterozoic rocks, which are folded in between the Archean bedrock. The seismic forward model was used to detect the surfaces of the geological 3D model reflections to

see if they are similar to the FVM reflection seismic section. Even though the Alaliesintie FVM seismic data is not directly comparable to the seismic forward model results, the results suggest that the seismic forward model can be used to simulate the reflection. The produced seismic forward model results present that the Sodankylä group rock contact would create strong reflections, and that the geological 3D model is suggesting possibilities and ideas for the reflections, which could indicate the same reflections as in the Alaliesintie seismic profile.

There are many ways to improve the understanding of the Alaliesintie seismic results. These include collecting new seismic data, borehole data, and improving the seismic forward model, which could be processed and reproduced with slightly different surface angles. To improve the geological 3D model, I recommend that another seismic profile should be designed and performed to cross the Alaliesintie. Additional borehole and borehole in situ measurements (density and acoustic velocity logs) would provide a means to test the reality of the interpreted lithological units their seismic responses.

ACKNOWLEDGMENTS

This master's thesis research was done for the Geological Survey of Finland (GTK). GTK funded the research by giving the licenses for all the programs I used during this study, and by supporting my work full time for three months in the summer of 2019 and part-time for two months in fall 2019. From GTK, I was also able to gain an excellent advantage in scientific knowledge from my supervisors Suvi Heinonen and Tuomo Karinen, to do this thesis. I am as well grateful for all the help and support I received from my supervisors from GTK and Ilmo Kukkonen at the University of Helsinki.

REFERENCES

Airo, M-L. and Kiuru, R. 2012. Petrofysiikan perusteet. The University of Helsinki, Division of Geophysics and Astronomy. Report Series in Geophysics, 68, 43–79.

Anderson, N. and Cardimona, S. 2002. Forward Seismic Modeling: The Key to Understanding Reflection Seismic and Ground Penetrating Radar (GPR) Techniques. Department of Geology and Geophysics, University of Missouri-Rolla.

Buske, S., Hlousek, F., and Jusri, T. 2019. XSoDEx Reflection Seismic Data Acquisition and Processing Report. Institute of Geophysics and Geoinformatics, TU Bergakademie Freiberg.

Eilu, P., Pankka, H., Keinänen, V., Kortelainen, V., Niiranen, T., and Pulkkinen, E. 2007. Characteristics of Gold Mineralization in the Greenstone Belts of Northern Finland. In: J. Ojala (Ed.), Gold in the Central Lapland Greenstone Belt, Finland. Geological Survey of Finland, Special Paper 44, 57–106.

EMERSON. 2019. SKUA-GOCAD application. Visited 31.08.2019. (https://www.pdgm.com/products/skua-gocad/)

Evins, P. and Laajoki, K. 2002. Early Proterozoic Nappe Formation: An Example from Sodankylä, Northern Baltic Shield. Geological Magazine 139, 73–87.

Gaal, G., Berthelsen, A., Gorbatschev, R., Kesola, R., Lehtonen, M., Marker, M., and Raase, P. 1989. Structure and Composition of the Precambrian Crust Along the POLAR Profile in the Northern Baltic Shield. Tectonophysics, 162, 1–25.

Geometrics Inc. 2020. Geometrics – Geode Seismic Recorder. Visited 04.02.2020. (https://www.environmental-expert.com/products/geometrics-geode-seismic-recorder-430751)

Hanski, E. and Huhma, H. 2005. Central Lapland Greenstone Belt. In: M. Lehtinen, P. Nurmi, and T. Rämö. (Eds.), Precambrian Geology of Finland: Key to the Evolution of the Fennoscandian Shield Developments in Precambrian. Geology Elsevier B.V. Amsterdam 14, 142–183.

Hanski, E., Huhma, H., and Perttunen, V. 2005. SIMS U-Pd, Sm-Nd Isotopic and Geochemical Study of an Arkosite Amphibolite Suite, Peräpohja Schist Belt: Evidence for ca. 1.98 Ga A Type Felsic Magmatism in Northern Finland. Bulletin Geological Society of Finland, Volume 77, 5–29.

Heinonen, S., Karinen, T., and Sormunen, R. 2018. XSoDEx- projektin seismisten heijastusluotausten kenttätyöt. Geologian Tutkimuskeskus, Espoo.

Hinze, W., Von Frese, R., and Saad, A. 2013. Gravity and Magnetic Exploration, Principles, Practice, and Applications. Cambridge University Press, 19–37.

Hlousek, F. and Buske, S. 2016. Fresnel Volume Migration of the ISO89-3D Data Set. Geophysical Journal International 207, 1273–1285.

Hölttä, P., Väisänen, M., Väisänen, J., and Manninen, T. 2007. Paleoproterozoic Metamorphism and Deformation in Central Lapland, In: J. Ojala. 2007 (Ed.), Gold in the Central Lapland Greenstone Belt, Finland. Geological Survey of Finland, Special Paper 44, 7–56.

Huhma, H., Hanski, E., Kontinen, A., Vuollo, J., Mänttäri, I., and Lahaye, Y. 2018. Sm-Nd and U-Pd Isotope Geochemistry of the Paleoproterozoic Mafic Magmatism in Eastern and Northern Finland. Bulletin, Geological Society of Finland 405, 150.

Kallweit, R. and Wood, L. 1982. The Limits of Resolution of Zero-Phase Wavelets. Geophysics, Volume 47, Number 7, 1035–1046.

Korsman, K., Koistinen, T., Kohonen, J., Wennerström, M., Ekdahl, E., Hankamo, M., Idaman, H., and Pekkala, Y. 1997. Bedrock Map of Finland 1:1 000 000. Geological Survey of Finland, Espoo.

Köykkä, J., Lahtinen, R., and Huhma, H. 2019. Province Evolution of the Paleoproterozoic Metasedimentary Cover Sequences in Northern Fennoscandia: Age Distribution, Geochemistry and Zircon Morphology. Elsevier. Precambrian research 331, 105–364.

Kozlovskaya, E., Narkilahti, J., Nevalainen, J., Hurskainen, R., and Silvennoinen, H. 2016. Seismic Observations at the Sodankylä Geophysical Observatory: History, Present, and the Future. Geoscientific instrumentation Methods and Data Systems, 370–380.

Kukkonen, I., Heikkinen, P., Ekdahl, E., Hjelt, S-E., Yliniemi, J., Jalkanen, E., and FIRE Working Group. 2006. Acquisition and Geophysical Characteristics of Reflection Seismic Data on FIRE Transects, Fennoscandian Shield. Geological Survey of Finland, Special Paper 43, 13–43.

Kukkonen, I., Heikkinen, P., Heinonen, S., Laitinen, J. and HIRE Working Group of the Geological Survey of Finland. 2009. HIRE Seismic Reflection Survey in the Suurikuusikko Gold Mining and Exploration area, North Finland, 5–48.

Kukkonen, I., Heinonen, S., Heikkinen, P., and Sorjonen-Ward, P. 2012. Delineating Ophiolite-Derived Host Rocks of Massive Sulphide Cu-Co-Zn Deposits with 2D High-Resolution Seismic Reflection Data in Outokumpu, Finland. Geophysics Volume 77, Number 5, 213–221.

Krebes, E. 2004. Seismic Forward Modeling. Article, Coordinated by Satinder Chopra. Department of Geology and Geophysics, University of Calgary, Calgary, 29–39.

Lahtinen, R. and Huhma, H. 2019. A Revised Geodynamic Model for the Lapland-Kola Orogen. Elsevier. Precambrian Research, 330, 1–19.

Lahtinen, R., Huhma, H., Sayab, M., Lauri, L-S., and Hölttä, P. 2018. Age and Structural Constraints on the Tectonic Evolution of the Paleoproterozoic Central Lapland Granitoid Complex in the Fennoscandian Shield. Tectonophysics 745, 305–325.

Lahtinen, R., Sayab, M., and Karell, F. 2015. Near-Orthogonal Deformation Successions in the Poly-Deformed Paleoproterozoic Martimo Belt: Implications for the Tectonic Evolution of Northern Fennoscandia. Precambrian Research 270, 22–38.

Langel, R. and Hinze, W. 1998. The Magnetic Field of the Earth's Lithosphere: The Satellite Perspective. Cambridge University Press, 250–279.

Lehtonen, M., Airo, M-L., Elju, P., Hanski, E., Kortelainen, V., Lanne, E., Manninen, T., Rastas, P., Räisänen, J., and Virransalo, P. 1998. The Stratigraphy, Petrology, and Geochemistry of the Kittilä Greenstone Area, Northern Finland. A Report of the Lapland Volcanite Project. Geological Survey of Finland, Report of Investigation 140, 144.

Leväniemi, H., Melamies, M., Mertanen, S., Heinonen, S., and Karinen, T. 2018. Petrophysical Measurements to Support Interpretation of Geophysical Data in Sodankylä, Northern Finland. Geological Survey of Finland, Applied Geophysics, Espoo. GTK Open Field Work Report 25, 1–4.

Luosto, U., Fluh E., Lund C., and POLAR Working Group. 1989. The Crustal Structure Along the POLAR Profile from Seismic Reflection Investigations. Tectonophysics 162, 51–85.

MacLeod, I., and Ellis, R. 2013. Magnetic Vector Inversion, A Simple Approach to the Challenge of Varying Direction of Rock Magnetization. ASEG-PESA, 23rd International Geophysical Conference and Exhibition, 11–14 August 2013, Melbourne, Australia. 1–2.

MacLeod, I., and Ellis, R. 2015. Quantitative Magnetization Vector Inversion. Extended Abstracts of 14th SAGA Biennial Technical Meeting and Exhibition 2015. 1–3.

Mutanen, T. 1989. Koitelaisen malmitutkimukset vuosina 1979–1989. Geologian tutkimuslaitos (Geological Survey of Finland). Sodankylä.

Mutanen, T. 1997. Geology and Petrology of the Akanvaara and Koitelainen Mafic Layered Intrusions and the Kevitsa-Satovaara Layered Complex, Northern Finland. Geological Survey of Finland. Espoo. Bulletin 395, 233.

Mutanen, T. and Huhma, H. 2001. U-Pd Geochronology of the Koitelainen, Akanvaara and Kevitsa Layer Intrusions and Related Rocks. Geological Survey of Finland, Special Paper 33, 229–246.

Niiranen, T. 2015. A 3D structural model of the central and eastern part of Kittilä terrane. Geological Survey of Finland, Archive report, 90, 1–15.

Niiranen, T., Lahti, I., Nykänen, V., and Karinen, T. 2014. Central Lapland Greenstone Belt 3D Modeling Project Final Report. Geological Survey of Finland, Report of Investigation 209, 5.

Niiranen, T., Lahti, I., and Nykänen, V. 2014 a. Chapter 3, 3D Model of the Kittilä Terrane and Adjacent Structures. In: Niiranen T., Lahti I., Nykänen V., and Karinen T. Ed., Central Lapland Greenstone Belt 3D Modeling Project Final Report. Geological Survey of Finland, Report of Investigation 209, 27–41.

Nironen, M. 2017a. Guide to the Geological Map of Finland – Bedrock 1:1 000 000. Major Stratigraphic Units, Metamorphism and Tectonic Evolution. Geological Survey of Finland. Special Paper 60, 41–69.

Nironen, M. 2017b. Structural Interpretation of the Peräpohja and Kuusamo Belts and Central Lapland, and a Tectonic Model for Northern Finland. Geological Survey of Finland. Report of Investigations 234, 53.

Nironen, M. and Mänttäri, I. 2003. Structural Evolution of the Vuotso Area, Finnish Lapland. Bullet. Geological Society of Finland 75, 93–101.

Patison, N., Korja, A., Lahtinen, R., Ojala, V., and the FIRE Working Group. 2006. FIRE Seismic Reflection Profiles 4, 4A and 4B: Insights into the Crustal Structure of the Northern Finland from Rauma to Näätämö. Geological Survey of Finland, Special Paper 43, 161–222.

Peltoniemi, M. 1988. Maa-ja Kallioperän geofysikaaliset tutkimusmenetelmät. Otava kustantamo, 515, 29–62

Price, N., and Cosgrove, J. 1990. Analysis of Geological Structures. Cambridge University Press, 476.

Salisbury, M., Milkereit, B., and Bleeker, W. 1996. Seismic Imaging f Sulphide Deposits: Part 1. Rock Properties. Economic Geology. 91, 821–828.

Salisbury, M., and Snyder, D. 2007. Application of Seismic Methods to Mineral Exploration, in Goodfellow, W.D., ed., Mineral Deposits of Canada: A Synthesis of Major Deposit-Types, District Metallogeny, the Evolution of Geological Provinces, and Exploration Methods: Geological Association of Canada, Mineral Deposits Division, Special Publication Number 5, 971–982.

Schön, J. 2011. Physical Properties of Rocks, A Workbook. Handbook of Petroleum Exploration and Production, 8. Elsevier, 226–227.

Shearer, P. 2009. Introduction to Seismology. 2 Edition. 32, 181–198.

Sheriff, R. 1995. Exploration seismology. 2 Edition. Cambridge University Press, Cambridge, 628.

Sheriff, R. and Geldart L. 1982. Exploration Seismology. Cambridge University, 275–346.

Simm, R. and Bacon, M. 2014. Seismic Amplitude: An Interpreter's Handbook. Cambridge University Press, 3–37.

Stein, S. and Wysession, M. 2003. An Introduction to Seismology, Earthquakes and Earth Structure. Blackwell Publishing, 29–111.

Tuomi, H. 2016. Seismic Forward Modelling Constraints for Seismic Ore Exploration at the Kylylahti Cu-Co-Zn-Ag-Au Sulfide Deposit. Master Thesis, University of Helsinki, Department of Geosciences and Geography, 40–43.

Ward, P., Härkönen, I., Nurmi, P., and Pankka, H. 1989. Structural Studies in the Lapland Greenstone Belt, Northern Finland and Their Application to Gold Mineralization. Geological Survey of Finland, Special Paper 10, 71–77.

Ylimaz, O. 2001. Seismic Data Analysis: Processing, Inversion, and Interpretation of seismic data. Volume 1–2. 2. Edition. Society of Exploration geophysicists, Tulsa, 2065.

ATTACHMENTS

Attachment 1

Surface geology observations around the Alaliesintie seismic survey in Sodänkylä

1: Layering, 2: Foliation, 3: Axial Plane, 4: Fault, 7:Contact, and 8: Joint

FID	DATE	TYPE	DIRECTION	DIP
0	11.6.1975	2	285	60
1	11.6.1975	1	295	55
2	11.6.1975	2	295	55
3	11.6.1975	2	290	60
4	11.6.1975	2	295	50
5	11.6.1975	1	295	50
6	11.6.1975	2	295	75
7		2	115	75
8	17.6.1975	1	290	15
9	17.6.1975	2	290	15
10	1.8.1975	2	330	25
11		2	280	80
12		2	160	15
13		2	90	35
14		2	295	85
15		1	290	50
16		2	290	50
17		1	285	40
18		2	300	50
19	15.6.1978	1	300	25
20	15.8.1984	2	360	25
21	11.6.1974	2	290	70
22	12.6.1974	1	290	20
23	12.6.1974	2	290	80
24	12.6.1974	1	285	30
25	12.6.1974	2	285	30
26	13.6.1975	2	300	30
27		2	115	55
28		1	80	48
29		1	88	45
30		2	15	48
31		1	40	53
32		2	110	85
33		1	245	82
34		1	80	84
35		1	255	85
36		1	285	85
37		1	250	85
38		1	70	85
39		1	75	85
40	14.8.1980	1	85	85
41		2	267	78
42		1	250	85
43		1	280	80
44		1	270	80

Attachment 1

Surface geology observations around the Alaliesintie seismic survey in Sodänkylä

1: Layering, 2: Foliation, 3: Axial Plane, 4: Fault, 7:Contact, and 8: Joint

FID	DATE	TYPE	DIRECTION	DIP
45		1	275	75
46		2	104	75
47		1	87	81
48		2	105	82
49		1	130	65
50		2	105	75
51		2	280	80
52		1	278	85
53		2	280	70
54		1	85	70
55		2	260	50
56		1	265	70
57		2	280	75
58		2	290	55
59		1	285	75
60		2	50	65
61		2	100	65
62		1	30	20
63		2	305	75
64	3.7.1981	2	70	60
65	17.8.1981	2	330	23
66		2	125	83
67	13.6.1974	8	145	85
68	13.6.1974	8	270	85
69	13.6.1974	8	155	60
70	13.6.1974	8	260	80
71	13.6.1974	8	145	60
72	13.6.1974	8	210	90
73	13.6.1974	8	110	90
74	14.6.1974	8	240	90
75	14.6.1974	8	270	90
76	14.6.1974	8	170	75
77	1.7.1976	2	90	90
78	1.7.1976	2	120	80
79	1.7.1976	2	120	80
80	1.7.1976	8	120	80
81	1.7.1976	2	105	25
82	1.7.1976	2	120	80
83	1.7.1976	2	120	80
84	1.7.1976	8	30	90
85	13.6.1981	2	75	68
86	13.6.1981	2	235	75
87	13.6.1981	2	30	75
88	13.6.1981	2	85	75
89	18.6.1981	2	270	65

Attachment 1

Surface geology observations around the Alaliesintie seismic survey in Sodänkylä

1: Layering, 2: Foliation, 3: Axial Plane, 4: Fault, 7:Contact, and 8: Joint

FID	DATE	TYPE	DIRECTION	DIP
90	18.6.1981	2	255	75
91	18.6.1981	2	255	80
92	27.6.1981	2	70	75
93	27.6.1981	2	95	75
94	27.6.1981	2	90	70
95	28.6.1981	2	210	55
96	28.6.1981	2	240	75
97	28.6.1981	2	68	50
98	28.6.1981	1	68	50
99	28.6.1981	2	80	60
100	17.7.1981	2	80	40
101		2	125	20
102	19.7.1981	2	52	40
103	19.7.1981	2	290	70
104	13.8.1981	1	315	55
105	13.8.1981	2	310	50
106	17.8.1981	2	300	60
107	18.8.1981	2	320	50
108	11.7.1981	1	310	60
109	13.6.1981	2	75	60
110	5.6.1980	2	270	78
111	5.6.1980	1	265	86
112	5.6.1980	1	187	74
113	5.6.1980	2	100	50
114	5.6.1980	2	250	74
115	5.6.1980	2	265	77
116	6.6.1980	2	240	72
117	6.6.1980	1	67	52
118	6.6.1980	1	80	54
119	6.6.1980	2	87	62
120	6.6.1980	1	90	52
121	6.6.1980	2	40	72
122	6.6.1980	2	81	62
123	6.6.1980	1	86	47
124	6.6.1980	2	72	42
125	6.6.1980	1	68	38
126	6.6.1980	2	86	50
127	6.6.1980	1	61	45
128	6.6.1980	2	78	41
129	6.6.1980	1	80	38
130	6.6.1980	2	89	68
131	6.6.1980	1	20	76
132	6.6.1980	2	45	72
133	6.6.1980	1	54	46
134	6.6.1980	2	90	82

Attachment 1

Surface geology observations around the Alaliesintie seismic survey in Sodänkylä

1: Layering, 2: Foliation, 3: Axial Plane, 4: Fault, 7:Contact, and 8: Joint

FID	DATE	TYPE	DIRECTION	DIP
135	6.6.1980	1	95	56
136	6.6.1980	1	75	58
137	6.6.1980	2	82	67
138	6.6.1980	1	270	80
139	7.6.1980	2	265	83
140	7.6.1980	2	93	87
141	7.6.1980	2	275	68
142	7.6.1980	1	270	65
143	7.6.1980	2	260	67
144	7.6.1980	2	274	57
145	7.6.1980	1	275	58
146	7.6.1980	1	235	64
147	7.6.1980	2	240	59
148	7.6.1980	2	125	41
149	7.6.1980	2	100	36
150	7.6.1980	1	75	20
151	8.6.1980	1	250	74
152	8.6.1980	2	78	79
153	9.6.1980	2	130	80
154	8.6.1980	2	260	68
155	2.7.1980	2	320	35
156		2	247	68
157		2	105	0
158		2	120	80
159		2	258	90
160		1	263	80
161		2	102	68
162		2	286	84
163		2	43	84
164		2	28	80
165		2	35	72
166		2	45	60
167		2	30	75
168		2	82	66
169		2	50	44
170		2	48	36
171		2	63	50
172		2	85	58
173		2	77	36
174		1	90	56
175		1	80	20
176		2	93	43
177		2	98	38
178		1	93	43
179		1	98	38

Attachment 1

Surface geology observations around the Alaliesintie seismic survey in Sodänkylä

1: Layering, 2: Foliation, 3: Axial Plane, 4: Fault, 7:Contact, and 8: Joint

FID	DATE	TYPE	DIRECTION	DIP
180		2	86	47
181		1	86	47
182		2	105	67
183		1	105	67
184		2	82	42
185		2	100	62
186		1	100	62
187		2	95	27
188		2	87	24
189		2	85	30
190		1	85	30
191		1	87	24
192		2	302	45
193		2	292	72
194		2	80	78
195		2	112	70
196		2	67	68
197		2	290	70
198		2	70	80
199		2	145	60
200		2	330	67
201		2	330	87
202		2	317	85
203		2	318	88
204		2	24	85
205		2	220	83
206		2	352	22
207		1	352	22
208		2	352	22
209		1	352	22
210		2	338	21
211		2	33	20
212		2	52	21
213		2	32	17
214		2	36	70
215		2	274	87
216		2	70	50
217		2	268	82
218		1	67	66
219		2	76	77
220		2	225	28
221		1	270	64
222		2	270	64
223		2	270	82
224		2	282	66

Attachment 1

Surface geology observations around the Alaliesintie seismic survey in Sodänkylä

1: Layering, 2: Foliation, 3: Axial Plane, 4: Fault, 7:Contact, and 8: Joint

FID	DATE	TYPE	DIRECTION	DIP
225		2	286	67
226		2	280	80
227		2	272	68
228		2	94	85
229		2	290	70
230		2	115	84
231		2	34	70
232		2	285	58
233		2	288	65
234		2	240	60
235		2	40	82
236		2	126	68
237		2	60	15
238		2	23	72
239		2	42	82
240		2	64	46
241		2	327	53
242		2	236	62
243		2	87	76
244		2	72	60
245		2	67	85
246		2	266	85
247		2	296	68
248		2	273	0
249		2	127	45
250		2	110	85
251		2	213	62
252		2	190	76
253		1	228	78
254		2	228	78
255		1	267	56
256		2	267	56
257		2	205	56
258		2	220	30
259		2	282	25
260		2	232	72
261		2	340	33
262		2	352	18
263		2	95	25
264		1	335	20
265		2	67	18
266		2	280	65
267		2	270	7
268		2	73	28
269		1	25	25

Attachment 1

Surface geology observations around the Alaliesintie seismic survey in Sodänkylä

1: Layering, 2: Foliation, 3: Axial Plane, 4: Fault, 7:Contact, and 8: Joint

FID	DATE	TYPE	DIRECTION	DIP
270		2	340	20
271		2	238	65
272		2	190	86
273		1	5	82
274		2	47	55
275		1	85	52
276		2	85	52
277		2	70	45
278		2	305	75
279		2	273	65
280		2	88	22
281		2	77	37
282		2	268	5
283		1	120	10
284		2	92	32
285		2	157	80
286		2	46	82
287		2	93	70
288		2	208	75
289		1	208	75
290		2	60	28
291		2	82	50
292		2	70	28
293		2	72	35
294		1	72	8
295		2	72	48
296		2	82	38
297		2	72	45
298		2	62	36
299		2	70	42
300		2	280	15
301		1	233	30
302		2	295	57
303		2	77	50
304		2	106	72
305		2	80	42
306		2	55	16
307		2	260	75
308		2	358	80
309		2	125	85
310		2	272	85
311	20.6.1982	2	90	50
312	30.6.1982	2	330	20
313	15.7.1982	2	340	65
314	12.6.1982	2	300	80

Attachment 1

Surface geology observations around the Alaliesintie seismic survey in Sodänkylä

1: Layering, 2: Foliation, 3: Axial Plane, 4: Fault, 7:Contact, and 8: Joint

FID	DATE	TYPE	DIRECTION	DIP
315	3.6.1982	2	2	65
316	2.7.1982	2	173	76
317	2.7.1982	1	25	20
318	2.7.1982	2	95	25
319	2.7.1982	2	95	25
320	2.7.1982	1	95	25
321	3.7.1982	2	80	43
322	3.7.1982	1	65	55
323	3.7.1982	2	65	55
324	3.7.1982	1	85	55
325	3.7.1982	2	85	55
326	3.7.1982	1	70	30
327	3.7.1982	2	70	30
328	8.7.1982	2	305	55
329	8.7.1982	2	320	65
330	8.7.1982	2	330	40
331	11.7.1982	1	80	27
332	15.7.1982	2	145	30
333	15.7.1982	1	305	30
334	20.8.1982	2	75	66
335	20.8.1982	1	75	66
336	20.8.1982	1	40	80
337	14.6.1982	2	305	55
338	3.6.1982	2	138	85
339	3.6.1982	2	275	60
340	18.6.1982	2	355	24
341	18.6.1982	2	20	21
342	18.6.1982	2	340	32
343	8.7.1982	2	140	25
344	8.7.1982	2	320	64
345	18.6.1982	2	360	45
346	18.6.1982	7	360	45
347	8.6.1983	2	5	65
348	24.8.1983	2	125	65
349	24.8.1983	1	125	65
350	20.6.1983	2	330	75
351	20.6.1983	2	308	52
352	28.7.1983	2	295	43
353	28.7.1983	2	290	90
354	11.8.1983	2	88	90
355	11.8.1983	2	85	90
356	11.8.1983	2	97	90
357	11.8.1983	2	75	80
358	19.8.1983	1	30	13
359	19.8.1983	2	30	13

Attachment 1

Surface geology observations around the Alaliesintie seismic survey in Sodänkylä

1: Layering, 2: Foliation, 3: Axial Plane, 4: Fault, 7:Contact, and 8: Joint

FID	DATE	TYPE	DIRECTION	DIP
360	19.8.1983	2	12	28
361	20.8.1983	1	20	24
362	20.8.1983	1	25	22
363	20.8.1983	2	360	15
364	18.8.1983	2	82	90
365	4.9.1984	1	75	19
366	4.9.1984	2	75	19
367	4.9.1984	1	270	90
368	28.5.1985	1	65	26
369	31.5.1985	1	104	57
370	31.5.1985	1	77	67
371	31.5.1985	2	77	67
372	31.5.1985	2	75	68
373	16.8.1985	2	270	53
374	6.9.1985	2	335	50
375	27.5.1985	1	25	22
376	28.5.1985	1	50	18
377	29.5.1985	2	64	25
378	29.5.1985	2	355	24
379	31.5.1985	2	81	60
380	31.5.1985	1	81	60
381	31.5.1985	1	80	42
382	31.5.1985	2	80	42
383	31.5.1985	1	83	62
384	16.8.1985	2	256	46
385	19.8.1985	1	255	42
386	23.9.1985	2	275	90
387	4.6.1987	2	5	30
388	27.7.1994	2	275	60
389	8.8.1984	1	305	30
390	9.8.1984	1	315	35
391	9.8.1984	1	305	70
392	9.8.1984	1	285	45
393	9.8.1984	1	295	70
394	10.8.1984	1	310	70
395	10.8.1984	1	305	70
396	10.8.1984	1	300	70
397	9.8.1984	1	295	45
398	9.8.1984	1	245	45
399	10.8.1984	1	305	70
400	10.8.1984	1	300	55
401	10.8.1984	1	305	35
402	19.7.1987	2	295	65
403	23.7.1987	1	75	80
404	29.7.1987	1	18	25

Attachment 1

Surface geology observations around the Alaliesintie seismic survey in Sodänkylä

1: Layering, 2: Foliation, 3: Axial Plane, 4: Fault, 7:Contact, and 8: Joint

FID	DATE	TYPE	DIRECTION	DIP
405	18.7.1987	1	295	45
406	18.7.1987	2	295	45
407	18.7.1987	1	295	30
408	18.7.1987	2	295	30
409	23.7.1987	1	80	80
410	23.7.1987	2	80	80
411	19.7.1987	1	300	45
412	19.7.1987	2	300	45
413	19.7.1987	2	278	65
414	19.7.1987	1	278	65
415		2	330	15
416	14.6.1973	1	260	80
417	14.6.1973	2	260	0
418	14.6.1973	2	270	85
419	14.6.1973	2	245	55
420	14.6.1973	1	90	55
421	18.6.1973	2	100	55
422	18.6.1973	2	35	40
423	14.6.1973	2	260	0
424	14.6.1973	2	260	90
425	18.6.1973	2	60	25
426	15.6.1973	1	10	15
427	29.6.1973	2	290	0
428	10.7.1973	2	295	60
429	10.7.1973	8	20	0
430	10.7.1973	2	290	45
431	12.9.1973	2	310	20
432		4	55	83
433	8.9.1999	3	345	13
434	8.9.1999	3	308	26
435	8.9.1999	2	60	80
436	8.9.1999	2	40	66
437	17.7.1975	8	150	90
438	17.7.1975	2	300	25
439	24.7.1975	2	270	90
440	24.7.1975	8	40	90
441	24.7.1975	2	240	80
442	24.7.1975	2	255	70
443	24.7.1975	2	100	50
444	24.7.1975	2	90	40
445	24.7.1975	2	90	40
446	24.7.1975	8	75	40
447	24.7.1975	8	20	90
448	24.7.1975	8	70	70
449	24.7.1975	8	310	80

Attachment 1

Surface geology observations around the Alaliesintie seismic survey in Sodänkylä

1: Layering, 2: Foliation, 3: Axial Plane, 4: Fault, 7:Contact, and 8: Joint

FID	DATE	TYPE	DIRECTION	DIP
450	29.7.1975	2	90	65
451	29.7.1975	2	290	80
452	29.7.1975	2	270	30
453	29.7.1975	2	90	45
454	30.7.1975	2	285	80
455	13.8.1975	2	270	85
456	13.8.1975	8	280	70
457	1.9.1975	2	265	30
458	1.9.1975	2	265	30
459		2	265	30
460	1.9.1975	2	265	30
461	24.7.1975	2	250	50
462	24.7.1975	2	90	30
463	29.7.1975	2	90	40
464	30.7.1975	2	285	60
465	30.7.1975	2	280	70
466	24.7.1975	2	255	85
467	1.9.1975	2	90	30
468	30.9.1980	2	65	60
469	30.9.1980	2	80	85
470	30.9.1980	2	280	65
471	30.9.1980	2	80	70
472	30.9.1980	2	80	55
473	30.9.1980	1	80	55
474	30.9.1980	2	80	40
475	30.9.1980	2	50	25
476	30.9.1980	2	275	30
477	30.9.1980	2	315	25
478	30.9.1980	2	270	80
479	30.9.1980	2	290	75
480	30.9.1980	2	315	60
481	1.10.1980	2	70	60
482	1.10.1980	2	260	75
483	8.7.2002	2	325	38
484	27.6.1974	8	110	0
485	27.6.1974	8	30	0
486	8.6.1976	2	310	85
487	8.6.1976	2	60	20
488	8.6.1976	2	60	30
489	8.6.1976	2	60	30
490	8.6.1976	2	75	70
491	14.6.1976	2	245	55
492	14.6.1976	2	230	80
493	8.6.1976	2	110	90
494	8.6.1976	1	90	30

Attachment 1

Surface geology observations around the Alaliesintie seismic survey in Sodänkylä

1: Layering, 2: Foliation, 3: Axial Plane, 4: Fault, 7:Contact, and 8: Joint

FID	DATE	TYPE	DIRECTION	DIP
495	8.6.1976	2	305	75
496	14.6.1976	2	330	80
497	14.6.1976	2	120	30
498	14.8.2008	2	10	15
499	14.8.2008	8	225	70
500	14.8.2008	8	140	70
501	2.10.2017	2	290	80
502	4.10.2017	2	285	0
503	4.10.2017	2	310	45
504	4.10.2017	2	33	80
505	5.10.2017	2	85	25
506	5.10.2017	2	310	85
507	5.10.2017	2	315	88
508	5.10.2017	2	105	30
509	5.10.2017	2	86	40
510	5.10.2017	2	74	83
511	6.10.2017	2	310	70
512	6.10.2017	2	115	80
513	6.10.2017	2	280	65
514	9.10.2017	2	310	35
515	9.10.2017	2	145	25
516	10.10.2017	2	270	55
517	10.10.2017	2	330	60
518	10.10.2017	2	10	35
519	10.10.2017	2	200	55
520	3.12.2018	2	245	15
521	3.12.2018	2	270	35
522	3.12.2018	2	10	65
523	3.12.2018	2	105	70
524	3.12.2018	2	39	80
525	3.12.2018	2	34	74
526	3.12.2018	2	304	80
527	15.8.2018	2	335	40
528	15.8.2018	2	300	20

Attachment 2
Petrophysical Rock Properties from the XSoDEx Survey

Sample information					P-wave velocity				S-wave velocity				Density		
y_proj	x_proj	Sample ID	Rock name	Part	(m/s)	Alaliesintie AVG. (m/s)	AVG. (m/s)	MED. (m/s)	(m/s)	Alaliesintie AVG. (m/s)	(m/s)	MED. (m/s)	AVG. (kg/m3)	Alaliesintie AVG.(kg/m3)	AVG. (kg/m3)
7524897	487633	MTM$-2017-61.1	Amphibole chlorite schist	A			1085	1085			767	626	2848	2843	2827
			Amphibole chlorite schist	B									2837		
7528875	466948	MTM$-2017-75.1	Amphibole chlorite schist		1085				626				2795		
7522327	493512	MTM$-2017-49.1	Amphibolite	A	6483	6355	6355	6343	3743	3669	3669	3662	2904	2908	2908
			Amphibolite	B	6343				3662				2909		
			Amphibolite	C	6240				3603				2911		
7524865	491095	MTM$-2017-55.1	Arkose quartzite	A	5432	5610	5410	5432	3136	3239	3123	3136	2679	2653	2618
			Arkose quartzite	B	5609				3238				2671		
7525135	490501	MTM$-2017-56.1	Arkose quartzite	A	5625				3248				2633		
			Arkose quartzite	B	5774				3334				2630		
7526796	469516	MTM$-2017-72.1	Arkose quartzite		4694				2710				2541		
7528341	467552	MTM$-2017-74.1	Arkose quartzite	A	5209				3007				2611		
			Arkose quartzite	B	5397				3116				2614		
7528717	466910	MTM$-2017-76.1	Arkose quartzite	A	5294				3056				2572		
			Arkose quartzite	B	5655				3265				2613		
7499887	490863	MTM$-2017-14.1	Felsic tuff		5859	5490	5675	5674.5	3383	3882	3276	3276	2762	2681	2722
7523363	493121	MTM$-2017-50.1	Felsic tuff		5490				3170				2681		
7509599	493524	MTM$-2017-28.1	Gabbro	A	5655	6186	6054	5975	3265	3571	3495	3450	2784	2926	2906
			Gabbro	B	5713				3298				2785		
7513072	497647	MTM$-2017-38.1	Gabbro	A	5663				3270				2903		
			Gabbro	B	5729				3308				2929		
7515970	497862	MTM$-2017-40.1	Gabbro		5664				3270				2920		
7516443	497364	MTM$-2017-41.1	Gabbro	A	6103				3524				2888		
			Gabbro	B	6378				3682				2886		
7517714	496896	MTM$-2017-42.1	Gabbro	A	5904				3409				2980		
			Gabbro	B	5673				3275				2973		
7518269	496893	MTM$-2017-43.1	Gabbro	A	5975				3450				2954		
			Gabbro	B	6397				3693				2940		
7519233	495881	MTM$-2017-44.1	Gabbro	A	6309				3643				2903		
			Gabbro	B	6205				3582				2913		
7520079	495649	MTM$-2017-46.1	Gabbro	A	6697				3867				2927		
			Gabbro	B	6741				3892				2902		
7526230	475726	MTM$-2017-66.1	Granite	A	4640		4466	4435	2679		2579	2561	2580		2583
			Granite	B	4607				2660				2572		
7526322	474324	MTM$-2017-67.1	Granite		4259				2459				2588		
7526049	472298	MTM$-2017-69.1	Granite	A	4309				2488				2592		
			Granite	B	4435				2561				2584		
7526629	470165	MTM$-2017-71.1	Granite		4347				2510				2582		
7527132	463537	MTM$-2017-77.1	Granite		4667				2694				2582		
7520735	494619	MTM$-2017-47.1	Granite gneiss		5199	5166	4713	5133	3002	2983	2721	2964	2602	2650	2618
7521715	494181	MTM$-2017-48.1	Granite gneiss		5133				2964				2697		
7526100	471006	MTM$-2017-70.1	Granite gneiss		2890				1669				2576		
7527805	468002	MTM$-2017-73.1	Granite gneiss	A	4768				2753				2610		
			Granite gneiss	B	5575				3219				2603		
7511193	497165	MTM$-2017-34.1	Granophyre		5703		4919	4591	3293		2840	2651	2798		2744
7512723	497378	MTM$-2017-37.1	Granophyre	A	4463				2577				2714		
			Granophyre	B	4591				2651				2721		
7526046	484121	MTM$-2017-65.1	Intermediate volcanic rock		4735	4735	4735	4735	2734	3348	3348	3348	2991	2991	2991
7524890	460922	MTM$-2017-81.1	Quartz vein	A	5924		6040	6039.5	3420		3487	3487	2638		2638
			Quartz vein	B	6155				3554				2638		
7503608	490566	MTM$-2017-20.1	Mica schist		5931	3845.5	3846	5338	3424	2220	2461	3082	2880	2717	2717
7524898	491210	MTM$-2017-54.1	Mica schist		3018				1742				2703		
7525231	486518	MTM$-2017-63.1	Mica schist	A	5351				3089				2650		
			Mica schist	B	5338				3082				2650		
7525253	485853	MTM$-2017-64.1	Mica schist		1675				967				2863		
7488224	487025	MTM$-2017-9.1	Komatiite	A	6513	5349	6146	6437	3760	3782	3548	3716	2944	2813	2926
			Komatiite	B	6437				3716				2933		
7500434	491078	MTM$-2017-17.1	Komatiite		5639				3256				2958		
7511361	497117	MTM$-2017-35.1	Komatiite		5843				3373				2876		
7524876	491682	MTM$-2017-53.1	Komatiite		5349				3088				2813		
7527036	463046	MTM$-2017-79.1	Komatiite	A	6523				3766				2985		
			Komatiite	B	6715				3877				2976		
7508570	491850	MTM$-2017-27.1	Quartz albite rock		4795		4795	4795	2768		3391	3391	2655		2655
7482197	482625	MTM$-2017-11.1	Quartzite		5349		5332	5349	3088		3079	3088	2640		2614
7508550	491574	MTM$-2017-25.1	Quartzite	A	5683				3281				2629		
			Quartzite	B	5582				3223				2632		
7526340	472512	MTM$-2017-68.1	Quartzite	A	5299				3059				2602		
			Quartzite	B	5433				3137				2602		
7525594	461880	MTM$-2017-80.1	Quartzite	A	4944				2854				2598		
			Quartzite	B	5036				2908				2594		
7488351	485410	MTM$-2017-10.1	Mafic volcanic rock		6465	5782	5632	5747.2	3733	3338	3251	3320	3115	3092	2931

Attachment 2
Petrophysical Rock Properties from the XSoDEx Survey

Sample information					P-wave velocity				S-wave velocity				Density		
y_proj	x_proj	Sample ID	Rock name	Part	(m/s)	Alaliesintie AVG. (m/s)	AVG. (m/s)	MED. (m/s)	(m/s)	Alaliesintie AVG. (m/s)	(m/s)	MED. (m/s)	AVG. (kg/m3)	Alaliesintie AVG.(kg/m3)	AVG. (kg/m3)
7488351	485410	MTM$-2017-10.1	Mafic volcanic rock		6465	5713	5747	5712.7	3733	3298	3318	3392	3115	2901	2997
7508480	491585	MTM$-2017-26.1	Mafic volcanic rock		6511				3759				3208		
7511060	496937	MTM$-2017-32.1	Mafic volcanic rock		4369				2522				2953		
7525359	490229	MTM$-2017-57.1	Mafic volcanic rock		6700				3868				3000		
7525030	487202	MTM$-2017-62.1	Mafic volcanic rock	A	5154				2976				2856		
			Mafic volcanic rock	B	5284				3051				2847		
7510977	497026	MTM$-2017-33.1	Metaquartzite	A	4498		4759	4758.5	2597		2747	2747	2774		2723
			Metaquartzite	B	5019				2898				2671		
7510329	497006	MTM$-2017-30.1	Metapyroxenite	A	6794		6935	6934.5	3923		4004	4004	3109		3110
			Metapyroxenite	B	7075				4085				3110		
7504685	491095	MTM$-2017-21.1	Black schist	A									2541		2523
			Black schist	B									2516		
			Black schist	C									2501		
			Black schist	D									2514		
7506383	491119	MTM$-2017-23.1	Black schist										2545		
7511041	496795	MTM$-2017-31.1	Peridotite		6468		6468	6468	3734		4574	3734	3018		3018
7500126	490775	MTM$-2017-15.1	Peridotitic komatiite		6464		6224	6211	3732		3593	3586	2971		2911
7500174	490921	MTM$-2017-16.1	Peridotitic komatiite	A	6211				3586				2908		
			Peridotitic komatiite	B	6583				3801				2909		
7502301	491323	MTM$-2017-19.1	Peridotitic komatiite		5909				3412				2934		
7505769	491301	MTM$-2017-22.1	Peridotitic komatiite		5953				3437				2831		
7518079	495255	MTM$-2017-45.1	Pyroxenite		6894	6894	6894	6894	3980	4875	4875	3980	3185	3185	3185
7510245	496866	MTM$-2017-29.1	Hornblende gabbro	A	6400	6907.5	6431	6410.5	3695	3988	3713	3701	3090	3294	3147
			Hornblende gabbro	B	6421				3707				3049		
7513330	497576	MTM$-2017-39.1	Hornblende gabbro	A	5799				3348				3080		
			Hornblende gabbro	B	6152				3552				3075		
7523501	492811	MTM$-2017-51.1	Hornblende gabbro	A	6837				3947				3293		
			Hornblende gabbro	B	6978				4029				3295		
7525575	488584	MTM$-2017-59.1	Serpentinite		4876	4876	4876	4876	2815	3448	3448	2815	2679	2679	2679
7507259	491536	MTM$-2017-24.1	Ultramafic volcanic rock		5979		5780	5779.5	3452		3337	3337	2935		2869
7511921	497166	MTM$-2017-36.1	Ultramafic volcanic rock		5580				3222				2803		
7499038	490219	MTM$-2017-12.1	Ultramafic veint rock	A	6381		6285	6278	3684		3629	3625	2894		2914
			Ultramafic veint rock	B	6509				3758				2891		
7499835	490625	MTM$-2017-13.1	Ultramafic veint rock	A	6075				3507				2934		
			Ultramafic veint rock	B	6175				3565				2938		
7501874	491539	MTM$-2017-18.1	Ultramafic volcanite	A	6214	5782.2	5869	5765	3588	6278	3388	3328	2997	2939.2	2964
			Ultramafic volcanite	B	5023				2900				2975		
7526032	488245	MTM$-2017-58.1	Ultramafic volcanite	A	5801				3349				2929		
			Ultramafic volcanite	B	5729				3308				2926		
			Ultramafic volcanite	C	5700				3291				2933		
7524786	487917	MTM$-2017-60.1	Ultramafic volcanite		5553				3206				2936		
			Ultramafic volcanite		6128				3538				2972		
7527259	463390	MTM$-2017-78.1	Ultramafic volcanite	A	6804				3928				3045		

Attachment 2
Petrophysical Rock Properties from the XSoDEx Survey

	Other measured rock properties										Resistivity (Galvanic)				
Sample ID	Mass (g)	Hight (cm)	Volume (cm3)	Porosity (%)	Susceptibility 10-6 (SI)	Remanence (mA/m)	Q-value	Declination (°)	Inclination (°)	Resistivity (ohmm)	R0.1 (ohmm)	R10 (ohmm)	R500 (ohmm)	PL (%)	PT (%)
MTM$-2017-61.1	167.7	11.5	58.9	3.02	36644	357	0.2								
	117.0	11.7	41.2	4.33	37531	909	0.6								
MTM$-2017-75.1	63.8	1.7	22.8	3.97	48575	373	0.2	346.8	54		2520	2450	2150	3	15
MTM$-2017-49.1	62.6	4.5	21.6	1.11	607	222	8.9	287.4	5.1		41400	38800	32900	6	21
	59.1	4.2	20.3	0.84	611	92	3.7	355.6	-4.4		17100	16500	15000	4	12
	33.9	2.5	11.7	0.95	619	185	7.3	285.3	41.3		10500	10200	9430	3	10
MTM$-2017-55.1	206.9	5.9	77.2	1.44	1481	37	0.6	121.6	40.4	0.055	2880	2790	2680	3	7
	86.2	2.5	32.3	1.77	1684	93	1.4	116.6	41.8		3140	3120	3000	1	4
MTM$-2017-56.1	205.3	6.0	78.0	0.62	1127	146	3.2	355.6	10.9		80200	74700	67700	7	16
	70.7	2.1	26.9	0.60	979	161	4.0	344.7	-41.3		49700	48400	45800	3	8
MTM$-2017-72.1	159.6	4.8	62.8	1.47	-20	78		81.4	-15.1	0.024	23400	23100	22700	1	3
MTM$-2017-74.1	201.9	5.9	77.3	0.75	3695	39	0.3	350.5	73.1		15600	15200	14800	3	5
	166.8	4.9	63.8	0.63	3063	34	0.3	262.9	58.2		5310	5120	4940	4	7
MTM$-2017-76.1	195.5	5.9	76.0	1.79	14	22		143.1	31	0.132	8270	8040	7750	3	6
	63.7	1.8	24.4	0.99	3	154		323.1	-17.7	0.16	17100	16600	15900	3	7
MTM$-2017-14.1	100.7	2.8	36.4	0.88	369	87		360	-18.4	0.766	5940	4120	2910	31	51
MTM$-2017-50.1	118.0	3.3	44.0	0.64	129	39		45	35.3	0.189	12000	11900	11500	1	4
MTM$-2017-28.1	213.8	5.9	76.8	1.20	108890	2942	0.7	310.8	75		1340	1290	1140	4	15
	65.3	1.8	23.4	1.07	110926	3014	0.7	358.6	66.2		2590	2480	2190	4	15
MTM$-2017-38.1	214.1	5.7	73.8	0.87	694	11	0.4	126.9	-31		17400	16900	16300	3	6
	167.2	4.3	57.1	0.93	775	59	1.9	285.3	14.7		16700	16200	15500	3	7
MTM$-2017-40.1	159.7	4.2	54.7	0.61	382	49	3.1	126.9	74.5		7560	7440	7100	2	6
MTM$-2017-41.1	224.9	6.0	77.9	0.53	866	230	6.5	322.4	33.4	7.16E-03	22700	21900	21000	4	7
	80.5	2.1	27.9	0.54	826	310	9.2	324.7	34.1	6.77E-03	19900	19500	18800	2	6
MTM$-2017-42.1	125.9	3.2	42.3	0.41	2583	3652	34.5	295.9	27.3	0.037	17600	17100	16400	3	7
	145.8	3.7	49.1	0.47	2086	2940	34.4	297.9	22.6	0.105	18400	17800	17100	3	7
MTM$-2017-43.1	230.9	6.0	78.2	0.60	489	10		338.2	-20.4		87300	83100	67700	5	22
	73.9	1.9	25.1	0.76	459	104		45	-3.1		86400	82700	71200	4	18
MTM$-2017-44.1	226.4	6.0	78.0	0.40	717	571	19.4	283.1	6.5		13200	12800	12100	3	8
	188.1	4.9	64.6	0.42	762	578	18.5	277.9	1.8		14500	14000	13200	3	9
MTM$-2017-46.1	225.9	5.9	77.2	0.27	337	33		346.8	9.7		140000	132000	93500	6	33
	169.8	4.5	58.5	0.48	302	86		143.1	31	0.307	30300	29800	28400	2	6
MTM$-2017-66.1	197.9	5.9	76.7	2.35	10567	133	0.3	6.4	0.8		28500	11800	10800	59	62
	187.0	5.6	72.7	2.74	11195	227	0.5	13.7	-7.5		7850	7250	6620	8	16
MTM$-2017-67.1	159.3	4.8	61.6	2.35	14459	167	0.3	141.5	46.2		15100	14400	13500	5	11
MTM$-2017-69.1	201.3	6.0	77.7	1.77	16598	119	0.2	301.6	44.5		14100	13200	12300	6	13
	162.0	4.8	62.7	2.00	15386	125	0.2	333.4	30.8		22400	21300	19900	5	11
MTM$-2017-71.1	159.7	4.7	61.8	1.60	4911	30	0.2	225	83.8		7660	7370	7030	4	8
MTM$-2017-77.1	120.2	3.6	46.6	2.34	14	93		7.1	74.5		11400	11400	11200	0	2
MTM$-2017-47.1	202.5	6.0	77.9	1.15	1922	21	0.3	338.2	-20.4		21900	20900	19500	5	11
MTM$-2017-48.1	105.4	3.0	39.1	1.36	253	86		82.9	69.9		25600	24300	22400	5	13
MTM$-2017-70.1	191.7	5.8	74.4	3.23	1454	30	0.5	65.2	22.7		2650	2560	2430	3	8
MTM$-2017-73.1	199.8	5.9	76.6	1.12	26	53		5	34.7		9290	8900	8560	4	8
	73.1	2.2	28.1	0.93	23	141		23.7	8.3	0.037	12300	12000	11600	2	6
MTM$-2017-34.1	212.4	5.8	75.9	1.17	21430	269	0.3	6.7	38.8		5620	5420	5100	4	9
MTM$-2017-37.1	211.8	6.0	78.0	1.41	12633	845	1.6	345.1	-11		35400	33000	30400	7	14
	82.6	2.3	30.4	1.52	22811	1550	1.7	336.8	-17		14400	13100	11900	9	17
MTM$-2017-65.1	163.1	4.3	54.5	1.21	707	30	1.0	82.9	44.8	0.039	21600	20600	19200	5	11
MTM$-2017-81.1	204.7	5.9	77.6	0.09	-8	46		85	21.3		>251296	>251296	>251296		
	157.8	4.6	59.8	0.07	-18	49		209.4	-26.1	0.027	>318809	>318809	>318809		
MTM$-2017-20.1	174.5	4.7	60.6	1.66	772	36	1.2	82.9	-58.2		8390	7810	7000	7	17
MTM$-2017-54.1	113.2	3.2	41.9	1.79	192	125					3820	3700	3490	3	9
MTM$-2017-63.1	54.3	4.5	20.5	1.12	106	84		323.1	65.6		5240	4920	4660	6	11
	30.8	2.4	11.6	1.12	115	321		296.6	53.3		5460	5180	4960	5	9
MTM$-2017-64.1	184.1	4.9	64.3	2.33	23607	3703	3.8				12700	11100	9660	13	24
MTM$-2017-9.1	227.8	5.9	77.4	0.82	690	24	0.8	126.9	38.7	0.409	4390	4120	3830	6	13
	129.8	3.4	44.3	0.77	707	53	1.8	328.4	21.5		3420	3320	3150	3	8
MTM$-2017-17.1	226.2	5.9	76.5	1.18	142410	5330	0.9	335	45.3		23500	18000	13500	23	43
MTM$-2017-35.1	213.6	5.7	74.3	0.51	47153	2553	1.3	53.3	67.2		76200	72500	60200	5	21
MTM$-2017-53.1	137.8	3.7	49.0	0.94	68266	6386	2.3				>403656	>403656	> 403656		
MTM$-2017-79.1	230.0	5.9	77.1	0.13	115006	10017	2.1	198.4	38.7		70700	54900	39700	22	44
	131.5	3.4	44.2	0.16	111001	13792	3.0	196.4	38.6		29700	23800	18800	20	37
MTM$-2017-27.1	152.0	4.4	57.3	1.38	131	53		276	25.2	0.225	3530	3410	3250	3	8
MTM$-2017-11.1	176.1	5.1	66.7	1.13	59	11		45	35.3	0.037	3260	3160	3020	3	7
MTM$-2017-25.1	112.2	3.3	42.7	0.35	-30	57		116.6	-24.1		89500	87400	83500	2	7
	95.0	2.8	36.1	0.33	-3	23		323.1	-31		136000	133000	117000	2	14
MTM$-2017-68.1	201.3	5.9	77.4	1.06	10259	302	0.7	14.6	26.1		18800	17700	16700	6	11
	101.1	3.0	38.9	0.98	8734	383	1.1	13.4	24.4		13300	12600	11700	5	12
MTM$-2017-80.1	197.0	5.8	75.8	1.06	1	29		94.4	-31.5	0.161	13000	12800	12500	2	4
	126.7	3.7	48.9	1.15	26	78		152.4	10.9		14500	14100	13700	3	6
MTM$-2017-10.1	91.5	2.3	29.4	0.10	1168	31	0.7	126.9	38.7	0.065	323000	280000	146000	13	55

Attachment 2
Petrophysical Rock Properties from the XSoDEx Survey

Other measured rock properties											Resistivity (Galvanic)				
Sample ID	Mass (g)	Hight (cm)	Volume (cm3)	Porosity (%)	Susceptibility 10-6 (SI)	Remanence (mA/m)	Q-value	Declination (˚)	Inclination (˚)	Resistivity (ohmm)	R0.1 (ohmm)	R10 (ohmm)	R500 (ohmm)	PL (%)	PT (%)
MTM$-2017-10.1	91.5	2.3	29.4	0.10	1168	31	0.7	126.9	38.7	0.065	323000	280000	146000	13	55
MTM$-2017-26.1	127.8	3.0	39.8	0.40	1185	38	0.8	158.2	59.1		19800	18100	15400	9	22
MTM$-2017-32.1	228.7	5.9	77.5	1.28	581	52	2.2	34.8	-10.1		20900	19700	18200	6	13
MTM$-2017-57.1	209.2	5.3	69.7	0.35	49413	933	0.5	325.5	53.2		35800	33100	30000	8	16
MTM$-2017-62.1	221.2	5.9	77.5	1.27	64710	986	0.4	54.7	44.5		1480	1440	1280	3	14
	85.8	2.3	30.1	1.26	73309	1010	0.3	57.3	40.1		1560	1550	1390	1	11
MTM$-2017-33.1	85.9	2.4	31.0	2.51	1526	189	3.0	344.7	73.7		567	578	563	0	1
	198.2	5.7	74.2	2.62	8591	72	0.2	20	51.1		767	768	744	0	3
MTM$-2017-30.1	239.8	5.9	77.1	0.16	33039	1072	0.8	312.8	60.9		145000	130000	86900	10	40
	180.5	4.4	58.0	0.21	26812	954	0.9	315	64.3		73500	69100	57400	6	22
MTM$-2017-21.1	139.4	11.0	54.9	6.32	182	49				0.016					
	155.6	9.5	61.9	6.46	162	36									
	92.5	10.3	37.0	6.92	115	53									
	161.9	7.0	64.4	6.97	154	22				0.082					
MTM$-2017-23.1	536.3	11.0	210.7	5.75	85	12									
MTM$-2017-31.1	201.1	5.1	66.6	0.44	22622	1816	2.0	301.8	40		>288911	>288911	>288911		
MTM$-2017-15.1	117.1	3.0	39.4	0.51	52677	4727	2.2	223.7	7.5		6150	5930	5380	4	13
MTM$-2017-16.1	225.4	5.9	77.5	0.85	22201	746	0.8	12.5	86.1		2880	2820	2670	2	7
	90.6	2.3	31.1	0.77	24651	795	0.8	162.6	84.5		3760	3750	3560	0	5
MTM$-2017-19.1	225.2	5.9	76.8	0.51	672	55	2.0	319.1	47.9		5200	5060	4910	3	6
MTM$-2017-22.1	131.0	3.5	46.3	2.13	495	34		253.3	21		9000	8550	7790	5	13
MTM$-2017-45.1	178.2	4.3	56.0	0.20	913	352	9.4	284.4	28.3	0.031	>341202	>341202	>341202		
MTM$-2017-29.1	233.1	5.8	75.4	0.41	5560	49	0.2	175.6	59.3		78000	69200	55100	11	29
	201.2	5.0	66.0	0.44	8409	184	0.5	225	36.4		17500	16300	14900	7	15
MTM$-2017-39.1	237.6	5.9	77.1	0.71	1065	26	0.6	360	0		28500	27500	25900	4	9
	76.9	1.9	25.0	0.73	1025	47	1.1	262.9	-7.1		29400	28600	27200	3	7
MTM$-2017-51.1	253.8	5.9	77.1	0.65	18480	1334	1.8	90.4	-25.7		36400	32400	27900	11	23
	83.3	1.9	25.3	0.68	20288	1341	1.6	85.4	-25.5		35800	31800	28800	11	20
MTM$-2017-59.1	206.1	5.9	76.9	2.32	94553	11276	2.9	171.8	21.3		>249239	>249239	>249239		
MTM$-2017-24.1	119.5	3.1	40.7	1.13	548	71	3.2	170.5	52.8		14200	13400	12400	6	13
MTM$-2017-36.1	222.6	6.1	79.4	1.00	73532	7370	2.5	127.7	38.2		>240645	>240645	>240645		
MTM$-2017-12.1	223.6	5.9	77.2	0.87	215600	9543	1.1	352.5	75.3		4580	3420	2620	25	43
	83.0	2.2	28.7	0.87	219630	9010	1.0	7.4	77.6		4570	3560	2770	22	39
MTM$-2017-13.1	229.5	6.0	78.2	1.05	875	62	1.7	82.9	61.7	0.058	6880	6260	5300	9	23
	180.1	4.7	61.3	0.87	1203	183	3.7	153.4	78.5		3410	3190	2990	6	12
MTM$-2017-18.1	81.0	2.0	27.0	2.04	669	34	1.2	306.9	-38.7	0.03	2830	2800	2700	1	5
	75.0	2.0	25.2	2.27	687	185	6.6	10.9	35.7		2330	2300	2230	1	4
MTM$-2017-58.1	62.1	4.4	21.2	1.79	69004	3971	1.4	325.9	49.6		2250	2010	1690	11	25
	62.1	4.4	21.2	1.74	49650	3650	1.8	322.9	47.8		1060	999	892	6	16
	31.3	2.3	10.7	1.70	73533	4284	1.4	341	47.9		1260	1150	972	9	23
MTM$-2017-60.1	149.8	3.9	51.0	1.02	10962	118	0.3	194.7	62		9770	8820	7930	10	19
	84.4	2.2	28.4	0.67	74947	5161	1.7	341.7	6.1		43700	38300	31700	12	27
MTM$-2017-78.1	233.4	5.9	76.6	0.16	873	103	2.9	306.9	24.7		159000	148000	97100	7	39